Diffusion of Diluents in Glassy Polymers

by

PAUL FRANKLIN NEALEY

Bachelor of Science, Chemical Engineering
Rice University, Houston, Texas, 1985

Submitted to the Department of Chemical Engineering
in partial fulfillment of the requirements for the degree of

DOCTOR OF PHILOSOPHY
in Chemical Engineering

at the
MASSACHUSETTS INSTITUTE OF TECHNOLOGY
May, 1994

Signature of Author_____
Department of Chemical Engineering
May 17, 1994

Certified by_____
Robert E. Cohen, Professor of Chemical Engineering
Thesis Advisor

and by_____
Ali S. Argon, Professor of Mechanical Engineering
Thesis Advisor

Accepted by_____
Robert E. Cohen
Chairman, Committee for Graduate Students

Diffusion of Diluents in Glassy Polymers

by

Paul Franklin Nealey

Submitted to the Department of Chemical Engineering on May 17, 1994,
in partial fulfillment of the requirements for the degree of
Doctor of Philosophy in Chemical Engineering.

Abstract

A central feature of a recently reported toughening mechanism observed in blends of a few volume percent low molecular weight polybutadiene(PB) in polystyrene (PS) is the localized plasticization of PS by PB in the immediate vicinity of crazes. The sorption of PB into the PS craze matter is driven by the significant concentrations of positive mean normal stress, σ, at the craze tip and along the craze borders, and throughout the fibrils. The required diffusion coefficient for PB in PS in these regions in craze growth experiments at 25 °C is approximately 10^{-12} cm^2/s.

The thermally-induced diffusion of low molecular weight PB in PS was measured with Forward Recoil Spectroscopy (FRES). Diffusion coefficients were determined for 3000 g/mol perdeuterated PB penetrating into a 350,000 g/mol PS matrix in the temperature range of 97 to 115 °C. The diffusion coefficients vary from 10^{-15} to 10^{-12} cm^2/s. The apparent activation energy, ΔE, is 99 kcal/mol. The values of D and ΔE are in good agreement with those found for the diffusion of photoreactive dye molecules in PS in the same temperature range. This implies that the PB molecule acts as a probe of PS matrix properties. The thermally-induced tracer diffusion of PB in PS did not proceed at a rate equivalent to the estimated rate required by the toughening mechanism until the temperature reached 115 °C, a temperature well above the T_g of PS.

The effect of stress on the diffusion of PB in PS was investigated by applying gas pressure. Hydrostatic pressure (negative mean normal stress) decreased D from 1.2×10^{-13} to 3.7×10^{-14} cm^2/s as the pressure increased from 0 to 11.3 MPa at 107 °C. On the other hand, D is expected to increase if the PS is subjected to a positive mean normal stress. However, even the largest value of σ in the vicinity of crazes can not fully account for the rapid diffusion of PB in PS in the toughening mechanism at 25 °C.

Diffusion in a model plasticizer/glassy polymer system consisting of resorcinol bis(diphenyl phosphate) (RDP) and a polyetherimide (Ultem™) was investigated to determine if a non-Fickian diffusion mechanism could account for the flux of PB into PS in the fringe layers of crazes. Volume fraction versus depth profiles of RDP in Ultem™ were measured with Rutherford Backscattering Spectroscopy (RBS) as a function of time, temperature, and externally applied stress when RDP was present in a limited supply. In the temperature range of 120 to 180 °C, diffusion front velocities varied from 10^{-4} to 10^{-1} nm/s. These experiments are comparable to the PB/PS system on the basis of the temperature difference, T_g-$T_{experiment}$. Under no experimental conditions did the front velocity attain a value of 10 nm/s, the minimum velocity required to account for the flux of PB in PS in the diffusion process of the toughening mechanism. Externally applied biaxial stresses in the plane normal to the direction of penetration had no effect on the diffusion.

The diffusion measurements in the PB/PS system and the RDP/Ultem™ system reveal that the physical properties of PS during the deformation process are dramatically different than the unstressed polymer or the stressed polymer prior to plastic deformation.

Thesis Supervisors: Robert E. Cohen, Professor of Chemical Engineering
Ali S. Argon, Professor of Mechanical Engineering

Acknowledgments

This research was supported primarily by NSF/MRL, through the Center for Materials Science and Engineering at M.I.T. under grant No. DMR-90-22933. Other sources of funding included the David H. Koch School of Chemical Engineering Practice at MIT, and a fellowship from Bayer AG.

I consider myself extremely fortunate to have had the opportunity to work with Professors R. E. Cohen and A. S. Argon. Their enthusiasm, interest, and insight created a supportive and intellectually challenging environment in which to learn and to conduct research.

Other people to whom my thanks are due include members of my thesis committee, W. M. Deen, and E. W. Merrill; Professor Kramer and his research group at Cornell University; and Roger Kambour of General Electric Co.

RBS and FRES experiments would have been impossible without the collaboration of John Chervinsky at the Cambridge Accelerator for Materials Science at Harvard University. Important sample preparation procedures were developed by Alexis Black when she worked as a UROP in our laboratory.

Finally, I will always value the experience of being part of the Cohen group. The frienships that I made in Boston contributed to both my education and my quality of life, and will surely be the most enduring aspect of my time at MIT.

Table of Contents

List of Figures

List of Tables

Chapter 1

Introduction

1.1 A New Toughening Mechanism for Glassy Polymers

Glassy polymers such as polystyrene (PS) and polymethyl methacrylate (PMMA) are important commercial materials because of their many attractive properties such as optical clarity, high strength, ease of processing, and low cost. Unfortunately, these materials are normally brittle and are not suitable for applications where a high resistance to fracture is required.[1] When glassy polymers are subjected to a tensile stress, a phenomenon known as crazing occurs.[2-4] Crazing is a dilatational process which allows the material to strain in response to the imposed tensile stress. The structure of a craze resembles two planes approximately 0.5 μm apart,[5] depending on the polymer and maturity of the craze, connected by fibrils of highly oriented material which has been drawn out of the craze walls. The planes are normal to the direction of the imposed tensile stress. Fibril diameters of 10 to 15 nm were measured with low angle electron diffraction,[6] and values of 20 to 40 nm have been reported in transmission electron microscopy studies.[7,8] Because of the fibrils, crazes are very different from cracks in that they are load bearing. Crazes in homopolymers generally initiate on the surface of the polymer or near a material defect, and they propagate at a craze flow stress well below the compressive yield stress of the material. A craze which was initiated on the surface, for example, would propagate in the shape of a half penny with increasing diameter. If a craze encounters any critical flaw in the material such as a dust particle, the craze can rupture and catastrophic brittle failure is the result if the flaw is larger than a critical value. In glassy homopolymers, these events are likely because of the comparatively high craze flow stress, and the materials undergo very little strain to fracture,[9-12] on the average.

For many years research has focused on improving the fracture resistance or toughness of glassy polymers.[1] One successful approach is to modify the material with rubber. Examples of so called rubber toughened glassy polymers are high impact polystyrene (HIPS), which is a graft copolymer of polybutadiene and polystyrene,[13-17] and acrylonitrile/butadiene/styrene (ABS).[16-18] In both of these materials, the rubber component occupies approximately 10 to 20 volume percent of the material in the form of composite particles of micron dimensions and high elastic flexibility, which act as effective craze initiators. When these materials are subjected to tensile stresses, a high density of active craze fronts is created. The crazes propagate at flow stresses which are on average, about half of the flow stress of the homopolymer. Crazes which propagate at this lower flow stress tend to survive encounters with what would otherwise be critical flaws in the homopolymer. The improved toughness is a result of significantly larger strains to fracture.[9-12]

Kruse found that the toughness of HIPS could be improved further by the addition of a low molecular weight polybutadiene (PB) component which was not grafted to the polystyrene.[19] In the course of investigating the solubility of the low molecular weight PB in PS, Gebizlioglu et al. observed dramatic increases in toughness in blends of just a few volume percent of low molecular weight PB in PS,[20,21] without the grafted rubber component. Figure 1.1 shows a schematic of typical stress-strain curves for the homopolymer and a toughened blend of perhaps 3 to 4 volume percent 3000 g/mol PB in PS in which the tensile toughness is defined as the area under the stress-strain curve.

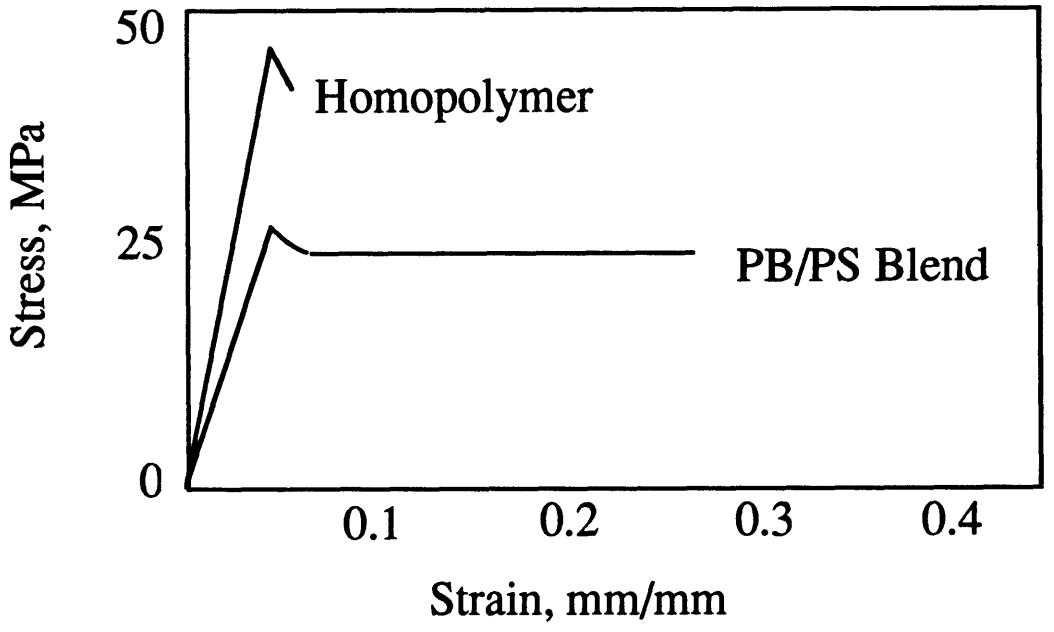

Figure 1.1 Schematic of a typical stress-strain plot for PS homopolymer and a toughened blend of a few volume percent of low molecular weight PB in PS.

Transmission electron microscopy (TEM) studies showed that the PB in these blends was phase separated in pools less than 0.2 μm in diameter. The pools can not act as craze initiators because they are 1) too small, and 2) have a very weak interfaces with the PS matrix.[10] Small angle x-ray scattering (SAXS) experiments revealed that the product of the craze flow stress and the mean fibril diameter was constant over a wide range of flow stress.[22] This is a signature that the crazes propagate according to the meniscus interface convolution mechanism as described by Argon and Salama,[23] but that the local plastic resistance is substantially lower than in the bulk material. The combination of the TEM and SAXS results indicated that the increased toughness observed in these blends was due to crazes which propagate at higher velocities rather than an increase in the density of active craze fronts.

Argon et al.[24] developed a model for the new toughening mechanism which explains the higher velocity craze growth and lower craze flow stress observed in the

blends of few volume percent low molecular weight PB in PS. The process is shown in a schematic in figure 1.2.

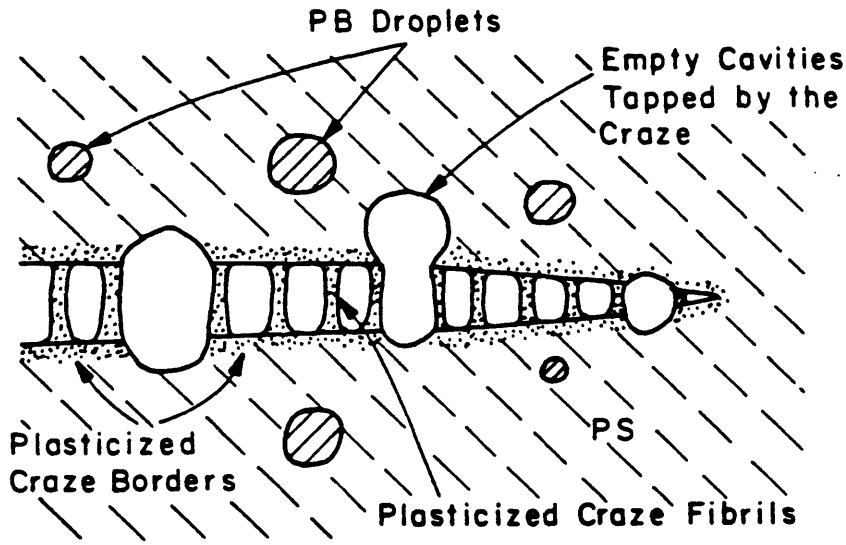

Figure 1.2 Craze propagating in a blend of a few volume percent low molecular weight PB and PS in which the PB is phase separated into small pools.

As crazes propagate in the blend, they intercept the randomly spaced, small pools of PB. The contents of the pools drain and wet the surfaces of the craze walls and fibrils. The critical nature of the pool size manifests itself in this process. If the pool is significantly larger than approximately 0.2 μm, the void left behind in the draining process becomes a critical flaw and the craze ruptures. PB penetrates into the PS in the immediate vicinity of crazes and locally plasticizes this material. The fibril drawing process is thus greatly facilitated and as a result, crazes propagate at higher velocities and at significantly lower craze flow stresses. The probability of premature failure due to encounters with flaws in

the material is reduced and the toughness is increased through larger strains to fracture (figure 1.1).

Local plasticization of the craze material is the key to this new toughening mechanism. The model of Argon et al.[24] is based on the interface convolution mechanism for craze growth in homopolymers[23] with a modification of the tensile plastic resistance of the PS due to the plasticization effects. The excellent agreement of the model to experimental craze velocity studies[20,24] combined with the SAXS experiments[22] discussed above is compelling evidence that plasticization indeed occurs. Confirmation of plasticization also comes from a TEM study of crazing in RC bimodal HIPS, a blend of the HIPS graft copolymer with free low molecular weight polybutadiene.[25] The free rubber component associates with the HIPS particles as well as phase separates in small pools in the PS matrix. Okamoto et al.[25] present micrographs of a sample before crazing, after crazing, and after healing the crazes for 36 hours at 110 °C. Crazes initiate at the HIPS particles and propagate into the matrix of PS and randomly dispersed free PB pools approximately 0.1 μm in diameter spaced approximately 0.5 μm apart. The crazes are shown to intercept small phase separated pools of PB only in the plane of the craze, similar to the schematic above. After healing, the PB that had been incorporated into crazes is reprecipitated in very small pools approximately 0.01 μm in diameter spaced approximately 0.01μm apart in a straight line which traces the exact path of a healed craze. Free rubber particles which had not been intercepted and incorporated by crazes remain unchanged throughout the entire micrograph series.

Polybutadiene phase separates in the morphology of small pools when blended with PS because of the large positive segmental interaction parameter for this system. At room temperature, the solubility of 3000 g/mol PB in high molecular weight PS is approximately 0.4 volume percent.[20] Normally PB would remain in equilibrium in a separate phase on the surface of the PS craze material after draining from the pools if the PS craze surfaces were stress free. However, significant concentrations of positive mean normal stress, σ,

or negative pressure, exist at the craze tip and in the plastic drawing zone at the craze borders, and throughout the fibrils.[7,24,26] The consequence of the positive mean normal stress is to increase the solubility of the PB is PS, C_∞, such that[24,27,28]

$$\frac{C_\infty(\sigma)}{C_\infty(\sigma=0)} = \exp\left(\frac{\sigma V_{PB}}{RT}\right) \tag{1.1}$$

where V_{PB} is the molar volume of PB, and R and T have their usual meanings. In the neighborhood crazes, the solubility of PB in PS must increase by orders of magnitude. This effect explains the thermodynamics behind the plasticization in that without the presence of stress, the PB could not possibly attain a volume fraction in PS that would lower the tensile plastic resistance to the extent required by the toughening mechanism.

An issue that is not resolved in the model of Argon et al.[24] is the diffusion process which delivers PB in sufficient quantities in the craze fringe layers to cause plasticization. The wetting and transport via a complex case II diffusion process are assumed to proceed at rates significantly higher than the rate of craze advance, and indeed this appears to be true for the experiments conducted by Gebizlioglu et al.[20] at room temperature in which the imposed strain rate was 1.4×10^{-4} s^{-1}. Subsequent mechanical experiments with blends of low molecular weight PB in PS demonstrate that the diffusion process is the limiting step in the toughening mechanism. Spiegelberg[29] showed that the increase in toughness begins to disappear when the material is subjected to strain rates greater than approximately 3×10^{-3} s^{-1}, and Piorkowska et al.[30] showed that at strain rates on the order of 1×10^{-2} s^{-1} in a notched Izod impact test, the blends showed no increase in toughness whatsoever. Tensile studies at subambient temperatures[29] (-20 °C) show no toughness increase for the blended material compared to the homopolymer. Gebizlioglu et al.[20] also demonstrated that the toughening phenomena disappear when the molecular weight of the PB is increased from 3000 g/mol to 6000 g/mol. The diffusion process is identified as the limiting step in the toughening mechanism because in all of the above experiments,

conditions were imposed which reduce the mobility of the PB in the blends, and no improvement in mechanical properties is observed.

1.2 The Diffusion Process

A lower bound estimate of the diffusion coefficient for low molecular weight PB in PS that occurs in the toughening mechanism is found from an order of magnitude analysis. Craze growth measurements by Spiegelberg[29] and Gebizlioglu et al.[20] indicate that a typical craze velocity in a toughened blend is approximately 10 to 100 nm/s. A characteristic length, l, in the system is of order 10 nm. This corresponds to the diameter of a fibril as well as to the thickness of the strain softened material in the fringe layer of the craze border which is drawn into fibrils.[31] The characteristic time, τ_{craze}, is calculated as the time necessary for the craze to advance one characteristic length, namely 0.1 to 1 s. Thus the lower bound estimate for the diffusion coefficient, D, is

$$D \approx \frac{l^2}{\tau_{craze}} \approx 10^{-12} cm^2 / s. \qquad (1.2)$$

The required flux of PB is a more difficult quantity to estimate because the volume fraction of PB in PS necessary to plasticize the craze matter is unknown. It is quite likely that the process is autocatalytic, where once a certain amount of PB penetrates the PS, the material begins to yield in response to the imposed stress, and the PB penetration accelerates. The diffusion process must depend on many interrelated parameters in this complex system.

Stress and plasticization are also important components in non-Fickian diffusion of more soluble plasticizers, usually vapors or solvents, in glassy polymers.[32-35] The term non-Fickian is used here to encompass so called anomalous and case II diffusion. Aspects of these diffusion mechanisms are, most likely, applicable to the diffusion process which

occurs in the toughening mechanism.[24] Systems which exhibit this type of behavior include Methanol/PMMA,[32] Iodohexane/PS,[32-34,36,37] and Dodecane/PS.[38] When the diffusant is present in an unlimited supply on the surface of the glassy polymer, non-Fickian diffusion is characterized by:

1. an induction period;
2. formation of a sharp diffusion front which separates plasticized material from the unperturbed glassy polymer substrate;
3. the existence of a small Fickian precursor diffusion profile ahead of the front;
4. linear weight gain with time (linear propagation of the diffusion front with time);
5. constant concentration of penetrant in the plasticized layer.

A schematic of the diffusion profiles at constant time intervals is shown in figure 1.3. The constant volume fraction in the plasticized layer is ϕ_0, the equilibrium swelling ratio.

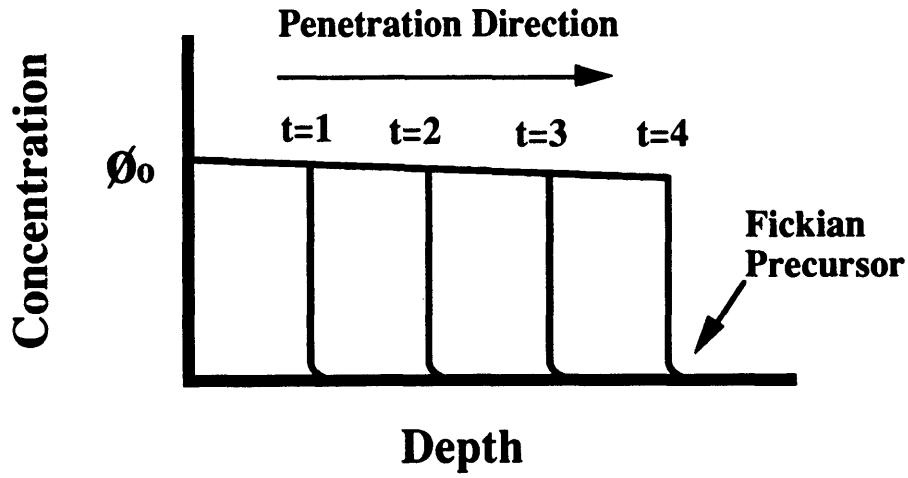

Figure 1.3 Schematic of non-Fickian diffusion profiles at integral times for a constant activity penetrant reservoir in contact with a glassy polymer.

Thomas and Windle[32] have developed a model which captures the fundamental aspects of this type of diffusion in these systems. They propose that the rate controlling step is the time dependent mechanical deformation of the polymer in response to the stress that is generated at the interface between the rubbery swollen material in the plasticized layer and the unswollen glassy polymer substrate. Consider the diffusion of a penetrant into a half plane as depicted at a snapshot in time in figure 1.4. The quantity ϕ_0 is the equilibrium swelling ratio of the penetrant in the polymer. The curve marked ϕ is the actual volume fraction of penetrant as a function of depth, and the curve marked ϕ_e is the local equilibrium concentration if the stress generated at the interface were zero.

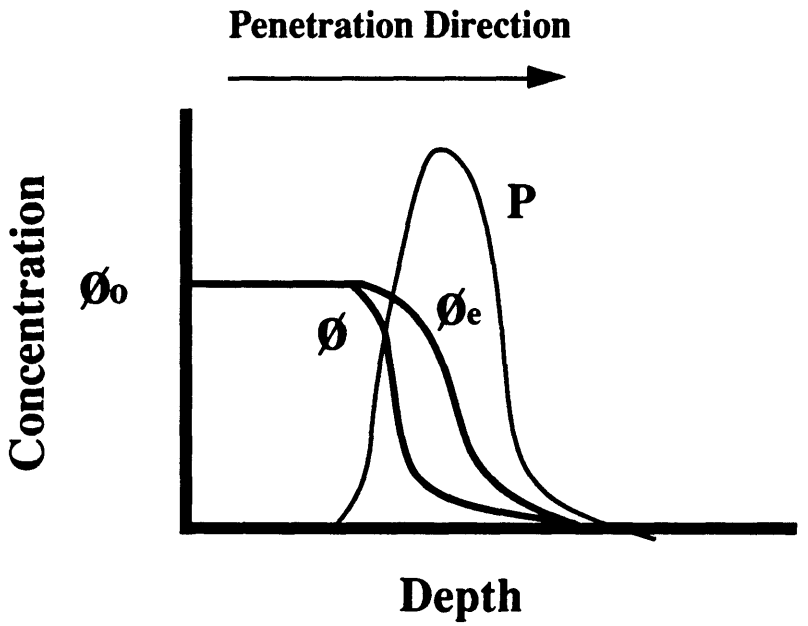

Figure 1.4 Schematic of non-Fickian diffusion profile where the curve marked ø is the actual concentraion profile, øe the local equilibrium concentration profile, and P the osmotic pressure.

The volume fraction ø increases towards its equilibrium value ϕ_e driven by the stress near the diffusion front. Thomas and Windle[32] equate the stress to an osmotic pressure, P, where

$$P = \frac{RT}{\bar{V}_p} \ln\left(\frac{\phi_e}{\phi}\right). \tag{1.3}$$

The osmotic pressure profile is marked P in figure 1.4, and values of P reach magnitudes as large as 50 to 100 MPa. The swelling rate at each material element is given by

$$\frac{\partial \phi}{\partial t} = \frac{P}{\eta} \tag{1.4}$$

where η, the elongational viscosity, is assumed to decrease exponentially with penetrant concentration such that

$$\eta = \eta_o \exp(-\alpha_v \phi). \tag{1.5}$$

Values of the constant α_v range from 10 to 30 in the model, and η_o is the equilibrium viscosity of the glassy polymer.

The flux of penetrant is derived from an expression of Fick's law in terms of chemical potential and the conservation of mass and is given by

$$\frac{\partial \phi}{\partial t} = \frac{\partial}{\partial x}\left(D(\phi)\frac{\phi}{\phi_e}\frac{\partial \phi_e}{\partial x}\right), \tag{1.6}$$

where the diffusion coefficient, D(ø), is assumed to increase exponentially with ø such that

$$D = D_o \exp(\alpha_D \phi). \tag{1.7}$$

Values of the constant α_D are the same order of magnitude as those for α_v. In equation 1.7, D_o is the tracer diffusion coefficient of the penetrant in the glassy polymer. Thus the

elongational viscosity and the diffusion coefficient change dramatically over a very short distance near the diffusion front. Thomas and Windle[32] have numerically integrated the coupled system of equations 1.4 and 1.6. Their model accurately predicts the correct shape of the diffusion profile, as well as the constant velocity of the diffusion front, and fits their experimental data from the methanol/PMMA system in all respects.

Elements of the non-Fickian diffusion model that may relate to the diffusion process in the toughening mechanism are the effect of stress as a driving force and the creation of a plasticized layer of material. In non-Fickian diffusion, the stress which drives the diffusion is generated internally. In the diffusion process in the toughened blends, an externally applied stress results in concentrations of positive mean normal stress in the craze borders. Perhaps the stress in the toughened blends not only increases the solubility of the PB in the PS, but initiates a non-Fickian diffusion mechanism as well. The material drawn into the crazes would originate from a plasticized layer, and this would explain the lower craze flow stress which ultimately leads to larger strains to fracture in the blends. In order to create a plasticized layer of sufficient thickness, the velocity of the non-Fickian diffusion front would have to be of the same order of magnitude or greater than the craze propagation velocity. Assuming no induction time for the diffusion, a front velocity of approximately 10 nm/s is required to account for the flux of PB in PS over the characteristic length, l. An important difference between the non-Fickian diffusion model and the diffusion process in the toughened blends is the boundary condition for the plasticizer. The Thomas and Windle model[32] and previous experimental work concerning non-Fickian diffusion[32-34,36,39] all consider an infinite reservoir of penetrant on the surface of the glassy polymer. In the toughened blends, PB is present only in a limited supply in the diffusion process, and this different boundary condition must be taken into account.

Brown[27] combined the Thomas and Windle theory[32] of non-Fickian diffusion with the Argon and Salama interface convolution mechanism for craze growth[23] to make some observations about environmental crazing. In terms of the Thomas and Windle model,[32]

environmental crazing occurs when the stress generated by the local plasticization exceeds the yield stress of the glassy polymer. In normal crazes in the glassy homopolymer, the thickness of the active zone, h, or strain softened layer adjacent to a craze border is much less than the distance between fibrils, λ, such that $h<<\lambda$.[40] Figure 1.5 shows a schematic of a craze cross section with these values labeled. In environmental crazing, the crazes act as conduits, so, again the penetrant is present in an unlimited supply at the craze surfaces.

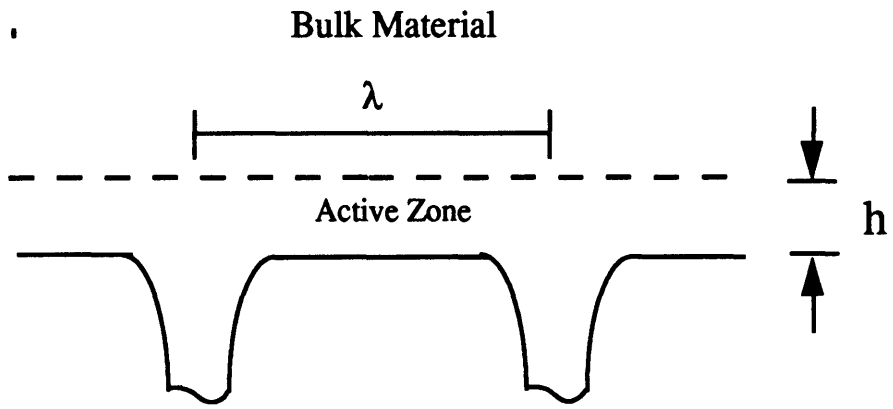

Figure 1.5 Craze fibrils spaced a distance λ apart with active zone of thickness h.

Brown[27] asserts that environmental plasticization may cause the active zone of material adjacent to a craze to be of significant thickness with respect to the craze fibril spacing, and have profound effect on the craze growth rate in that the rate varies as h^3. This problem can be considered as the question, 'A ceiling is painted with a Newtonian fluid of thickness h, the paint drips onto the floor, how far apart are the drips and under what circumstances is the distance apart controlled by h?' One regime of Brown's analysis considers a scenario where the propagation of the craze front is sufficiently fast such that the thickness h corresponds to both the thickness of the strain softened layer and the depth of penetration of the plasticizing agent. The craze growth rate is shown to be controlled by a combination of the non-Fickian diffusion process[32] and the meniscus instability process.[23] This framework seems to be applicable to the diffusion process in the toughened blends.

However, the question still remains, 'How does PB penetrate into PS from a limited supply on the craze surface at a rate which is sufficient to affect a layer of thickness h on the time scale of craze propagation?'

1.3 Research Objectives

Information concerning the rate of penetration of PB into PS is key for understanding the toughening mechanism and its limitations. Diffusion data is also a prerequisite for the future extension of models such as Brown's to describe the complicated and mutually dependent deformation and diffusion processes which occur in the toughened blends. The objectives of this research project were:

1. Develop the sample preparation procedures and experimental techniques to measure diffusion data in the low molecular weight PB/PS system. Diffusion coefficients are expected to be of order 10^{-12} cm^2/s. This implies that the technique must be able to determine volume fraction versus depth profiles over distances of order 1μm in order for reasonable time frame experiments to be conducted. Sensitivity is also an issue in that volume fractions of PB in PS are expected to be as low as 0.4 percent.
2. Experimentally determine the effect of stress on the solubility and diffusion of PB in PS.
3. Investigate non-Fickian diffusion with a limited supply boundary condition in a model plasticizer /glassy polymer system.
4. Determine the effect of an externally applied stress on non-Fickian diffusion in which the effect of stress on solubility and diffusion is not coupled.
5. Use the results of the experimental observations to describe the diffusion process in the toughened blends on a more fundamental level.

1.4 References

(1) Bucknall, C. B. *Toughened Plastics*; Applied Science Publishers LTD: London, 1977.

(2) Hsaio, C. C. *J. Appl. Phys.* **1950**, *21*, 1071.

(3) Cheatham, R. G.; Dietz, A. G. H. *Trans. ASME* **1952**, *74*, 31.

(4) Sauer, J. A.; Hsaio, C. C. *Trans. ASME* **1953**, *75*, 895.

(5) Michler, G. H. *J. Mater. Sci.* **1990**, *25*, 2321.

(6) Berger, L. L. *Macromolecules* **1989**, *22*, 3162.

(7) Lauterwasser, B. D.; Kramer, E. J. *Phil. Mag.* **1979**, *39*, 469.

(8) Beahan, P.; Bevis, M.; Hull, D. J. *J. Mater. Sci.* **1972**, *8*, 162.

(9) Argon, A. S.; Cohen, R. E.; Gebizlioglu, O. S.; Schwier, C. E. In *Advances in Fracture Research, International Conference on Fracture*; Pergamon Press: New Delhi, India, 1984; pp 427.

(10) Argon, A. S.; Cohen, R. E.; Gebizlioglu, O. S. In *Mechanical Behavior of Materials-V*; Pergamon Press: Beijing, China, 1987; pp 3.

(11) Argon, A. S. In *International Conference on Fracture*; Pergamon Press: Houston, Texas, 1989; pp 2661.

(12) Argon, A. S. In *Tenth Riso International Symposium on Metallurgy and Materials Science:Materials Architecture*; Riso National Laboratory, Roskilde, Denmark, 1989; pp .

(13) Hall, R. A. *J. Mater. Sci.* **1990**, *25*, 183.

(14) Okamoto, Y.; Miyagi, H.; Kakugo, M. *Macromolecules* **1991**, *24*, 5639.

(15) Bucknall, C. B.; Clayton, D.; Keast, W. E. *J. Mater. Sci.* **1972**, *7*, 1443.

(16) Bucknall, C. B.; Stevens, W. W. *J. Mater. Sci.* **1980**, *15*, 2950.

(17) Cigna, G.; Maestrini, C.; Castellani, L.; Lomellini, P. *J. of Appl. Polym. Sci.* **1992**, *44*, 505.

(18) Chen, C. C.; Sauer, J. A. *J. of Appl. Polym. Sci.* **1990**, *40*, 503.

(19) Kruse, R. L. *US Patent 4154715* **1979**,

(20) Gebizlioglu, O. S.; Beckham, H. W.; Argon, A. S.; Cohen, R. E.; Brown, H. R. *Macromolecules* **1990**, *23*, 3968-3974.

(21) Gebizlioglu, O. S.; Cohen, R. E.; Argon, A. S.; Beckham, H. W.; Qin, J. *US Patents 5115028 and 5223574* **1993**,

(22) Brown, H. R.; Argon, A. S.; Cohen, R. E.; Gebizlioglu, O. S.; Kramer, E. J. *Macromolecules* **1989**, *22*, 1002.

(23) Argon, A. S.; Salama, M. M. *Phil. Mag.* **1977**, *36*, 1217.

(24) Argon, A. S.; Cohen, R. E.; Gebizlioglu, O. S.; Brown, H. R.; Kramer, E. J. *Macromolecules* **1990**, *1990*, 3975-3982.

(25) Okamoto, Y.; Miyagi, H.; Mitsui, S. *Submitted to Macromolecules* **1993**,

(26) Bagepalli, B. S. Sc. D. Thesis, MIT, 1984.

(27) Brown, H. R. *J. Polym. Sci, Polym. Phys. Ed.* **1989**, *27*, 1273-1288.

(28) Nealey, P. F.; Cohen, R. E.; Argon, A. S. *Macromolecules* Submitted for publication.

(29) Spiegelberg, S. H. PhD Thesis, MIT, 1993.

(30) Piorkowska, E.; Argon, A. S.; Cohen, R. E. *submitted for publication* **1993**,

(31) Miller, P.; Kramer, E. J. *J. Mater. Sci.* **1991**, *26*, 1459.

(32) Thomas, N. L.; Windle, A. H. *Polymer* **1982**, *23*, 529-542.

(33) Hui, C.; Wu, K.; Lasky, R. C.; Kramer, E. J. *J. Appl. Phys.* **1987**, *61*, 5137-5149.

(34) Hui, C.; Wu, K.; Lasky, R. C.; Kramer, E. J. *J. Appl. Phys.* **1987**, *61*, 5129-5136.

(35) Lustig, S. R.; Caruthers, J. M.; Peppeas, N. A. *Chemical Engineering Science* **1992**, *47*, 3037-3057.

(36) Lasky, R. C. Ph.D. Thesis, Cornell University, 1986.

(37) Lasky, R. C.; Kramer, E. J.; Hui, C. *Polymer* **1988**, *29*, 673-679.

(38) Kim, D. Ph. D. Thesis, Purdue University, 1992.

(39) Wu, J. C.; Peppas, N. A. *J. of Polym. Sci., Polym. Phys. Ed.* **1993**, *31*, 1503-1518.

(40) Kramer, E. J. *Adv. Polym. Sci.* **1983**, *52/3*, 1.

Chapter 2

Ion Beam Analysis

2.1 Introduction

The ion beam analysis techniques employed in this research are Rutherford Backscattering Spectroscopy (RBS) and Forward Recoil Spectroscopy (FRES). Both of the techniques determine relative populations of elements within approximately 0.5 μm of the surface of a sample as a function of depth . RBS is most sensitive to medium and heavy atomic mass elements, and FRES probes relative populations of deuterium and hydrogen. Diffusion experiments are performed with model systems in which the depth profile of a labeled component can be determined. The measurements were made at the Cambridge Accelerator for Materials Science located at Harvard University. The purpose of this chapter is to give the reader enough background information to be able to read RBS or FRES data, especially for the specific model systems described in later chapters. For a more general and comprehensive description of the techniques and their many applications, see Feldman[1] and Chu.[2]

RBS and FRES have been used to study diffusion in polymers only in the last decade, initially and most extensively by Kramer and coworkers at Cornell University. Historically, the high energy beam of alpha particles was thought to damage polymeric samples to such a degree that no useful information could be obtained. This is due to the fact that polymer samples are discolored and clearly degrade somewhat in a typical experiment. However, the data do not change with beam exposure during a normal collection period, and thus the degradation does not change the spatial distribution of elements in the sample. Green and Kramer measured tracer diffusion coefficients of perdeuterated polystyrenes in hydrogenated polystyrene matrices with FRES in different

molecular weight regimes to experimentally verify polymer diffusion theories such as the reptation model.[3-9] Composto and Kramer determined mutual diffusion coefficients with FRES in a system of compatible polymers to prove the so called fast theory of mutual diffusion.[10-12] Lasky, Gall, and Kramer measured volume fraction versus depth profiles of 1-iodo-n-alkanes in polystyrene with RBS to experimentally test and modify the Thomas and Windle[13] theory of case II diffusion.[14-18] The powerful and proven ability of RBS and FRES to measure diffusion profiles in polymers demonstrates their suitability to investigate the diffusion process which occurs in the toughening mechanism described in Chapter 1.

2.2 General Concepts

In both RBS and FRES a high energy beam of monoenergetic alpha particles, 4He+ or 4He++, in the range of 2 to 3 MeV, is directed towards the sample. A small fraction of the fast, light MeV He ions have essentially elastic collisions with nuclei in the sample. Chemical bonding energies, for example, are inconsequential, and the energy transfer in the two-body collisions can be calculated with the equations for the conservation of energy and momentum. This assumes that the close-impact collisions are governed by Coulomb repulsion between two positively charged nuclei. If the nucleus in the sample (target atom) is much heavier than the incident He ion, then a scattering event occurs where the incident ion retains most of the energy in the collision. These events are the basis for RBS. If the nucleus in the sample is less massive than the incident He ion, namely that of a hydrogen or deuterium atom, then most of the energy is transferred to the lighter nucleus in the recoil collision. These events are the basis for FRES. In both techniques, the identity of the target atom is determined by the energy of either the backscattered particle or the forward recoiled particle. Deviations from this simple picture of classical scattering in a central-force field occur at low and high energies[1], but do not concern us here. More detailed

calculations of the energy transfer in these elastic collisions are presented later in the chapter for specific RBS and FRES experiments.

The likelihood that a collision will occur is related to the concept of the scattering cross section, σ_S. If the number of incident particles is Q, the atomic density of the sample is N, and the thickness of a thin sample is t, then the number of detected particles in the experiment is $Q_D=\sigma_S QNt$. The simplest form of the scattering cross section as derived by Rutherford[19] is

$$\sigma_s(\theta)=\left(\frac{Z_1 Z_2 e^2}{4E}\right)^2 \bullet \frac{1}{\sin^4(\theta/2)} \qquad (2.1)$$

where θ is the angle between the incident beam and the scattered beam, Z_1 is the atomic number of the incident atom (2 for He), Z_2 is the atomic number of the target atom, e is charge of an electron, and E is the energy of the incident ion immediately prior to the collision. Geiger and Marsden[20] experimentally verified equation 2.1 in their classic experiments with thin metal foils. In both the RBS and FRES experiments, the geometry is fixed and only one value of θ is of interest. From equation. 2.1, σ_S is proportional to $(Z_2)^2$. RBS is therefore more sensitive to heavy atoms than light atoms because heavy atoms are much better scatterers. σ_S is also inversely proportional to the square of E. Thus the yield of scattered particles will increase rapidly with decreasing energy.[2] For 2 MeV He ions ($Z_1=2$) incident on silver ($Z_2=47$) with $\theta=180°$, σ_S is approximately 3×10^{-24} cm^2. A typical monolayer of solid contains approximately 10^{15} atoms/cm^2. Therefore, a 2 MeV He particle will on average traverse a large number of monolayers before being scattered from its path. Equation 2.1 is valid when the mass of the target atom, M_2, is much greater than the mass of the incident ion, M_1. A more general equation for σ_S is widely employed in quantitative analysis of RBS data, especially when lighter target atoms are involved.[2]

The majority of the incident ions traverse a significant amount of material before having a collision. In fact, ion implantation in thick samples is the primary process and the small probability of scattering or recoil events which are monitored in RBS or FRES is the secondary process. The high energy ions lose energy as they traverse material mainly through excitation and ionization processes in inelastic collisions with electrons. Some energy is also lost in small angle scattering events with nuclei, but this is negligible in comparison.[1] These discrete atomic scale events sum in such a way that the energy loss through a material can be considered a macroscopic property. Consider a simple experiment shown in figure 2.1 where incident particles with energy E are transmitted through a thin sample of thickness Δx.

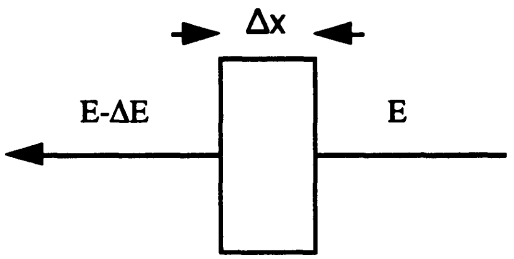

Figure 2.1 Energy loss through a sample of thickness Δx.

ΔE depends on the density and composition of the sample, and on E. The energy loss function, dE/dx (eV/nm), is given by[2]

$$\lim_{\Delta x \to 0} \frac{\Delta E}{\Delta x} = \frac{dE}{dx}(E). \qquad (2.2)$$

Typical values of dE/dx are 200 to 300 eV/nm for MeV He particles. Another way to express the energy loss function is with the stopping cross section ε (eV/atom/cm^2) which is defined as

$$\varepsilon = \left(\frac{1}{N}\right)\frac{dE}{dx} \tag{2.3}$$

where N (atoms/cm^3) is the atomic density. Values for dE/dx and/or ε have been measured over the years for most of the elements and many compounds for a wide range of energies.[21-23] When the stopping cross section has not been tabulated for a particular compound, A_mB_n, then ε can be approximated with Bragg's Rule such that[1]

$$\varepsilon^{A_mB_n} = m\varepsilon^A + n\varepsilon^B. \tag{2.4}$$

To calculate the loss function in equation 2.3, the molecular density of the compound, N_{comp}, is found as follows:

$$N_{comp}(molecules/cm^3) = \frac{\rho(g/cm^3)}{\left(mM_A(g/mol) + nM_B(g/mol)\right)} \bullet N_{AV} \tag{2.5}$$

where ρ is the density of the compound, M_i is the atomic weight of element i in the compound, and N_{AV} is the Avogadro constant. The energy loss is directly proportional to the path length of material traversed, and knowledge of material stopping cross sections allows a depth scale to be readily determined for the energy spectra of detected particles in RBS or FRES.

Statistical fluctuations are observed in the energy loss over a given path length in a homogeneous material because the total loss is the sum of many discrete events. If the distribution of energy E of the incident beam in figure 2.1 is a delta function, then the distribution of energies about E-ΔE emerging from the film is approximated by a gaussian function. This phenomenon is called energy straggling. As Δx increases, the energy straggling is approximated with a gaussian function with increasing full width at half maximum (FWHM). The total energy resolution of RBS or FRES, δE_1, is a combination

of the energy straggling , δE_s, and the detector resolution, δE_d. The detector resolution in turn depends on the finite detector acceptance angle, as well as an inherent energy broadening in the electronics equal to 15 to 20 keV FWHM. The two contributions are assumed to be independent and satisfy Poisson's statistics, and the total energy resolution, δE_1, is[1]

$$(\delta E_1)^2 = (\delta E_d)^2 + (\delta E_s)^2. \tag{2.6}$$

Later in the chapter, the relationships between total energy resolution and depth resolution are discussed for the specific RBS and FRES experiments. The way in which δE_1 manifests itself in RBS or FRES data is to broaden or smear the peaks. The mathematical description is that the data is a convolution of the actual distribution of elements in the sample with the gaussian function whose FWHM is δE_1.

2.3 Rutherford Backscattering Spectroscopy

The configuration of the RBS experiment is shown in figure 2.2. A 2.0 MeV beam of alpha particles (4He+) 2 mm in diameter is directed towards the sample such that the beam is normal to the sample surface. An annular surface barrier detector subtends a solid angle of 14.2×10^{-3} sr., and is placed at an angle such that the center of the annulus is 176° from the incident beam.

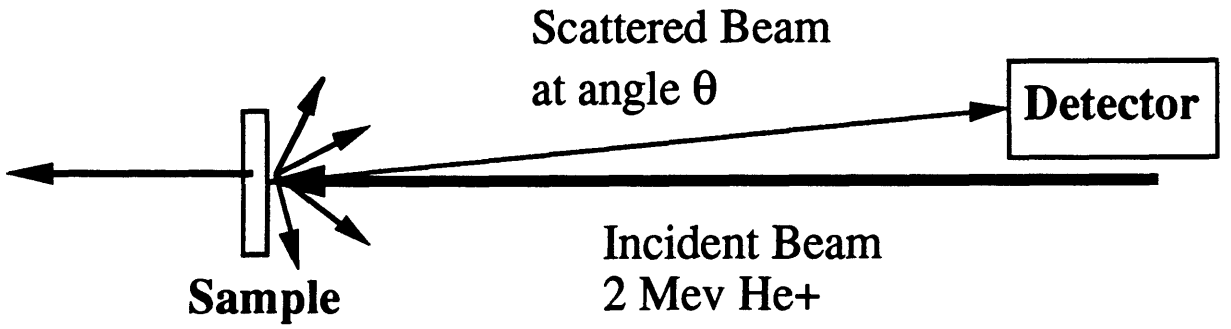

Figure 2.2 Configuration of RBS experiment, θ=176°.

The detector is connected to a multichannel analyzer and the particles which reach the detector are counted as a function of their energy. The energy range of interest, 0 to approximately 2 MeV, is divided into 1024 channels such that each channel spans approximately 2 keV.

The particles which reach the detector result from elastic collisions with nuclei in the sample as in the schematic below (figure 2.3).

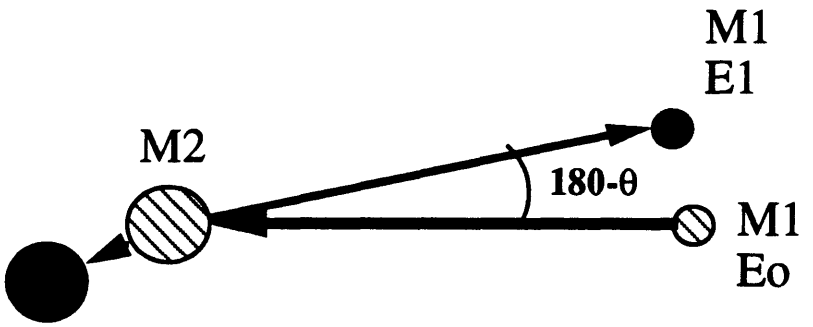

Figure 2.3 Schematic of elastic collision in RBS.

For M1<M2, the ratio of the energy of the particle after the collision, E_1, to the energy of the incident particle, E_0, is found by the conservation of kinetic energy and momentum to be[1]

$$\frac{E_1}{E_0} = K = \left[\frac{\left(M_2^2 - M_1^2 \sin^2\theta\right)^{0.5} + M_1 \cos\theta}{M_2 + M_1}\right]^2 . \qquad (2.7)$$

This ratio is called the kinematic factor, K. In the RBS experiment, M_1 (4He) and θ (176°) are fixed, and K is a function of the target atom mass, M_2. Table 2.1 contains the values[1] of K at θ=180° for the elements of interest in the RBS experiments presented in Chapter 5.

Table 2.1 Kinematic Factors at θ=180°.

Element	K
Au	0.922
P	0.595
O	0.36
N	0.309
C	0.25

The difference in energy transfer as a function of the mass of the target atom results in an energy spectrum of detected particles with peaks which are separated on an elemental basis.

To illustrate how depth profiling is accomplished in RBS, consider an elastic collision which occurs at a depth Δx and results in a backscattered particle that reaches the detector. The schematic of such an event is shown in figure 2.4.

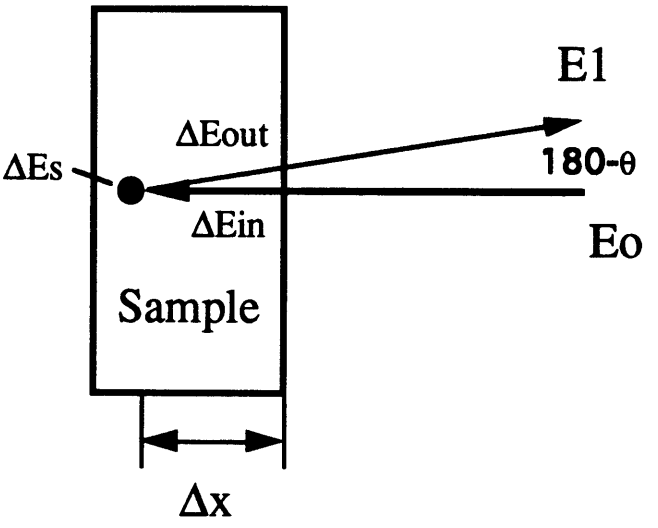

Figure 2.4 Schematic of energy losses for a collision at depth Δx in the sample.

The energy loss of the He ion on the inward path, ΔE_{in}, is

$$\Delta E_{in} \cong \Delta x \bullet \left(\frac{dE}{dX}\right)_{E_o}. \tag{2.8}$$

Remember that the loss function dE/dx depends on energy. In equation 2.8, dE/dx is shown to be a constant evaluated at E_0. This approximation is valid for small Δx or equivalently small ΔE_{in}. In actual data analysis, Δx is usually divided into a number of sections and ΔE_{in} is found iteratively. Immediately before the collision the incident particle will have an energy $E_{\Delta x}$, where

$$E_{\Delta x} = E_o - \Delta E_{in}. \tag{2.9}$$

The energy loss in the elastic collision, ΔE_s, is

$$\Delta E_s = (1-K)E_{\Delta x}. \tag{2.10}$$

Finally, the energy the particle loses as it exits the sample, ΔE_{out}, is

$$\Delta E_{out} \cong \frac{\Delta x}{\cos\theta} \bullet \left(\frac{dE}{dx}\right)_{E_1}. \tag{2.11}$$

Again, dE/dx is a function of energy but for small Δx can be assumed constant as indicated in equation 2.11. ΔE_{out} is usually found in an iterative calculation similar to that described for ΔE_{in}. Combining equations 2.8 through 2.11, the energy of the particle which reaches the detector, E_1, is

$$E_1 = E_o - \Delta E_{in} - \Delta E_s - \Delta E_{out}. \tag{2.12}$$

For a particular element in the sample, the energy of a backscattered particle is a unique function of depth. The energy scale is almost but not quite linear with depth. The loss function dE/dx increases as E decreases. The energy lost through a given thickness of material near the surface will be less than the energy lost through the same thickness of material deeper in the sample. In energy terms, a channel that spans 2 keV at energies for particles backscattered from a specific element near the surface corresponds to a thicker slice of sample than a channel that spans 2 keV at energies for backscattered particles for the same element deeper in the sample.

With this background information, a representative RBS experiment from the research described in Chapter 5 can now be explained in detail. Consider a typical sample in which a diffusant (RDP) with chemical formula $C_{30}O_8H_{24}P_2$ and density 1.3 g/cm^3 has diffused from the surface into a thick substrate material (Ultem™) with chemical formula $[C_{37}N_2O_6H_{24}]_n$ and density 1.27 g/cm^3. The sample is analyzed with RBS in the configuration shown in figure 2.2 with a total beam dose of 15 μC. The beam dose is measured by integrating the beam current over the data collection time. RBS data for the sample is shown in figure 2.5. The data is plotted in terms of channel number and counts.

In order to convert channel numbers to energy, a calibration standard is analyzed which consists of a ~2 Å discontinuous layer of gold on a silicon wafer. The channel number of particles backscattered from surface gold and surface silicon are found from the RBS data. The incident beam energy is 2 MeV, and the kinematic factor, K, is known for Au and Si for the geometry of the experiment. Application of equation 2.7 yields the energy of the backscattered particles from surface Au and Si. With these two points (channel $number_i$,$energy_i$, i=1,2), the linear relation for energy as a function of channel number is obtained. The energies of the backscattered particles are indicated in figure 2.5 on the top axis. Based on the values of K in table 2.1 and equation 2.7, backscattered particles from the surface of the sample from phosphorous, oxygen, nitrogen, and carbon atoms have energies of approximately 1.19, 0.72, 0.62, and 0.5 MeV respectively. Backscattered particles at energies between 1.19 and 0.72 MeV can only result from collisions with phosphorous atoms below the surface of the sample because there are no elements in the sample with atomic masses between those of P and O. The nitrogen peak appears as a shoulder on the oxygen peak because there is overlap of the oxygen and nitrogen peaks. Particles backscattered from nitrogen on the surface have the same energy (0.62 MeV) as particles backscattered from oxygen atoms at a given depth in the sample. The oxygen and nitrogen peaks both overlap with the carbon peak which appears at approximately 0.5 MeV.

The yields of backscattered particles from different elements, or in other words the heights of the peaks, are used to calculate the relative atomic concentrations of the elements at a particular depth. For example, if the height of the phosphorous peak from surface collisions is $H_{P,S}$, and the height of the oxygen peak from surface collisions is $H_{O,S}$, then the ratio of oxygen atomic density near the surface, $N_{O,S}$, to phosphorous atomic density near the surface, $N_{P,S}$, is

$$\frac{N_{O,S}}{N_{P,S}} \cong \frac{H_{O,S}}{H_{P,S}} \bullet \left.\frac{\sigma_{SP}}{\sigma_{SO}}\right|_{E_o} . \tag{2.13}$$

Since the diffusant (RDP) is the only species in the sample which contains phosphorous, the volume fraction of RDP near the surface of the sample can be calculated from equation 2.13 and the chemical formulae of the diffusant and the substrate material. In figure 2.5, $H_{O,S}$=347, $H_{P,S}$=101. The ratio of scattering cross sections,[2] σ_{SP}/σ_{SO}=3.866 evaluated at 1 MeV, and is assumed not to be significantly different at 2 MeV. $N_{O,S}/N_{P,S}$ is thus equal to 13.3. If N_S is total atomic density near the surface, and ø is the volume fraction of RDP, $C_{30}O_8H_{24}P_2$, in the substrate material, $C_{37}N_2O_6H_{24}$, then

$$\frac{N_{O,S}}{N_{P,S}} = \frac{N_S\phi\frac{6}{69} + N_S(1-\phi)\frac{8}{64}}{N_S\phi\frac{2}{64}} = 13.3 \tag{2.14}$$

Solving for ø in equation 2.14, we find that the volume fraction of RDP near the surface is 0.27.

The energy scale is converted to a depth scale with equations 2.8 through 2.12. The energy loss function for the substrate material is computed with Bragg's Rule and the known chemical formula and density of the of the substrate material (equations 2.4 and 2.5). 4He stopping cross sections for the elements from 0.4 to 4 MeV are tabulated in both Feldman[1] and Chu.[2] The loss function does not change significantly with diffusant volume fraction if the volume fraction is low, or if the loss function of the diffusant is nearly equal to the loss function of the substrate material as in this particular system. In figure 2.4, the depth of penetration of the diffusant (the back edge of the phosphorous peak) corresponds to a detected energy, E_1, equal to 1.09 MeV. Using the values ($(dE/dx)_{2\ MeV}$=184 eV/nm, $(dE/dx)_{1.1\ MeV}$=253 eV/nm, θ=176°, E_o=2 MeV, and

K=0.595, the penetration depth is calculated to be 251 nm. The procedure outlined above therefore shows that the relative heights of the peaks as a function of energy are readily converted to volume fraction RDP as a function of depth. In this sample, the volume fraction of diffusant is constant throughout the first 251 nm of the sample and a sharp front exists between the layer affected by diffusion and the rest of the substrate material.

The edges of the peaks in figure 2.5 are broadened by energy straggling and the energy resolution of the detector. The depth resolution, δt, of the RBS technique is related to the energy resolution by[1]

$$\delta t = \frac{\delta E_1}{K(dE/dx)_{in} + \frac{(dE/dx)_{out}}{|\cos\theta|}}. \qquad (2.15)$$

For $\delta E1$ equal to 15 to 20 keV FWHM, the depth resolution for phosphorous near the surface ($(dE/dx)_{2\ MeV}$=184 eV/nm, $(dE/dx)_{1.2\ MeV}$=245 eV/nm, θ=176°, and K=0.595) is 42 to 56 nm.

The solid line drawn through the data in figure 2.5 was calculated with RUMP, a software package developed at Cornell University for RBS data analysis. The program was purchased from Computer Graphics Service in Lansing, NY. RUMP performs rigorous iterative calculations based of the equations and concepts discussed above.[24,25] The software was used to analyze data in the following way. A distribution of species in the sample is proposed on the basis of a model in the SIM subroutine. Based on the densities and chemical formulae of the species, a spatial distribution of elements is calculated. The program produces 'simulated' RBS data for the proposed distribution of elements for the geometry and known energy resolution of the experiment. The 'simulated' data is compared to the experimental data in a subroutine called PERT. The distribution of species in the 'simulated' sample is changed iteratively until the best least squares fit of the 'simulated' data to the experimental data is obtained. For the example in figure 2.5, the

solid line is drawn for a 'simulated' sample which has a layer of material 257 nm thick which is 0.26 volume fraction RDP followed by an infinitely thick layer of substrate material. The parameters in the 'simulated' sample which were allowed to vary were the thickness of the mixed layer, and the volume fraction of the diffusant in that layer. Figures 6 and 7 show the sensitivity of the fits to the thickness of the 'simulated' mixed layer and the volume fraction RDP in the 'simulated' layer. The excellent agreement between the rough calculations discussed here and the rigorous iterative calculations performed with RUMP underscores the ability of RBS to yield quantitative results.

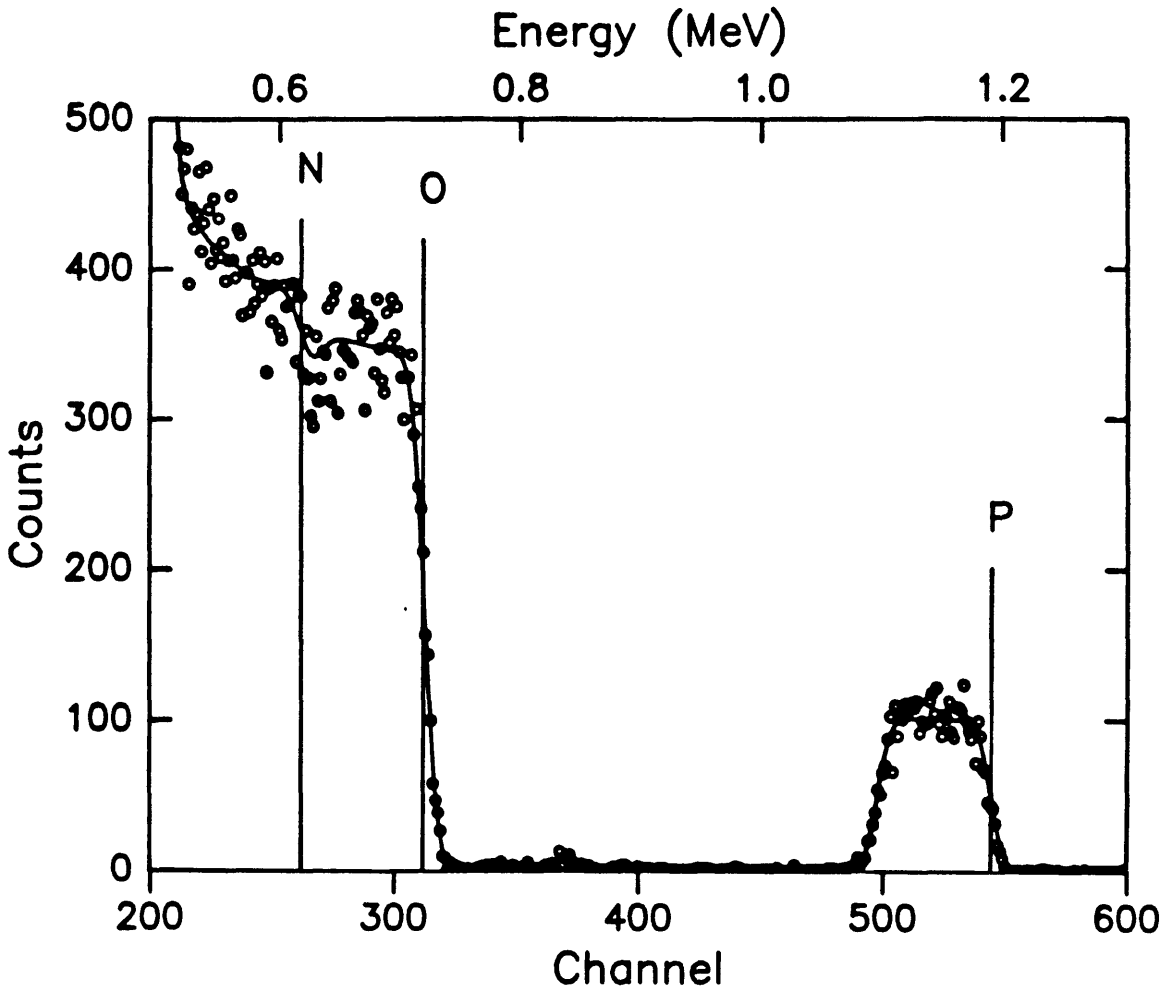

Figure 2.5 Typical RBS data for a sample in which RDP has diffused into Ultem™.

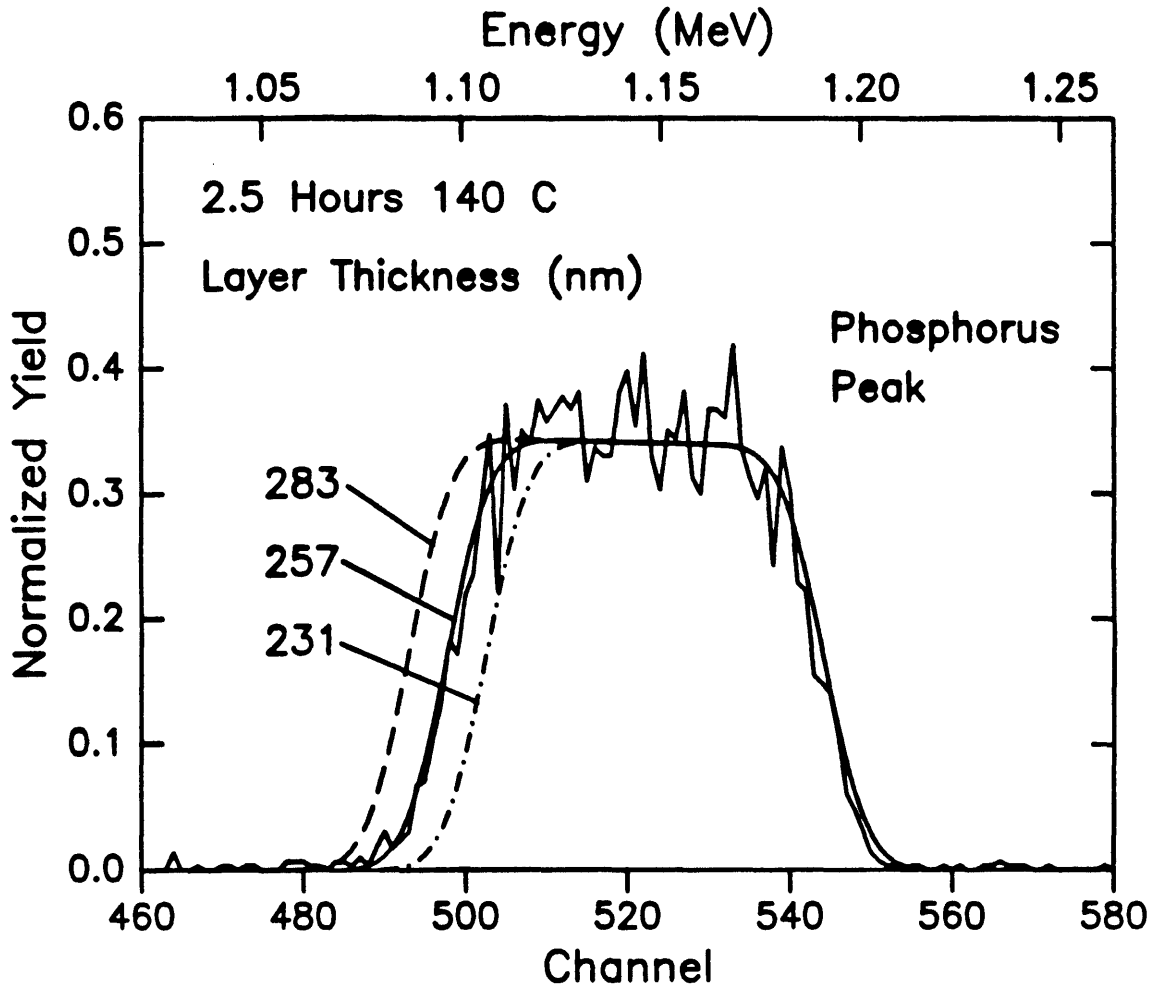

Figure 2.6 Sensitivity of RUMP fit to RBS data with variation of the 'simulated' penetration depth.

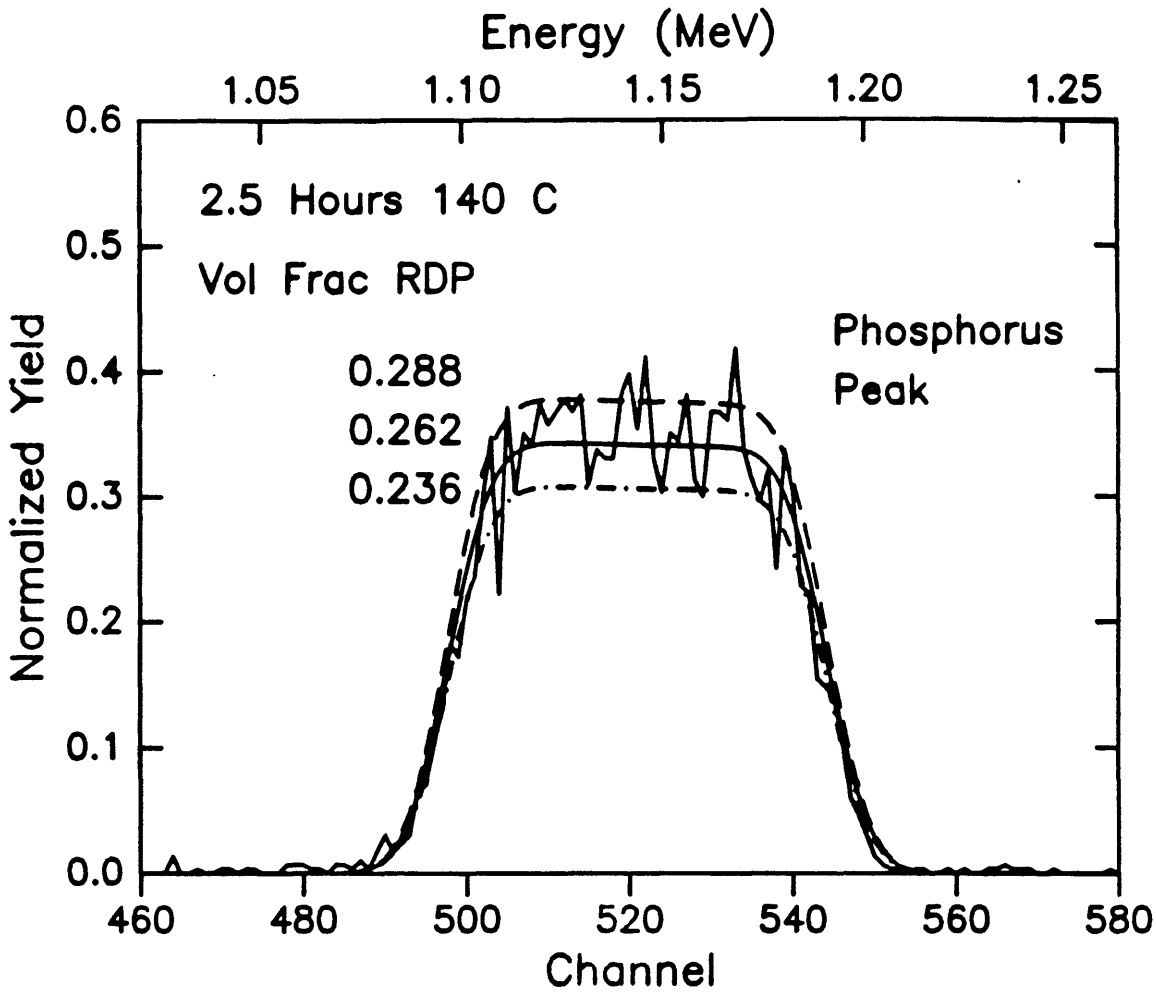

Figure 2.7 Sensitivity of RUMP fit to RBS data with variation of the 'simulated' RDP volume fraction .

2.4 Forward Recoil Spectroscopy

Many of the concepts and equations discussed in the context of RBS experiments also apply in FRES. RBS probes the volume fraction versus depth profile of medium to heavy atomic weight elements in the sample based on differences in energy and yield of backscattered particles. FRES probes the volume fraction versus depth profile of light elements, namely deuterium and hydrogen, based on differences in energy and yield of recoiled particles. Diffusion profiles are typically determined for a deuterated species which has penetrated into a hydrogenated matrix. The configuration of the experiment is shown in figure 2.8.[26,27]

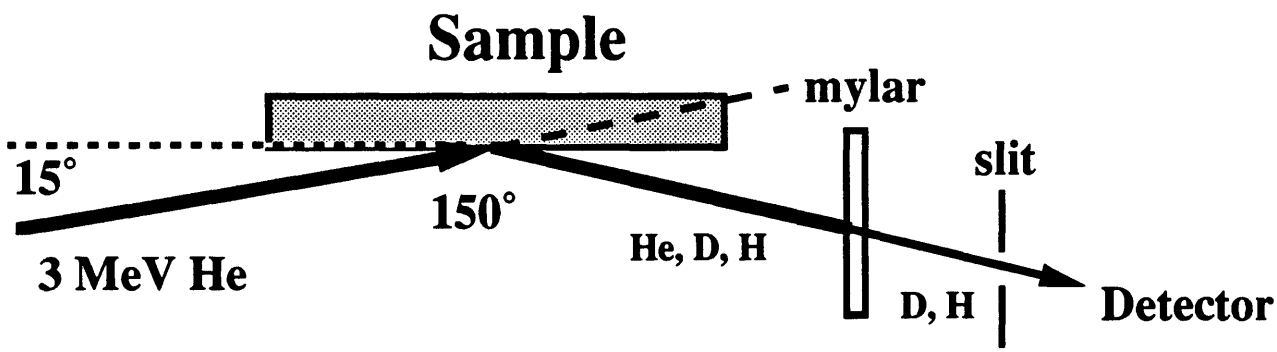

Figure 2.8 Configuration of the FRES experiment.

A 3 MeV beam of alpha particles ($4He^{++}$) is directed towards the sample at a glancing angle of 15°. Some of the incident ions are scattered from heavy elements in the sample, and another small percentage of the incident ions have collisions with deuterium and hydrogen nuclei in the sample which result in recoiled deuterium and hydrogen ions. Only the particles which are recoiled at an angle 150° from the incident beam are collected. The angle is defined by placing a slit in front of the detector which subtends a solid angle of 6.3×10^{-3} steridians. A large number of He ions are scattered from the sample at this

angle, too. A mylar foil is placed in front of the slit that is just thick enough to stop all of the scattered He ions, but will allow the smaller recoiled deuterium and hydrogen particles to pass through with some loss of energy. The thickness of the mylar is 11.5 μm. Deuterium and hydrogen particles are counted as a function of their energy with a detector, amplifier, and multi-channel analyzer. The energy range of interest, 0 to 2 MeV, is divided into 512 channels with approximately 4 keV/channel. Data is usually collected for a total beam dose 15 μC which is determined by integrating the beam current over the collection period.

A schematic of elastic collision which results in a recoiled particle at the angle of the detector is presented in figure 2.9.

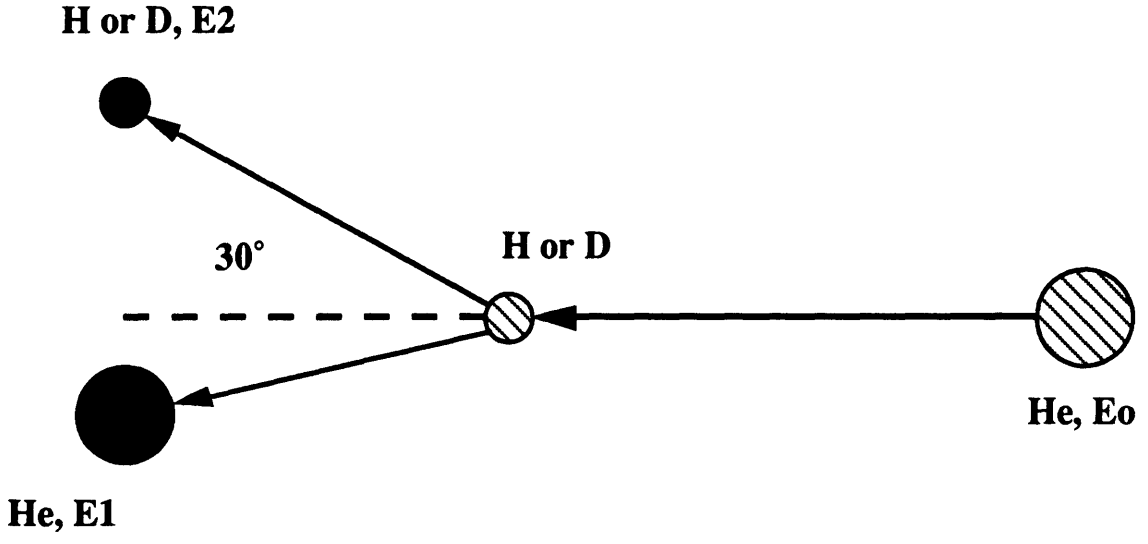

Figure 2.9 Elastic Recoil Collision in FRES.

The ratio of energies between the recoiled particle and the incident particle is[1]

$$\frac{E_2}{E_1} = K' = \frac{4M_{He}M_{H\,or\,D}}{\left(M_{He} + M_{H\,or\,D}\right)^2}\cos^2 30, \qquad (2.16)$$

where K' is the recoil kinematic factor whose value is 0.48 and 0.67 for hydrogen and deuterium respectively. This difference in energy transfer in the elastic collisions is the reason why the deuterium and hydrogen peaks are separated in the energy spectra of a FRES experiment.

Depth profiling in FRES is most easily illustrated with an example in which energy losses are calculated along each step of a recoil event which occurs at a depth Δx in the sample. A schematic of the process is shown in figure 2.10.

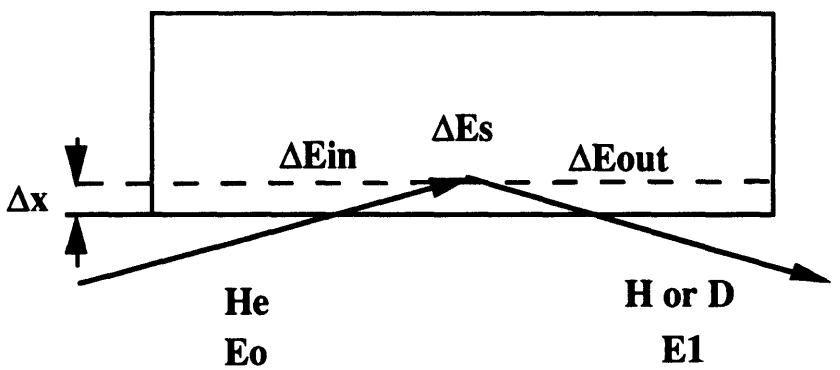

Figure 2.10 Schematic of recoil event in FRES.

The energy loss along the inward path of the incident ion, ΔE_{in}, is

$$\Delta E_{in} \cong \frac{\Delta x}{\sin(15^\circ)}\left(\frac{dE}{dx}\right)_{He,E_o}, \qquad (2.17)$$

where the energy loss function is indicated by a subscript to be for a He ion. The energy of the He ion immediately before collision, $E_{\Delta x}$, is

$$E_{\Delta x} = E_o - \Delta E_{in}. \tag{2.18}$$

The energy loss in the elastic collision, ΔE_s, is

$$\Delta E_s = (1 - K')E_{\Delta x}. \tag{2.19}$$

On the outward path, the energy loss is calculated for with the loss function of the recoiled particle such that

$$\Delta E_{out} \cong \frac{\Delta x}{\sin(15°)}\left(\frac{dE}{dx}\right)_{H\,or\,D,E_1}. \tag{2.20}$$

Recoiled particles also lose energy in the mylar foil, ΔE_{mylar}, and the detected energy, E_d, is found by combining equations 2.17 to 2.20 such that

$$E_d = E_o - \Delta E_{in} - \Delta E_s - \Delta E_{out} - \Delta E_{mylar}. \tag{2.21}$$

Thus the detected energy for a recoiled hydrogen or deuterium particle is a unique function of the depth in the sample from which the particle originated.

The yield of recoiled particles, either hydrogen or deuterium, is related to the scattering cross section of each element. In contrast to the RBS experiment where values of σ are tabulated and/or calculated, the ratio of deuterium and hydrogen cross sections in the geometry of the FRES experiment are determined experimentally. The ratio is assumed to remain constant in the energy range of interest. Data is collected for a calibration sample which is 210 nm thick and is a homogeneous blend of 0.277 volume fraction perdeuterated polystyrene and 0.723 volume fraction hydrogenated polystyrene (figure 2.11). The ratio of scattering cross sections is found using equation 2.13 and the known ratio of atomic

densities in the sample. Since the ratio of cross sections is assumed constant in this energy range, the integrated areas under the peaks are used instead of the peak heights in equation 2.13 for improved statistical accuracy . In this sample the ratio is 1.48. The cross sections are strong functions of the geometry of the experiment and this calibration standard is run and analyzed every time that FRES experiments are performed. The calibration standard is also used to relate channel number to energy. Knowledge of the recoil kinematic factors, the incident ion energy, and the thickness of the mylar foil allows the calculation of the energies of deuterium and hydrogen recoiled from the surface of the sample. The channel numbers which correspond to these energies is found from the experimental data. A linear relationship is thus determined for energy as a function of channel number, and the energies are indicated on the top axis of figure 2.11.

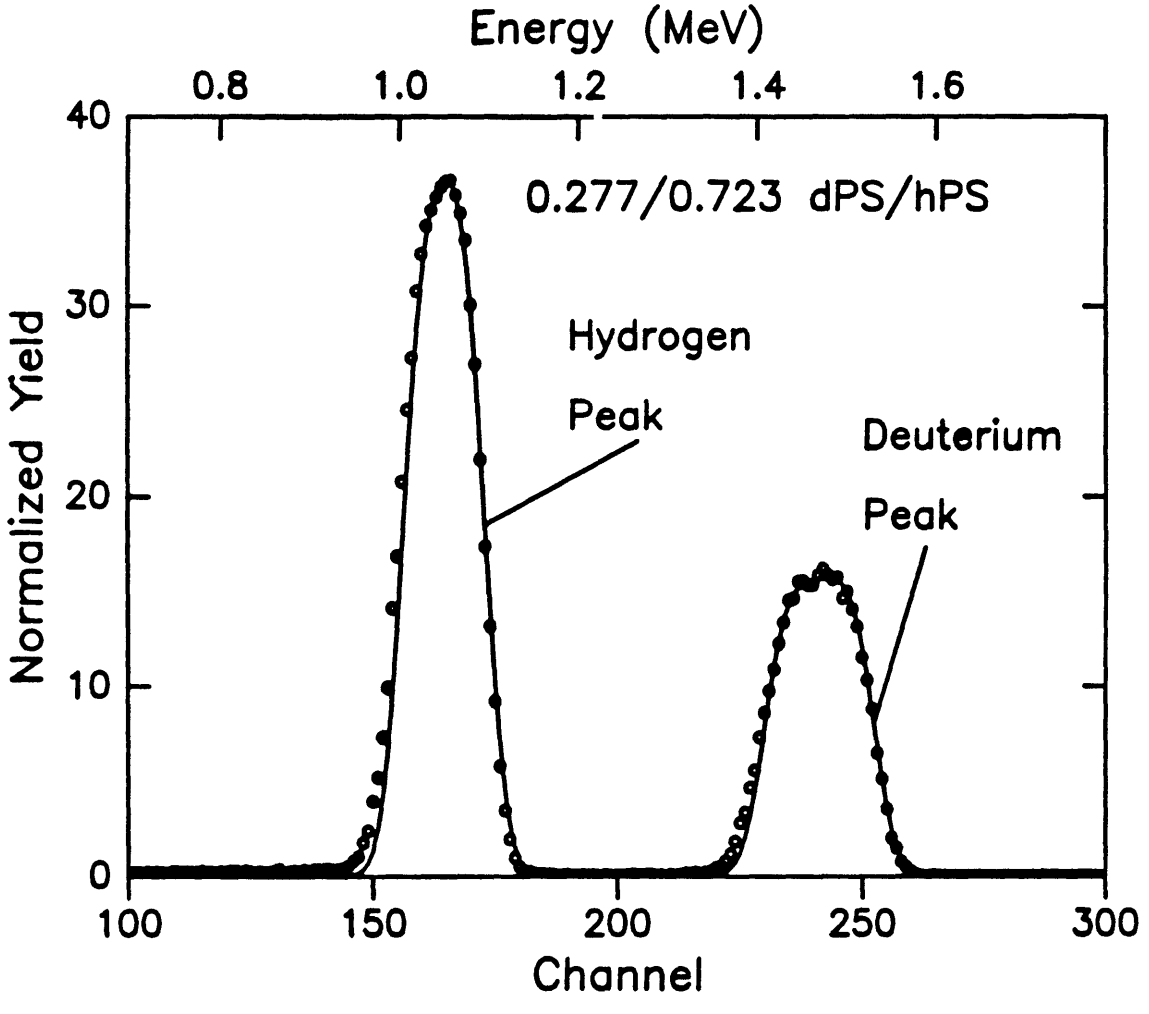

Figure 2.11 FRES data from a homogeneous blend of 0.277/0.723 dPS/hPS which is 210 nm thick.

Diffusion coefficients are determined for a deuterated species penetrating into hydrogenated matrix from the volume fraction versus depth profile of deuterium obtained with Forward Recoil Spectroscopy. The concepts and principles required to read FRES data are the same as RBS data. In Chapters 3 and 4, tracer diffusion measurements of perdeuterated polybutadiene in polystyrene are described in detail. The energy difference between the deuterium peak and the hydrogen peak corresponds to a depth in PS of approximately 600 nm. Thus the volume fraction of the deuterated species in the sample can be analyzed without overlap of the two peaks over this distance. In reasonable time scale experiments, penetration depths of this order allow diffusion coefficients to be determined between 10^{-12} to 10^{-16} cm^2/s.

The energy resolution of the FRES experiment with this geometry and a 3 MeV beam is approximately 45 keV. This corresponds to a depth resolution of approximately 80 nm. Energy straggling through the mylar foil is the limiting factor in the resolution. However, there are many other important factors that became apparent during the extension of the capabilities of the Cambridge Accelerator for Materials Science to perform FRES. For example, the intersection of the circular incident beam of alpha particles with the sample surface at the glancing angle is an ellipse. If the incident beam is 2 mm in diameter (as in the RBS experiment), then the ellipse becomes elongated to such an extent that angular differences between the beam and the detector over the elliptical irradiated area of sample dominate and adversely affect the energy resolution. For this reason, a 1 mm beam was used at the expense of reducing the beam current by a factor of four, and increasing the data collection time accordingly. Normally a 1 mm x 1 cm vertical slit is placed in front of the detector to define the acceptance angle. In the geometry of the RBS experiment, the resulting difference in scattering angle between particles passing through the middle of the slit compared to the ends of the slit are insignificant. At the glancing angle geometry of the FRES experiment, significant distribution of acceptance angles results from the use of a vertical slit. The strong geometric dependence of the recoil kinematic factor (equation 2.14)

and the scattering cross sections require that the acceptance angle be better defined. If the subtended solid angle is reduced, for example, by using a 1 mm x 0.5 cm slit, then fewer counts are recorded for the same beam dose and the statistical significance of the data is adversely affected. The solution is to place a curved slit in front of the detector. If the slit is a distance q from the center of the beam spot on the sample surface, then the curvature of the slit should follow the function q•tan(30°). The width of the slit defined an acceptance angle of 30° ± 0.5°.

One of the most difficult problems in setting up the FRES experiment was the precise and reproducible determination of the angle between the beam and sample, and the angle between the beam and the detector. Again, knowledge of the angles is critical because of the strong dependence of K' on the geometry of the experiment. A sample holder was designed which held samples at a fixed angle to the sample chamber via pins in an stationary flange. A laser was installed which pointed directly down the collimated path of the beam. With this tool, the beam position could be verified in relation to the sample holder so that a 15° between the beam and the sample surface was assured. The laser was reflected on itself from a goniometer to find the position where the sample was normal to the beam. The goniometer could then be rotated until the reflected laser light passed through the slit to illuminate the detector. By monitoring the detector leakage current at a low bias voltage as a function of the angle of the goniometer, the angle between the beam and the detector was found within ± 0.05°.

2.5 References for Chapter 2

(1) Feldman, L. C.; Mayer, J. W. *Fundamentals of Surface and Thin Film Analysis*; Elsevier Science Publishing Co., Inc.: New York, New York, 1986.

(2) Chu, W. K.; Mayer, J. W.; Nicolet, M. A. *Backscattering Spectroscopy*; Academic Press: New York, NY, 1978.

(3) Green, P. F.; Mills, P. J.; Palmstrøm, C. J.; Mayer, J. W.; Kramer, E. J. *Phys. Rev. Lett.* **1984**, *53*, 2145-2148.

(4) Green, P. F. Ph D Thesis, Cornell University, 1985.

(5) Green, P. J.; Mills, P. J.; Kramer, E. J. *Polymer* **1986**, *27*, 1063-1066.

(6) Green, P. F.; Kramer, E. J. *Macromolecules* **1986**, *19*, 1108-114.

(7) Green, P. F.; Kramer, E. J. *J. Mat. Res.* **1986**, *1*, 202-205.

(8) Green, P. F. *Macromolecules* **1991**, *24*, 3373-3376.

(9) Green, P. F.; Adolf, D. B.; Gilliom, L. R. *Macromolecules* **1991**, *24*, 3373-3382.

(10) Composto, R. J.; Mayer, J. W.; Kramer, E. J.; White, D. M. *Phys. Rev. Lett.* **1986**, *57*, 1312.

(11) Composto, R. J. PH D Thesis, Cornell University, 1987.

(12) Composto, R. J.; Kramer, E. J.; White, D. M. *Macromolecules* **1988**, *21*, 2580.

(13) Thomas, N. L.; Windle, A. H. *Polymer* **1982**, *23*, 529-542.

(14) Gall, T. P.; Lasky, R. C.; Kramer, E. J. *Polymer* **1990**, *31*, 1491-1499.

(15) Hui, C.; Wu, K.; Lasky, R. C.; Kramer, E. J. *J. Appl. Phys.* **1987**, *61*, 5137-5149.

(16) Hui, C.; Wu, K.; Lasky, R. C.; Kramer, E. J. *J. Appl. Phys.* **1987**, *61*, 5129-5136.

(17) Lasky, R. C. Ph.D. Thesis, Cornell University, 1986.

(18) Lasky, R. C.; Kramer, E. J.; Hui, C. *Polymer* **1988**, *29*, 673-679.

(19) Rutherford, E. *Phil. Mag.* **1911**, *21*, 669.

(20) Geiger, H.; Marsden, E. *Phil. Mag.* **1913**, *25*, 606.

(21) Ziegler, J. F. *Helium Stopping Powers and Ranges in All Elements*; Pergamon Press: New York, 1977.

(22) Ziegler, J. F.; Chu, W. K. *At. Nucl. Data Tables* **1974**, *13*, 463-489.

(23) Anderson, H. H.; Ziegler, J. F. *Hydrogen Stopping Powers and Ranges in All Elements*; Pergamon: Oxford, 1977.

(24) Doolittle, L. R. *Nucl. Inst. Meth.* **1985**, *B9*, 344.

(25) Doolittle, L. R. *Nucl. Inst. Meth.* **1986**, *B15*, 227.

(26) Turos, A.; Meyer, O. *Nucl. Instr. and Meth.* **1984**, *B4*, 92-97.

(27) Mills, P. J.; Green, P. F.; Palmstrøm, C. J.; Mayer, J. W.; Kramer, E. J. *Appl. Phys. Lett.* **1984**, *45*, 957-959.

Chapter 3

Solubility and Diffusion of Polybutadiene in Polystyrene at Elevated Temperatures

3.1 Abstract

The thermally - induced diffusion of low molecular weight perdeuterated polybutadiene (dPB) in polystyrene (PS) was measured with Forward Recoil Spectroscopy (FRES). Diffusion coefficients were determined for 3000 g/mole dPB penetrating into a 350 000 g/mole PS matrix in the temperature range of 97 to 115 °C. The diffusion coefficients vary from 10^{-15} to 10^{-12} cm^2/s. The apparent activation energy is 99 kcal/mole.

Solubility limits for dPB in PS at temperatures ranging from 105 °C to 160 °C were also determined with FRES. The results were used to construct a portion of the binodal curve for this polymer system. The derived value of the Flory - Huggins interaction parameter, χ, is 0.055 and 0.048 at 105 °C and 160 °C respectively.

3.2 Introduction

A central and limiting process in a recently reported toughening mechanism in blends of polystyrene (PS) and polybutadiene (PB)[1,2] is the stress enhanced solubility and subsequent diffusion of the low molecular weight PB rubber into the glassy PS. The diffusion is restricted to regions in the immediate neighborhood of advancing crazes, where the local deformation - induced stress fields are favorable for enhancing the PB solubility. The PB locally plasticizes the material drawn into crazes, and the crazes advance more rapidly and at lower applied stresses in the blends than in pure PS. Based

on results from craze velocity measurements[3] in blends of PS and 3000 g/mole PB and a characteristic length for diffusion equal to the diameter of a craze fibril[2], the estimated diffusion coefficient for the PB is 3 x 10^{-12} cm^2/s. Information concerning the rate of polymer - polymer interdiffusion for PB/PS is necessary to probe the limitations of the proposed toughening mechanism.

Blends of polybutadiene and polystyrene exhibit upper critical solution temperatures. The segmental interaction parameter for this system is large enough and positive such that blends of PB and PS phase separate into virtually pure components at temperatures below 200 °C. Hence this polymer pair is generally termed immiscible. Previous polymer - polymer interdiffusion studies have not included this type of system. In our experiments, the molecular weight of the PB is low enough that a miscibility of approximately 3 volume percent in PS can be achieved near 120 °C. Conversely, the high molecular weight PS is completely immiscible in the PB. Polymer - polymer interdiffusion across an interface between pure low molecular weight PB and pure high molecular weight PS is essentially penetration of the PB into the PS across a stationary interface. The temperature dependence of this diffusion provides a means to probe the changing properties of the PS matrix.

Forward Recoil Spectroscopy has been discussed extensively in the recent literature as a means for determining diffusion coefficients for polymer - polymer systems. Some of the research has centered on self - diffusion measurements to probe mechanisms of diffusion in various regimes of molecular weight[4-8]. Other studies have examined mutual diffusion in miscible polymer systems[9-13]. FRES has also been used to measure solubility limits of deuterated polystyrene in brominated polystyrene, a partially miscible polymer system[14]. This technique is capable of measuring atomic concentrations on the order of 0.1 % and diffusion coefficients in the range of 10^{-12} to 10^{-16} cm^2/s. FRES is expected to be a viable method to measure solubilites and determine diffusion coefficients in our low molecular weight PB/PS system.

3.3 Experimental

Polymers

The polystyrene used in this study was supplied by Polysar (M_W = 350 000 g/mole, M_n = 170 000 g/mole). Perdeuterated polybutadiene (dPB) was synthesized in our laboratory via homogeneous anionic polymerization in benzene using n-butyl lithium initiator. The perdeuterated butadiene was obtained from Cambridge Isotope Laboratories and purified as described by Cheng[15]. M_W was determined to be 3000 g/mole and the polydispersity 1.04 based on size exclusion chromatography and an in - line viscometer. Deuterium NMR experiments show that the microstructure of the dPB is 12 % 1,2, and 88 % 1,4 cis and trans addition. With the exception of the n-butyl and proton end groups, the polymer is greater than 97 % deuterated based on proton NMR results.

Sample Preparation

All samples were prepared in a similar manner. A piece of silicon wafer was washed in distilled water to remove any dust particles, rinsed with high purity ethanol, and dried by spinning at 3000 rpm in air. A polystyrene layer was deposited on the wafer in a spin coating process with solutions of PS in toluene. The samples were annealed in a vacuum oven for at least 8 hours at approximately 100 °C to remove any residual solvent. The objective was to create a bilayer sample consisting of dPB on top of the PS. We were unable to form a coherent film with the low molecular weight dPB. Instead heterogeneous films of randomly mixed dPB and PS were made by spin coating solutions of blends of dPB and PS in toluene in which the PS accounted for 30 to 40 percent of the total polymer by weight. Thus, the dPB/PS blend layer was spun onto a glass slide, floated onto the surface of a water bath, and picked up with a PS - coated wafer. The glass slides were cleaned in a 50 % aqueous solution of hydrofluoric acid,

rinsed in distilled water, rinsed with ethanol, and dried by spinning at 3000 rpm in air. Each sample was dried in a vessel with a nitrogen purge at room temperature for at least 12 hours. Care was taken in each preparation step to minimize the exposure of the dPB to oxygen, UV light, and heat to reduce the possibility of cross-linking.

The samples were heated in a thin-walled copper chamber after it was evacuated and back filled with pure argon and maintained at a constant pressure of 1.2 atmospheres. In each experiment, the sample and chamber were immersed in an oil bath at a given temperature for a specific period of time. In this way the sample temperature reached 90 % of its final steady state value after 20 seconds and 99 % after 40 seconds. The temperature of the bath itself dropped approximately 0.5 °C immediately after insertion of the sample chamber and regained a steady state value ($\pm$ 0.1 °C) after approximately 2 minutes. The error in reported temperature is greater for those samples which were treated for short time periods. The minimum time period used in these experiments was 5 minutes.

Forward Recoil Spectroscopy

All of the samples were analyzed with Forward Recoil Spectroscopy (FRES) at the Cambridge Accelerator for Materials Science at Harvard University to determine concentration versus depth profiles of dPB in PS. This technique allows direct measurement of the diffusion profile of the deuterated species in the hydrogenated matrix for penetration depths in the range of 500 nm. Given this depth and a 5 minute minimum experimental time period for accurate temperature control, the largest diffusion coefficient that can be measured is approximately 10^{-12} cm^2/s.

The configuration of the FRES experiment is shown in figure 3.1. The sample is irradiated with a 1 mm diameter beam of 3 M eV alpha particles ($4He^{++}$) at a glancing angle of 15°. The beam dose for all samples was 15 μC. The slit defines the angle of detection to be 150° $\pm$ 0.5° from the incident beam and subtends a solid angle of 6.3×10^{-3} steridians. The mylar foil placed in front of the detector is 11.5 μm in

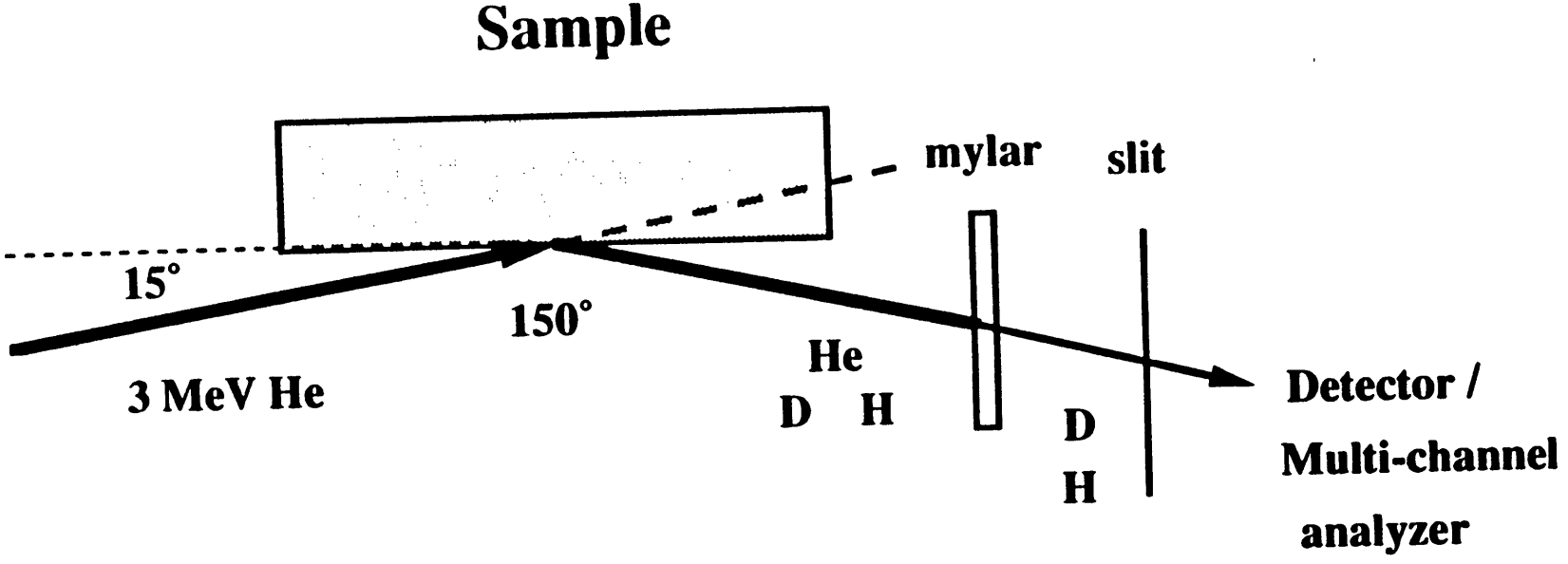

Figure 3.1 Configuration of FRES experiment.

thickness. The energy resolution in the experiments was 45 k eV. Details of this technique are described elsewhere[4, 8, 16].

3.4 Results

Some of the samples were held at temperatures ranging from 105 °C to 160 °C for time periods of 15 hours to 1 hour. The dPB/PS blend layer in these samples was approximately 80 nm thick and was 67 % dPB and 33 % PS by weight, and the pure PS substrate layer was approximately 490 nm thick. A schematic of a typical sample for the solubility experiments is shown in figure 3.2. The amount of dPB present is more than enough to saturate the PS substrate layer in the present experiment in the temperature range studied, and the thickness of the PS layer allows the determination of the composition at the polymer silicon interface. Figures 3.3 and 3.4 show the FRES data for samples held for 1 hour at 159.6 °C and 119.9 °C. The dPB has diffused into the PS layer and the relatively flat concentration profiles indicate that the samples have approached equilibrium. More deuterium is recoiled at energies between about 1.2 and 1.45 M eV in the sample held at the higher temperature. The sample held at 159.6 °C thus has a higher concentration of dPB in the PS layer than the sample held at 119.9 °C. The use of these data to determine the solubility of dPB in PS as a function of temperature is explained in the Discussion section.

Other samples were held at temperatures ranging from 115.2 °C to 96.5 °C for time periods of 5 to 2010 minutes. In these experiments the dPB/PS blend layer was approximately 35 nm thick and was 59 % dPB and 41 % PS by weight. The pure PS substrate layer was approximately 4 μm (4000 nm) thick. A schematic of a typical sample in the diffusion experiments is shown in figure 3.5. Diffusion times were chosen to obtain concentration profiles which would go to zero in penetration depths of order 200 nm. The temperature and time period for each experiment is tabulated in Table 3.1.

Table 3.1 - Experimental Diffusion Times

Temperature (°C)	Diffusion Time (minutes)
115.2	5
113.4	5
111.5	5
109.7	8
109.4	10
107.9	10
107.4	15
105.9	20
105.4	20
103.4	75
101.5	240
100.3	420
99.6	511
98.7	767
96.5	2010

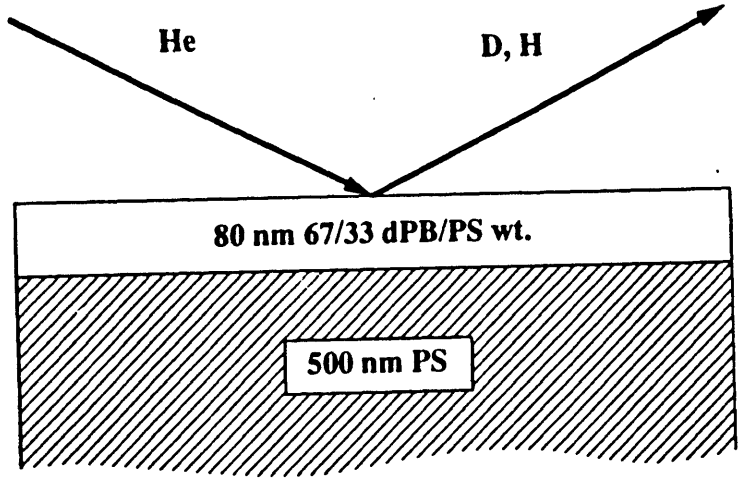

Figure 3.2 Schematic of a typical sample in the solubility experiments.

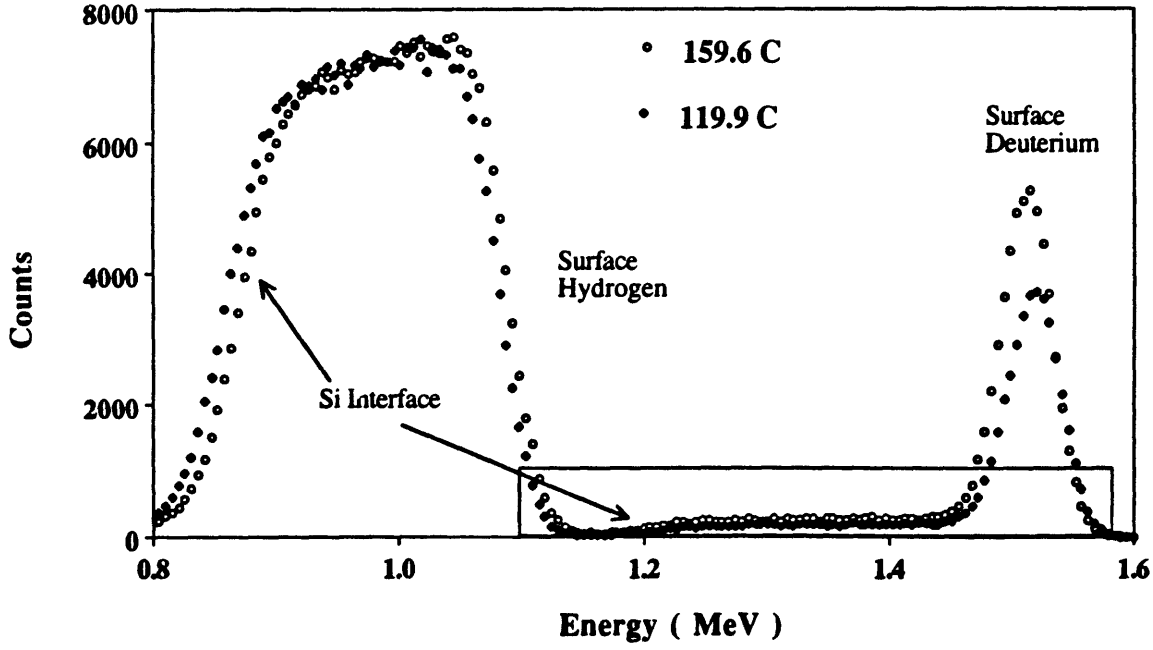

Figure 3.3 Overview of FRES data for samples held for 1 hour at 159.6 and 119.9 °C.

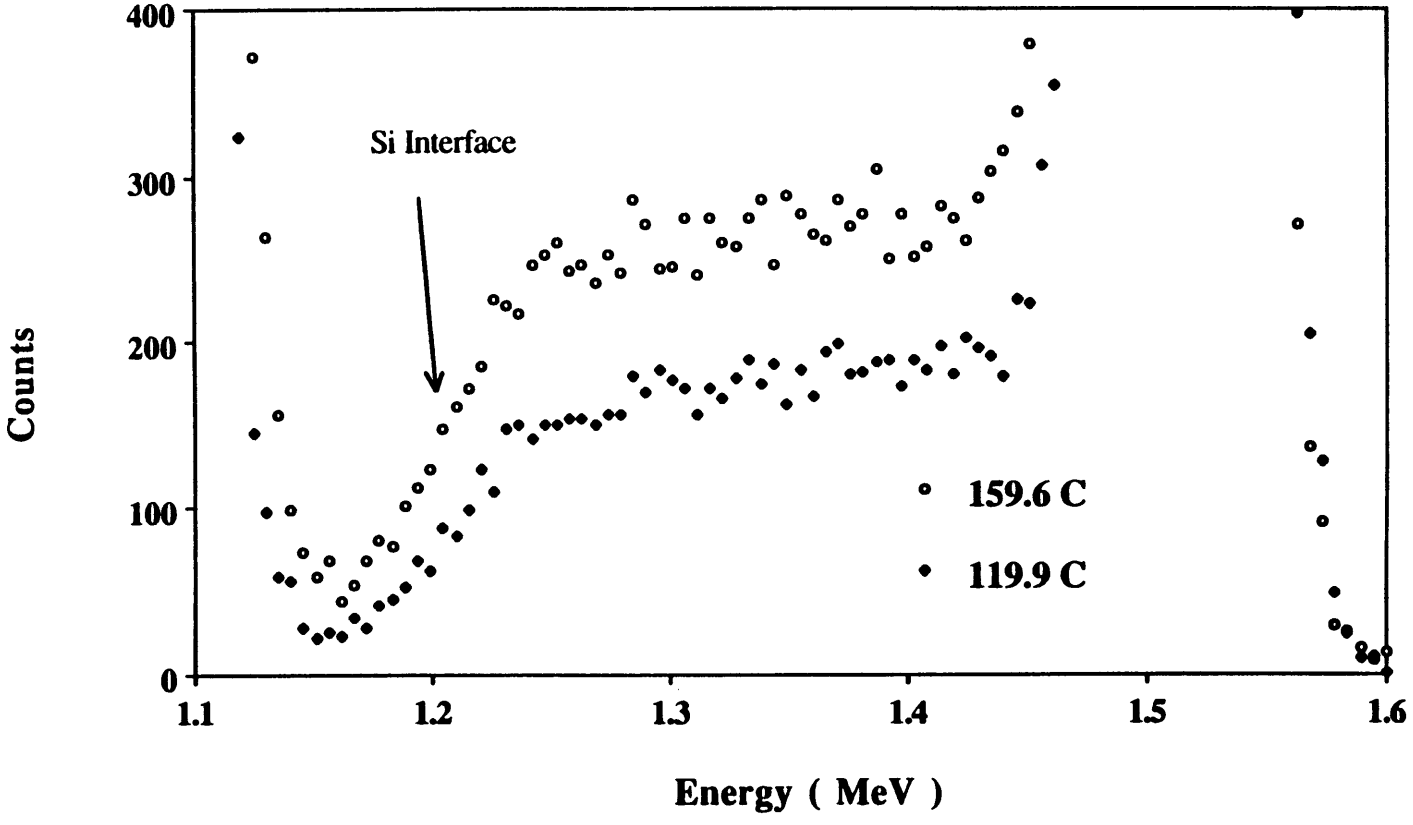

Figure 3.4 Expanded view of the deuterium profiles for samples held for 1 hour at 159.6 and 119.9 °C.

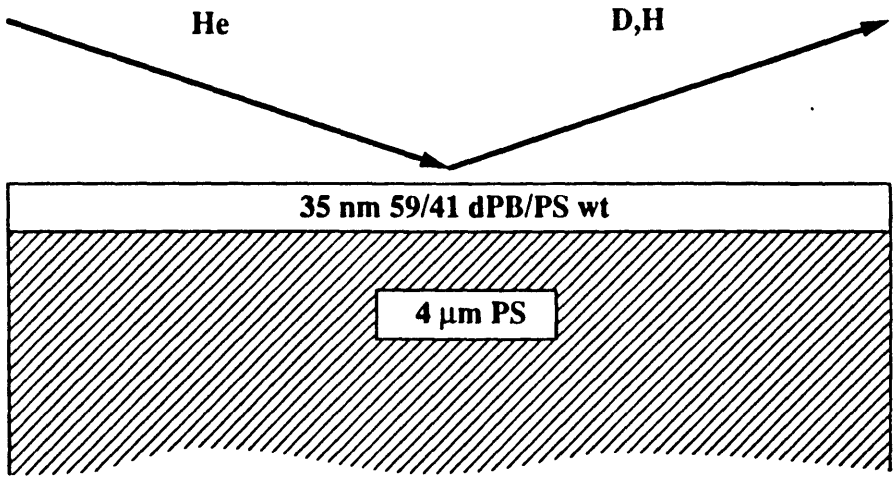

Figure 3.5 Schematic of a typical sample in the diffusion experiments.

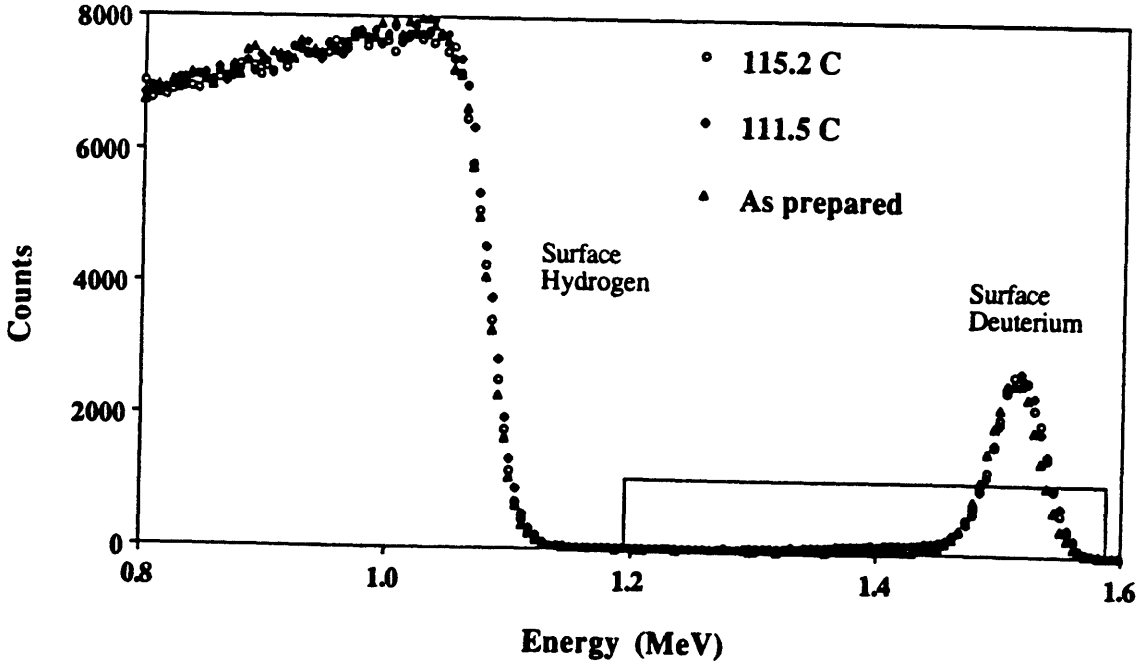

Figure 3.6 Overview of FRES data for samples held for 5 min at 115.2 and 111.5 °C and an unheated sample.

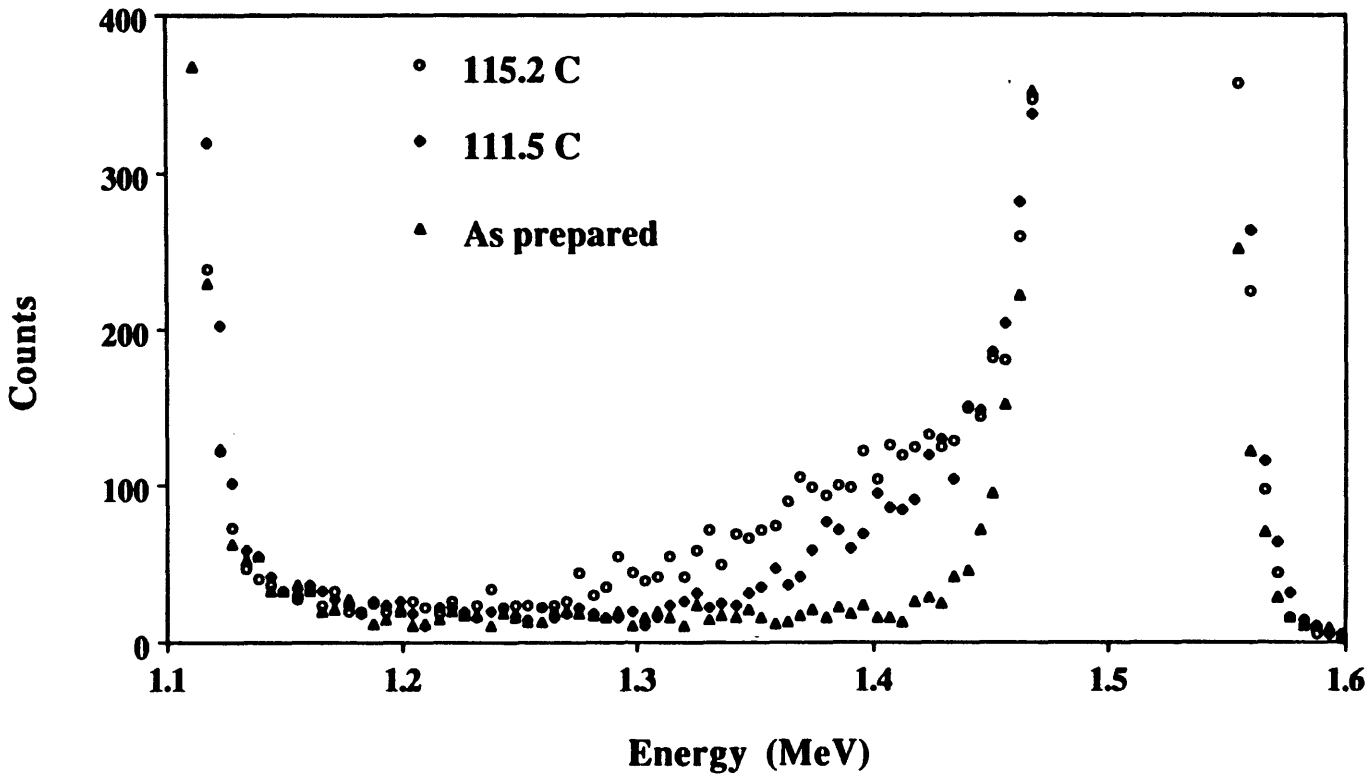

Figure 3.7 Expanded view of the deuterium profiles for samples held for 5 min at 115.2 and 111.5 °C and an unheated sample.

Figures 3.6 and 3.7 show the profiles obtained for samples held for 5 minutes at 115.2 °C and 111.5 °C, respectively, compared to an unheated sample. From figure 3.6 we can conclude that the sample preparation procedure is very reproducible. The identical deuterium peaks in the FRES data at approximately 1.5 M eV show that all of the samples have an equal amount of dPB in the thin, initially blended surface layer. Figure 3.7 shows clearly that there is penetration of dPB into the PS in both annealed samples, and that the penetration at 115.2 °C is markedly deeper than at 111.5 °C for the same diffusion time period. All three samples exhibit a consistent non-zero value for the counts of deuterium in the range of energy between the deuterium and hydrogen peaks. These counts are attributed to events when two particles of lower energy reach the detector at the same time and are counted as one single higher energy particle. This background is termed pulse pile-up. A model to extract diffusion coefficients from these data is developed in the following section.

3.5 Discussion

Solubility limits and diffusion coefficients were determined from the FRES results with the aid of the RUMP software package developed for Rutherford Backscattering and FRES data analysis at Cornell University.[17, 18] The software was purchased from Computer Graphics Service in Lansing, New York. This program performs complex iterative simulations of FRES data given the specific parameters of the experimental configuration and the physical and chemical characteristics of the species in the sample description. RUMP calculates simulations in terms of counts and energy. These axes are readily transformed to concentration and depth and some of the data is presented in this form.

Figures 3.8 and 3.9 show the FRES data and the simulation of the sample held for 1 hour at 139.9 °C. A schematic of the sample is shown in figure 3.2. A calibration

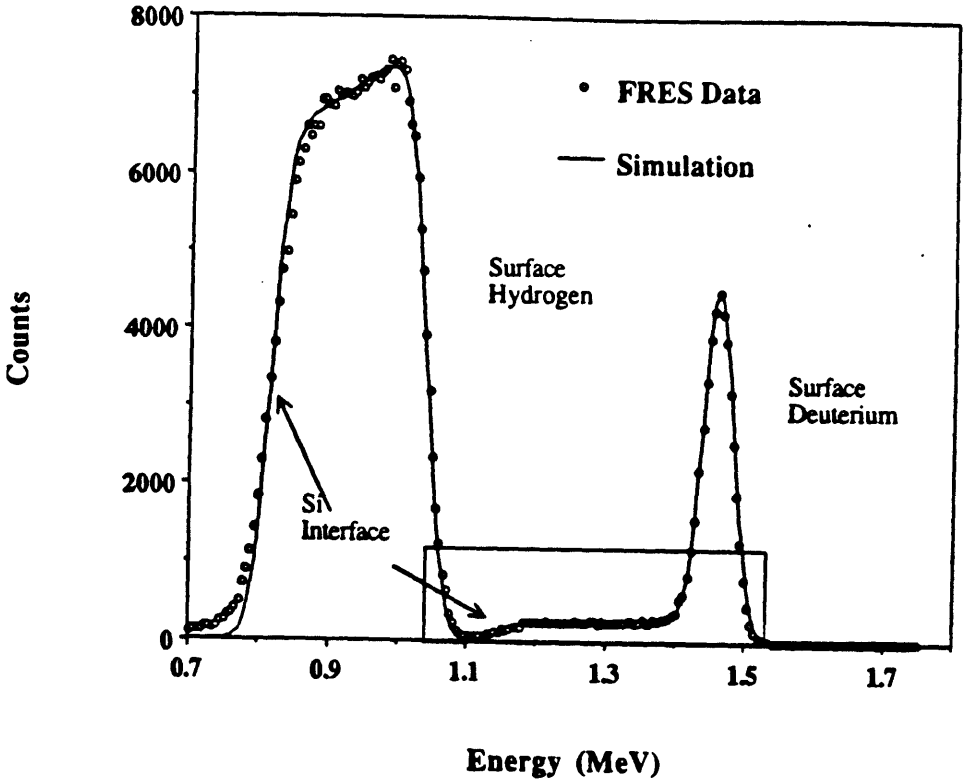

Figure 3.8 Overview of FRES data and simulation for a sample held for 1 hour at 139.9 °C.

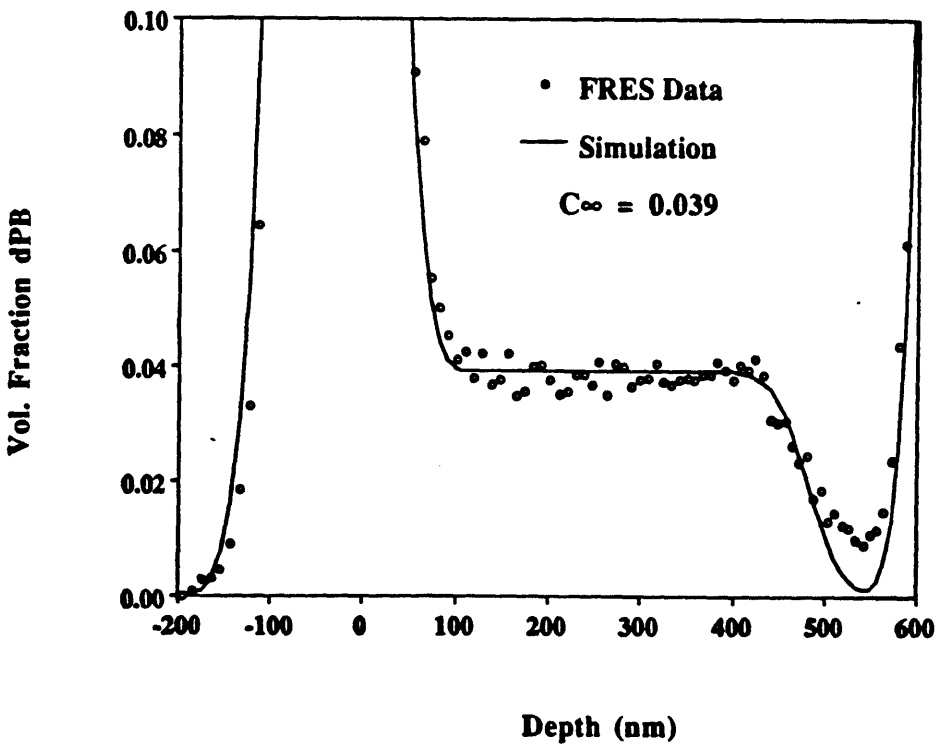

Figure 3.9 Expanded view of the deuterium profile and simulation for a sample held for 1 hour at 139.9 °C plotted in terms of volume fraction versus depth.

sample of known composition is used to establish the relative cross sections of deuterium and hydrogen. The height of the hydrogen peak is used to normalize the counts or concentration axis for small errors in measured beam dose from sample to sample. The concentration of dPB in the PS is modeled as constant throughout the layer. We assume that the polymer system has reached an equilibrium, phase - separated state in which one phase consists of a homogeneous mixture of PS saturated with a small volume fraction of dPB, and the other phase is pure dPB. The best fit of this model to the experimental data in figure 3.9 is achieved with a solubility of 0.039 volume fraction dPB in PS at 139.9 °C.

In similar experiments, the solubility limits were found at 9 temperatures ranging from 105 °C to 160 °C. The measured solubilites ranged from 0.027 to 0.043 volume fraction dPB in the PS rich phase. The data are presented in figure 3.10. To construct a portion of the binodal curve from these points for this polymer system, we use an expression for the free energy of mixing per unit volume, ΔG_m, given by[19]

$$\Delta G_m = RT\left[\frac{\phi_{PS}\ln(\phi_{PS})}{V_{PS}} + \frac{\phi_{PB}\ln(\phi_{PB})}{V_{PB}}\right] + \Lambda\phi_{PS}\phi_{PB} \tag{3.1}$$

where Λ, the segmental interaction parameter, has a constant and temperature dependent term

$$\Lambda = \lambda_O + \lambda_t \cdot T\,(^{\circ}C), \tag{3.2}$$

and where ϕ is the volume fraction, V is the molar volume, and where R and T have their usual meaning. Normally Λ also has a concentration dependent term. The volume fraction of dPB solubilized in the high molecular weight PS does not change enough in the temperature range of our experiments to make the calculation of the concentration

dependence meaningful. The Flory - Huggins interaction parameter $\chi = \Lambda V_{PB} / xRT$ where x is the degree of polymerization of the PB.

ΔG_m is plotted as a function ϕ_{PS} at a particular temperature and the points of double tangency determine the binodal composition of the two phases in equilibrium. The calculated concentration of PS in the PB rich phase is so small that it is effectively zero. The set of points of tangency on the PS rich side of the curves for various temperatures defines the binodal curve. The solid line in figure 3.10 represents the best non - linear least squares fit[20] to the data and corresponds to values of $\lambda_O = 0.71$ and $\lambda_t = -0.00020$. The value of χ is thus 0.055 and 0.048 at 105 °C and 160 °C respectively.

We have specifically chosen the expression of the interaction parameter in equation (3.2) to compare our results to those of Roe and Zin[19]. They determined binodal curves based on light scattering experiments for polymer systems of PB (94 % 1,4 addition, 6 % 1,2 addition, M_n = 2350 g/mole) and three polystyrenes with M_w = 2400, 3500, and 5480 g/mole. If the ϕ dependent term in their expression for Λ (ϕ is always close to 1 in our system) is added to the constant term in their expression, we calculate average values of λ_O and λ_t in their experiments to be 1.05 and -0.0022 respectively. The binodal curve for our polymers predicted with these values is plotted in figure 5 as the dashed line.

The major difference in the interaction parameter determined from the present FRES results and that of Roe and Zin is in the temperature dependence. This difference is responsible for the larger curvature in the dashed line in figure 3.10. The molecular weights of the polybutadienes in both studies are similar. The use of perdeuterated polybutadiene instead of its protonated analog is not expected to have a significant effect on λ_t. However, the 1, 2 content of the PB in the Roe and Zin study was 6% compared to a 1, 2 content of 12 % in the dPB used in this study. In addition, the polystyrene molecular weights in the Roe and Zin experiments were 60 to 150 times smaller than the molecular weight of the PS in the present study suggesting that λ_t is a function of

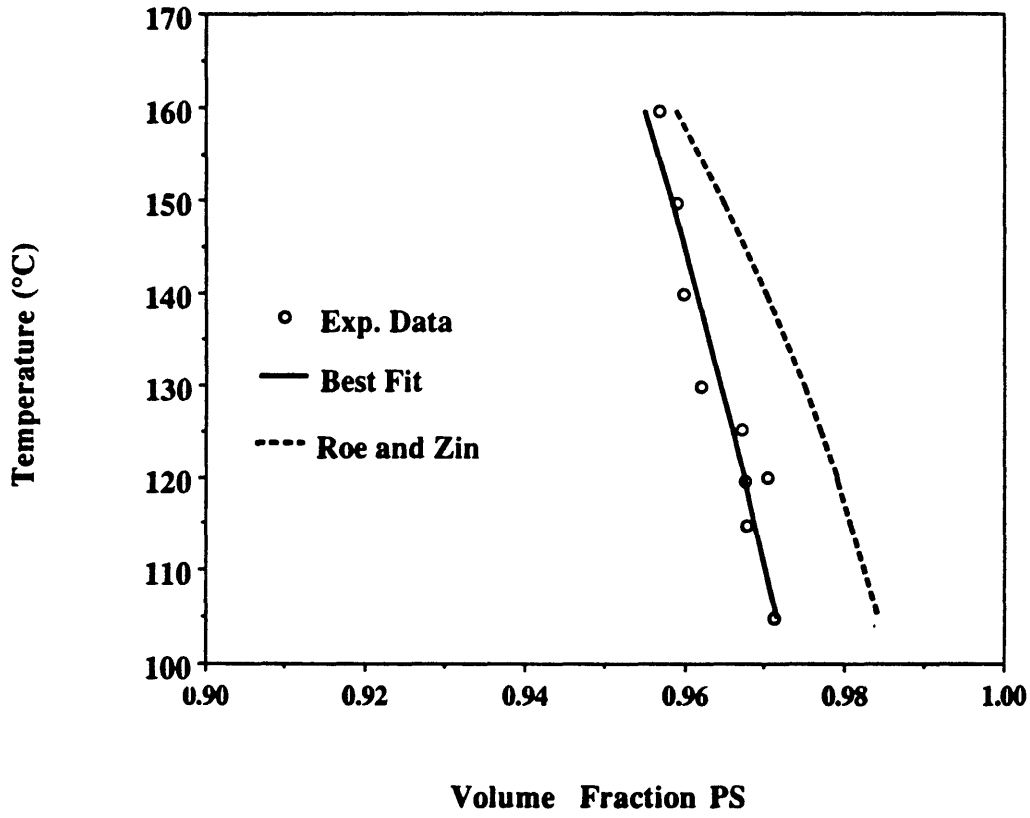

Figure 3.10 Plot of temperature versus the solubity of dPB in PS. • denotes solubilites determined from FRES data. The solid line is the best fit of a binodal curve to the data with $\Lambda = 0.71 - 0.00020(T\ ^\circ C)$. The dashed line is the binodal curve calculated for $\Lambda = 1.05 - 0.0022(T\ ^\circ C)$ which is based on the results of Roe and Zin.

molecular weight. In fact, the temperature dependence of Λ in the Roe and Zin experiments decreases with increasing PS molecular weight (λ_t = -0.0026, -0.0023, and -0.0016 for M_{wPS} = 2400, 3500, and 5480 g/mole). Our results produced λ_t = -0.00020 at M_{wPS} = 350 000 g/mole.

We extract diffusion coefficients from the samples in which the concentration of dPB decays with depth in the PS layer. Figures 3.11 and 3.12 show the FRES data and the simulations for a sample held 15 minutes at 107.4 °C. A schematic of the sample is shown in figure 3.5. We assume that the blended dPB/PS surface layer (whose detailed morphology is unknown) rapidly transforms to a layer of pure dPB on top of a layer of PS saturated with dPB when heated to the temperature of a diffusion experiment. Evidence to support this assumption was obtained from Secondary Ion Mass Spectroscopy analysis of annealed samples which revealed a significant concentration enhancement of dPB on the surface compared to the unannealed samples[21]. The PS saturated with dPB is simulated as a layer 13.5 nm thick based on mass balance considerations.

The concentration profile of dPB in the PS layer is modeled as Fickian diffusion of a species at constant concentration at the interface diffusing into a half space. The constant concentration in this case is the equilibrium solubility limit, C_∞, of the dPB in PS at the temperature of the experiment. The concentration profile is given by[22]

$$C(x,t) = C_\infty \operatorname{erfc}\left[\frac{x}{\sqrt{4Dt}}\right] \tag{3.3}$$

where x is the depth of penetration, D is the diffusion coefficient, and t is time. The baseline of non-zero values for the concentration of dPB at depths greater than the penetration depth of dPB is simulated as pulse pile-up described above.

The value of C_∞ in the model of the concentration profile is an important parameter in the determination of D. Figure 3.11 shows the fit obtained when C_∞ is equal to 0.029, the value determined from the point at 107.4 °C along the binodal curve that was fitted to the solubility data given above. The best value for D using this value for C_∞ in a least squares fit between the simulation and the FRES data is 2.43×10^{-13} cm^2/s. However, the simulated concentration profile using this C_∞ and D underestimates the experimental data at the front of the diffusion profile and overestimates the concentration of dPB at greater depths (Figure 3.11). We therefore consider the diffusion coefficients found with values of C_∞ from the experimentally determined binodal curve to be upper bounds at each temperature.

A second approach to find D was to perform a two parameter fit in which C_∞ and D are both varied to find the combination that yields the best possible fit between the simulation and the FRES data. The best combination for the sample held 15 minutes at 107.4 °C is shown in figure 3.12) where $C_\infty = 0.044$ and $D = 1.51 \times 10^{-13}$ cm^2/s. In all of the samples studied, the C_∞ values employed in the two parameter fits were higher than those obtained from the binodal curve developed in the solubility experiments; at times, the difference was as much as a factor of 2. Possible explanations for the inconsistency include the difficulty in precisely determining the location of the dPB/PS interface, the steepness of the concentration profile in this region, a concentration dependent diffusion coefficient, and the error associated with describing the baseline as pile-up. We consider the diffusion coefficients found with two parameter fits to be lower bounds at each temperature. The values of D presented in the discussion below are an average of the upper and lower bounds, and the average D differs from the bounds by $\pm$ 5 to 30 % . The value of D at 107.4 °C is thus 1.97×10^{-13} $cm^2/s \pm 23$ %.

Diffusion coefficients were determined for 3000 g/mole dPB diffusing into a high molecular weight PS matrix in the temperature range of 97 °C to 115 °C. The diffusion coefficients range from 10^{-15} to 10^{-12} cm^2/s. The data are presented in figure 3.13 in a

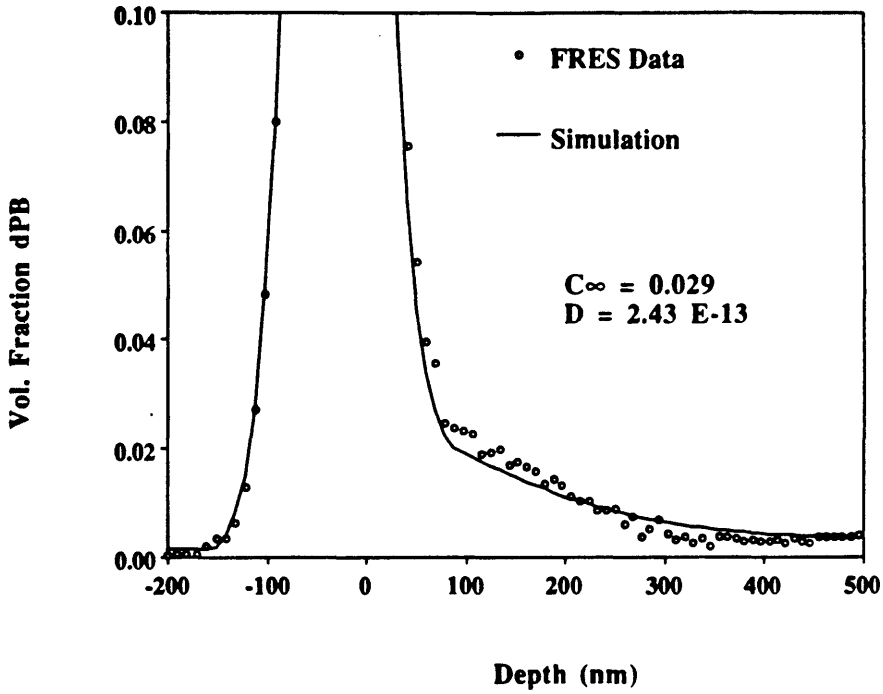

Figure 3.11 Expanded view of the deuterium profile and simulation in terms of volume fraction versus depth for a sample held 15 min at 107.4 °C. The simulation employs a value of C_∞ which was determined from the binodal curve fit to the experimental solubility data.

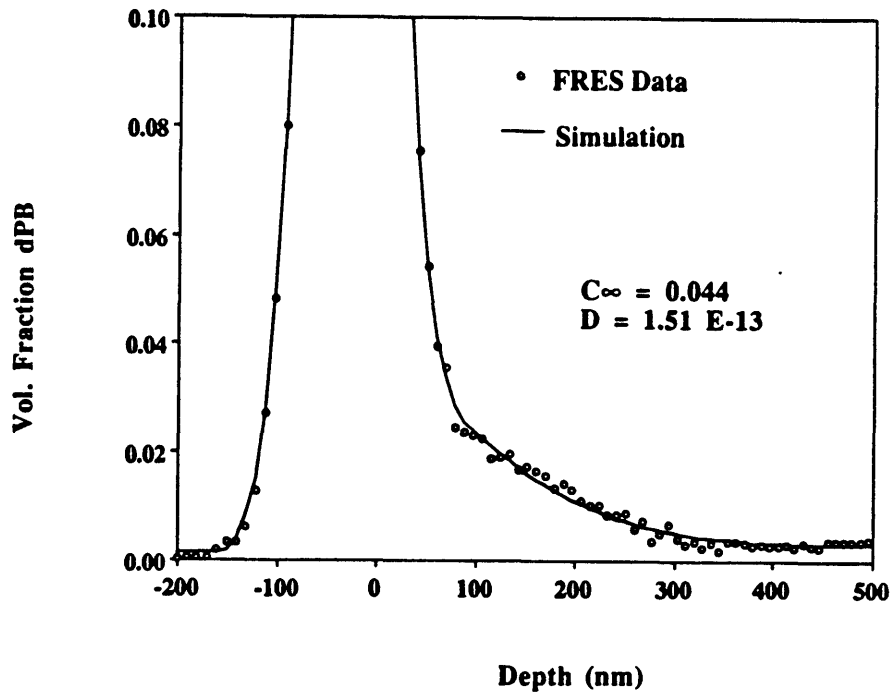

Figure 3.12 Expanded view of the deuterium profile and simulation in terms of volume fraction versus depth for a sample held 15 min at 107.4 °C. The simulation employs the best two-parameter fit for values of C_∞ and D.

semilog plot of D versus $1000/T$. We were unable to measure diffusion coefficients at temperatures higher than 115 °C because of the uncertainty of the sample temperature at short times in the oil bath. Longer times at higher temperatures result in penetration depths which extend out of the deuterium window of the FRES experiment and/or place the boundary conditions of the diffusion model in question. Conversely, measurements of diffusion coefficients at temperatures below 97 °C are possible but require very long time periods.

The solid line in figure 3.13 represents the best fit of an Arrhenius expression, $D=D_O exp(\Delta E_{act} / RT)$, to the data. The apparent activation energy, ΔE_{act}, is 99 kcal/mole. The temperature dependence of polymer - polymer interdiffusion at temperatures less than 100 °C above T_g is not usually well described by an Arrhenius equation, particularly when a wide range of temperature is considered. The data usually exhibit curvature not accounted for by the temperature independent activation energy of the Arrhenius equation and so a more appropriate expression such as the WLF equation is generally employed. Our data do not span a large enough range to merit a fit beyond the Arrhenius equation. The value of ΔE_{act} in this polymer system can be compared with data from other researchers by finding the local slope of their data,

$$\frac{d(\ln D)}{d(1/T)} = \frac{\Delta E_{act}}{R}, \tag{3.4}$$

evaluated in the temperature range of our experiments.

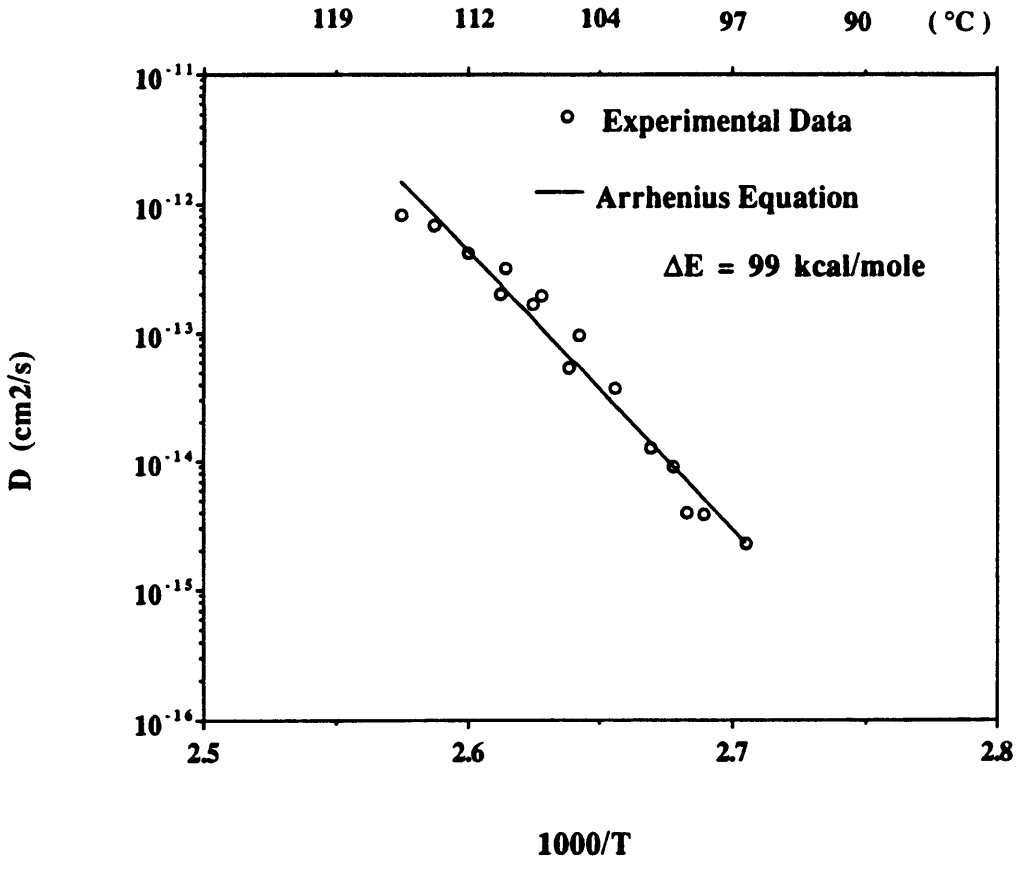

Figure 3.13 Semilog plot of D versus 1000/T. The solid line represents the best fit of an Arrhenius equation to the data with ΔE_{act} = 99 kcal/mole.

Green and Kramer have studied the temperature dependence of PS (55000 < M (g/mole) < 430000) diffusing into a PS matrix ($2x10^7$ g/mole) with FRES[23]. They determined tracer diffusion coefficients in the range of 10^{-12} cm^2/s to 10^{-16} cm^2/s for temperatures between 220 °C to 130 °C. The temperature dependence was modeled with the WLF type equation,

$$\log_{10}\left(\frac{D}{T}\right) = A' - \frac{B}{T - T_\infty} \tag{3.5}$$

where A' is a constant, $B = 710$, and $T_\infty = 49$ °C. The local slope at T = Tl is equal to

$$\left.\frac{d(\ln(D))}{d\left(1/T\right)}\right|_{T=T_l} = \left.\frac{\Delta E_{act}}{R}\right|_{T=T_l} = \left.-\frac{2.303BT^2}{(T - T_\infty)^2} - T\right|_{T=T_l}. \tag{3.6}$$

If we extrapolate the fitted equation beyond the temperature range of the experiments by Green and Kramer to the average temperature in this study, 107 °C, we calculate an apparent activation energy for the PS/PS tracer diffusion at 107 °C to be 140 kcal/mole.

In another series of experiments, Green and Kramer measured the diffusion of low molecular weight polystyrenes in a PS matrix (M = 2 x 10^7 g/mole)[6]. These experiments were conducted at 112, 118, and 120 °C. We chose a PS oligomer of molecular weight 11200 g/mole to compare to the dPB diffusant on the basis of approximately equal chain length. At 112 °C, the diffusion coefficient for the PS/PS system is approximately 2 x 10^{-15} cm^2/s, two orders of magnitude smaller than the diffusion coefficient we measured in the dPB/PS system at 111.5 °C. Diffusion rates in the PS/PS experiments may have been influenced by the presence of approximately 10 volume percent diffusant species which could have altered the properties of the matrix.

The apparent activation energy for the PS/PS diffusion between 112 and 120 °C is 60 kcal/mole, 40 percent less than the value obtained for the dPB/PS diffusion between 97 and 115 °C. We expect the activation energy to be significantly lower in the higher temperature range. The WLF equation used to describe the overall temperature dependence of the diffusion coefficients exhibits a high degree of curvature in this region.

Comparison of the activation energies for PS/PS diffusion and dPB/PS diffusion is not ideal in this temperature range. In the PS/PS system, both the diffusant and the matrix polymers are approaching their glass transition temperatures. The activation energy reflects drastically decreasing mobility for both species. This is evident especially in the case of high molecular weight PS diffusing into a high molecular weight PS matrix. In our dPB/PS experiments, the dPB is approximately 200 °C above its glass transition temperature. The activation energy at 107 °C reflects primarily the changing properties of the PS matrix. The change in mobility of the dPB molecule with temperature in this range is in contrast insignificant.

Tracer diffusion in high molecular weight PS near the glass transition temperature has been measured for photo reactive dye molecules. Ehlich and Sillescu[24] measured the diffusion of tetrahydrothiophene-indigo (TTI, 256 g/mole) in PS (270 000 g/mole) between 78 and 160 °C. Kim et al. [25]determined diffusion coefficients for tetraethyl[3.3](1,4)naphthaleno-(9,10)anthracenophane-2,2,15,15 tetracarboxylate (cyclophane, 674 g/mole) in PS (422 000 g/mole). The tracer diffusion coefficients were determined by forced Raleigh scattering in samples containing less than 0.5 % TTI and in samples containing less than 0.04 % cyclophane. The values obtained for TTI at 97, 105, and 112 °C were 3×10^{-15}, 1×10^{-13}, and 1×10^{-12} cm^2/s respectively. The value for cyclophane at 107 °C is approximately 1×10^{-14} cm^2/s. The diffusion coefficients determined for dPB in PS at 96.5, 105.4 and 111.5 °C were 2×10^{-15}, 7×10^{-14}, and 3×10^{-13} cm^2/s, and within the same order of magnitude. The apparent activation energy for the TTI diffusion at 107 °C is calculated to be 92 kcal/mole from the

local slope of the WLF equation used to describe[24] the temperature dependence of the diffusion coefficient above T_g. In a similar way, the apparent activation energy for cyclophane[25] at 107 °C is calculated to be 109 kcal/mole. These values compare favorably with the 99 kcal/mole apparent activation energy found for the diffusion of dPB in PS. The fact that the rigid dye molecules and the low molecular weight dPB are diffusing at similar rates and with similar apparent activation energies implies that both types of experiments are probing the changing properties of the PS matrices near the glass transition temperature.

The largest diffusion coefficient we measured was 8.4×10^{-13} cm^2/s at 115.2 °C. The estimated minimum D required in the crazing mechanism at room temperature is 3×10^{-12} cm^2/s. At room temperature, the dPB is still well above its glass transition temperature. Evidence from the thermally - induced diffusion measurements above suggests that the diffusion in the crazing mechanism is controlled by the PS matrix properties. The local concentration of negative pressure and tuft drawing processes of craze growth must alter the properties of the PS in these regions to such a degree that the PB becomes significantly more soluble in the PS and the diffusion rate is quite substantially increased.

3.6 Summary

FRES is a viable technique to measure both solubilites and diffusion coefficients in the dPB/PS polymer system. The solubility of the 3000 g/mole dPB is only 2 to 4 volume percent in 350 000 g/mole PS in the temperature range from 100 to 160 °C. A binodal curve was determined with the segmental interaction parameter $\Lambda = 0.71$ ($\Lambda = \chi x RT/V_{PB}$) with little temperature dependence. We conclude that Λ is a function of molecular weight to explain the difference between our results and the Roe and Zin values found for a system with similar molecular weight polybutadiene but with

low molecular weight PS. Tracer diffusion coefficients were measured for dPB in PS which ranged from 10^{-15} to 10^{-12} cm^2/s in the temperature range from 97 to 115 °C. The apparent activation energy is 99 kcal/mole. The values of the diffusion coefficients and the apparent activation energy are in good agreement with those found for the diffusion of photo reactive dye diffusion in PS in the same temperature range. This implies that dPB molecule, like the dye molecules, is acting as a probe of the changing properties of the PS matrix.

3.7 References for Chapter 3

(1) Gebizlioglu, O. S.; Beckam, H. W.; Argon, A. S.; Cohen, R. E.; Brown, H. R. *Macromolecules* **1990**, *23*, 3968-3974.

(2) Argon, A. S.; Cohen, R. E.; Gebizlioglu, O. S.; Brown, H. R.; Kramer, E. J. *Macromolecules* **1990**, *1990*, 3975-3982.

(3) Spiegelberg, S. H.; Argon, A. S.; Cohen, R. E. *J. Appl. Polym. Sci.* in press.

(4) Green, P. J.; Mills, P. J.; Kramer, E. J. *Polymer* **1986**, *27*, 1063-1066.

(5) Green, P. F.; Mills, P. J.; Palmstrøm, C. J.; Mayer, J. W.; Kramer, E. J. *Phys. Rev. Lett.* **1984**, *53*, 2145-2148.

(6) Green, P. F. Ph D Thesis, Cornell University, 1985.

(7) Green, P. F.; Kramer, E. J. *Macromolecules* **1986**, *19*, 1108-114.

(8) Mills, P. J.; Green, P. F.; Palmstrøm, C. J.; Mayer, J. W.; Kramer, E. J. *Appl. Phys. Lett.* **1984**, *45*, 957-959.

(9) Green, P. F. *Macromolecules* **1991**, *24*, 3373-3376.

(10) Green, P. F.; Adolf, D. B.; Gilliom, L. R. *Macromolecules* **1991**, *24*, 3373-3382.

(11) Composto, R. J.; Mayer, J. W.; Kramer, E. J.; White, D. M. *Phys. Rev. Lett.* **1986**, *57*, 1312.

(12) Composto, R. J. PH D Thesis, Cornell University, 1987.

(13) Composto, R. J.; Kramer, E. J.; White, D. M. *Macromolecules* **1988**, *21*, 2580.

(14) Bruder, F.; Brenn, R. *Macromolecules* **1991**, *24*, 5552-5557.

(15) Cheng, P. L. Ph D Thesis, Massachusetts Institute of Technology, 1986.

(16) Feldman, L. C.; Mayer, J. W. Elsevier Science Publishing Co., Inc.: New York, New York, 1986.

(17) Doolittle, L. R. *Nucl. Inst. Meth.* **1985**, *B9*, 344.

(18) Doolittle, L. R. *Nucl. Inst. Meth.* **1986**, *B15*, 227.

(19) Roe, R.-J.; Zin, W.-C. *Macromolecules* **1980**, *13*, 1221-1228.

(20) Ferrier, N. J., personal communication.

(21) Eschner, A.; Holm, R., personal communication.

(22) Crank, J. Oxford University Press: Oxford, U.K., 1975.

(23) Green, P. F.; Kramer, E. J. *J. Mat. Res.* **1986**, *1*, 202-205.

(24) Ehlich, D.; Sillescu, H. *Macromolecules* **1990**, *23*, 1600-1610.

(25) Kim , H.; Waldow, D. A.; Han, C. C.; Tran-Cong, Q.; Yamamoto, M. *Polymer Communications* **1991**, *32*, 108-114.

Chapter 4

The Effect of Gas Pressure on the Solubility and Diffusion of Polybutadiene in Polystyrene

4.1 Abstract

Tracer diffusion of 3000 g/mole perdeuterated polybutadiene (dPB) into high molecular weight polystyrene (PS) was measured with Forward Recoil Spectroscopy (FRES) in the temperature range from 90 to 110 °C in the presence of argon and helium pressures up to 11.3 MPa. The diffusion coefficient for dPB in PS at 107 °C increases from 1.2×10^{-13} to 8.7×10^{-13} cm^2/s as the argon pressure is increased from atmospheric pressure to 11.3 MPa. When helium is the pressurizing medium, the diffusion coefficient for dPB in PS at 107 °C decreases from 1.2×10^{-13} to 3.7×10^{-14} cm^2/s as the pressure is increased from atmospheric pressure to 11.3 MPa. The results are explained in the framework of competing hydrostatic pressure and plasticization effects. The solubility of dPB in PS is independent of pressure, irrespective of the gas used as the pressurizing medium.

4.2 Introduction

The tracer diffusion of large molecules in polymers provides a sensitive probe of the dynamics of the polymer matrix. For example, the tracer diffusion coefficient (D) of 3000 g/mol perdeuterated polybutadiene (dPB) in polystyrene (PS) varies over two orders of magnitude in the temperature range from 96 to 115 °C.[1] The values of D as well as the apparent activation energy for the diffusion in this range near the PS glass transition temperature compare favorably to tracer diffusion measurements of photoreactive dye

molecules in PS at the same temperatures.[2,3] In all of these experiments, the diffusion is coupled to the dynamics of the PS matrix, and small changes in temperature in this range result in large differences in matrix mobility and thus large variations in the measured diffusion coefficient.

Above the glass transition temperature, the temperature dependence of the diffusion coefficient is usually well described by a WLF equation in which the relationship between D and the temperature difference, $T_{experiment} - T_g$, is readily apparent. Conditions which increase T_g decrease mobility, and those which decrease T_g increase mobility. The effect of hydrostatic pressure is to increase T_g.[4] However, some gases at high pressure are sufficiently soluble in PS so that they can act as plasticizers and lower T_g. Wang et al.[5] described the reduction in T_g of PS as a function of carbon dioxide pressure. They found that T_g went through a minimum near 20 MPa of CO_2 pressure and explained their results in terms of the competing effects of hydrostatic pressure and plasticization. This same framework of competing hydrostatic pressure and plasticization effects should be relevant to the behavior of the diffusion coefficient of dPB in PS in the presence of helium or argon gas pressure. On the other hand, neither hydrostatic pressure nor dissolved gas is expected to change the equilibrium solubility of dPB in PS as we will clarify below. Experiments were performed to examine the validity of these presumptions.

4.3 Experimental

Polymers

The polystyrene used in this study was supplied by Polysar (M_W = 350 000 g/mole, M_n = 170 000 g/mole). Perdeuterated polybutadiene (dPB) was synthesized in our laboratory via homogeneous anionic polymerization in benzene using n-butyl lithium initiator. The perdeuterated butadiene was obtained from Cambridge Isotope

Laboratories and purified as described by Cheng.[6] Molecular weight was 3000 g/mole and the polydispersity was 1.04 based on size exclusion chromatography and an in - line viscometer. Deuterium NMR experiments showed that the microstructure of the dPB was 12 % 1,2, and 88 % 1,4 cis and trans addition. With the exception of the n-butyl and proton end groups, the polymer is greater than 97 % deuterated based on proton NMR results.

Sample Preparation

All samples were prepared in a similar manner. A piece of silicon wafer was washed in distilled water to remove any dust particles, rinsed with high purity ethanol, and dried by spinning at 3000 rpm in air. A polystyrene layer was deposited on the wafer in a spin coating process with solutions of PS in toluene. The samples were annealed in a vacuum oven for at least 8 hours at approximately 100 °C to remove any residual solvent and to relax stresses caused by the spin coating process. The objective was to create a bilayer sample consisting of dPB on top of the PS. We were unable to form a coherent film with the low molecular weight dPB. Instead heterogeneous films of dPB and PS were employed successfully as in our previous work.[1] These films were made by spin coating solutions of blends of dPB and PS in toluene in which the PS accounted for 30 to 40 percent of the total polymer by weight. Thus, the dPB/PS blend layer was spun onto a glass slide, floated onto the surface of a water bath, and picked up with a PS - coated wafer. Each sample was dried in a vessel with a nitrogen purge at room temperature for at least 12 hours. Care was taken in each preparation step to minimize the exposure of the dPB to oxygen, UV light, and heat to reduce the possibility of cross-linking.

The samples were heated in a brass sample chamber which was connected to a gas cylinder. The chamber was evacuated and back filled with argon or helium and the pressure was maintained constant with a regulator. The pressure was read from the gauge of the regulator with an accuracy of 50 kPa. The maximum pressure attainable was 11.3

MPa. In each experiment, the sample and chamber were immersed in an oil bath at a given temperature for a specific period of time. In this way the sample temperature reached 90 % of its final steady state value after 80 seconds and 99 % after 180 seconds. The temperature of the bath itself dropped approximately 0.6 °C immediately after insertion of the sample chamber and regained a steady state value (± 0.1 °C) after approximately 2 minutes. The error in reported temperature is greater for those samples which were treated for short time periods. The minimum time period used in these experiments was 15 minutes. Each sample was quenched to room temperature to 'freeze' the concentration versus depth profile for subsequent analysis, and then the gas pressure was released.

Forward Recoil Spectroscopy

All of the samples were analyzed with Forward Recoil Spectroscopy (FRES) at the Cambridge Accelerator for Materials Science at Harvard University to determine concentration versus depth profiles of dPB in PS. This technique allows direct measurement of the diffusion profile of the deuterated species in the hydrogenated matrix for penetration depths in the range of 500 nm. Given this depth and a 5 minute minimum experimental time period for accurate temperature control, the largest diffusion coefficient that can be measured is approximately 10^{-12} cm^2/s. Details of this technique and the data analysis are described elsewhere.[1, 7-9]

4.4 Results and Discussion

Solubility limits and diffusion coefficients were determined from the FRES results with the aid of the RUMP software package developed for Rutherford Backscattering and FRES data analysis at Cornell University.[10, 11] The software was purchased from Computer Graphics Service in Lansing, New York. This program performs complex iterative simulations of FRES data given the specific parameters of the

experimental configuration and the physical and chemical characteristics of the species in the sample description.

Solubility Experiments

Some of the samples were held at temperatures of 106.7, 119.7 and 159.0 °C and gas pressures of either atmospheric pressure or 11.3 MPa for time periods of 1 to 24 hours. The dPB/PS blend layer in these samples was approximately 80 nm thick and was 67 % dPB and 33 % PS by weight, and the pure PS substrate layer was approximately 500 nm thick. A schematic of a typical sample for the solubility experiments is shown in figure 4.1. The amount of dPB present is more than enough to saturate the PS substrate layer in the present experiment in the temperature range studied. Figures 4.2 shows the FRES data for a representative sample held at 119.7 °C for 2 hours under 11.3 MPa argon pressure. Normalized yield is proportional to the concentration of dPB, and depth in the sample increases as energy or channel number decreases. The dPB has diffused from the thin blended reservoir layer on the surface (1.47 to 1.56 MeV) into the initially homogeneous PS layer and the relatively flat concentration profile (1.22 to 1.44 MeV) indicates that the sample has reached equilibrium. The back edge of the sample corresponds to an energy of approximately 1.18 MeV. The solid line through the data is the best fit of a simulation to the data in which the concentration of dPB is assumed to be constant in the PS layer. For this sample, the solubility limit of dPB in PS, C_∞, is determined to be 0.027 volume fraction.

Figure 4.3, 4.4, and 4.5 show the solubility of dPB in PS determined from the FRES data for a number of different samples. The samples in figure 4.3, figure 4.4, and figure 4.5 were held at 106.7, 119.7, and 159.0 °C respectively at atmospheric pressure and at 11.3 MPa of gas pressure. Because the error in the solubility values is approximately 10 percent, there is no meaningful effect of either helium or argon gas pressure on the solubility of dPB in PS in the temperature range of the experiments. The

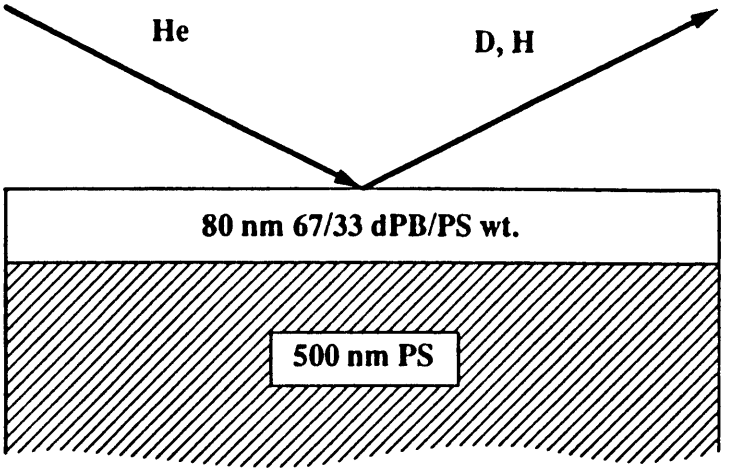

Figure 4.1 Schematic of a typical sample in the solubility experiments.

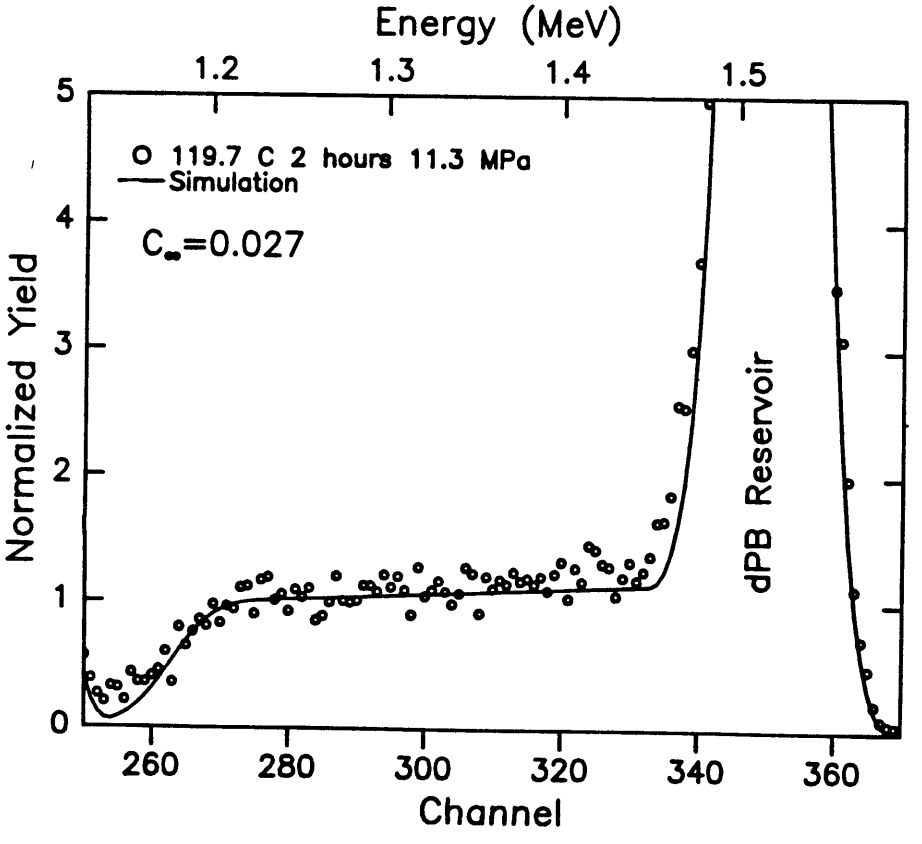

Figure 4.2 FRES data and simulation for a sample held for 2 hours at 119.7 °C with 11.3 MPa of argon. The solubility of dPB in PS in this sample is 0.027 volume fraction.

observed absence of any effect of pressure on the solubility of dPB in PS can be predicted from a thermodynamic analysis as follows: We are considering a case in which the molecular weights of the polymers are very different. We have observed that the low molecular weight polybutadiene (PB) is somewhat soluble in the high molecular weight PS and the solubility of the PS in the PB is negligible. We may then address the expected influence of pressure on solubility by considering a thermodynamic system at constant temperature in which PS, saturated with the low molecular weight PB, is in equilibrium with a reservoir of PB. At equilibrium, the chemical potential of the pure PB in the reservoir, μ_{PB}^{pure}, must be equal to μ_{PB}^{blend}, the chemical potential of the PB dissolved in the PS. These two quantities depend on pressure as follows:[12]

$$\mu_{PB}^{pure} - \mu_{PB}^{ref} = PV_{PB} \tag{4.1}$$

$$\mu_{PB}^{blend} - \mu_{PB}^{ref} = RT\ln[\gamma C_{\infty}] + P\bar{V}_{PB} \tag{4.2}$$

where μ_{PB}^{ref} is the chemical potential of pure PB at P=0 and temperature T, V_{PB} is the molar volume, $\bar{V}_{PB}$ is the partial molar volume, γ is an activity coefficient, and C_{∞} is the volume fraction of PB in PS at equilibrium. V_{PB}, $\bar{V}_{PB}$, and γ may be considered to be functions of pressure.

The most general case would be to consider that the PB reservoir pressure, P^{res}, and the pressure on the blend, P^{blend}, are not identical so that

$$RT\ln[\gamma C_{\infty}] + P^{blend}\bar{V}_{PB} = P^{res}V_{PB}. \tag{4.3}$$

Using Equation 4.3 it is possible to compare the equilibrium solubility of PB in PS for two different conditions of pressure as follows:

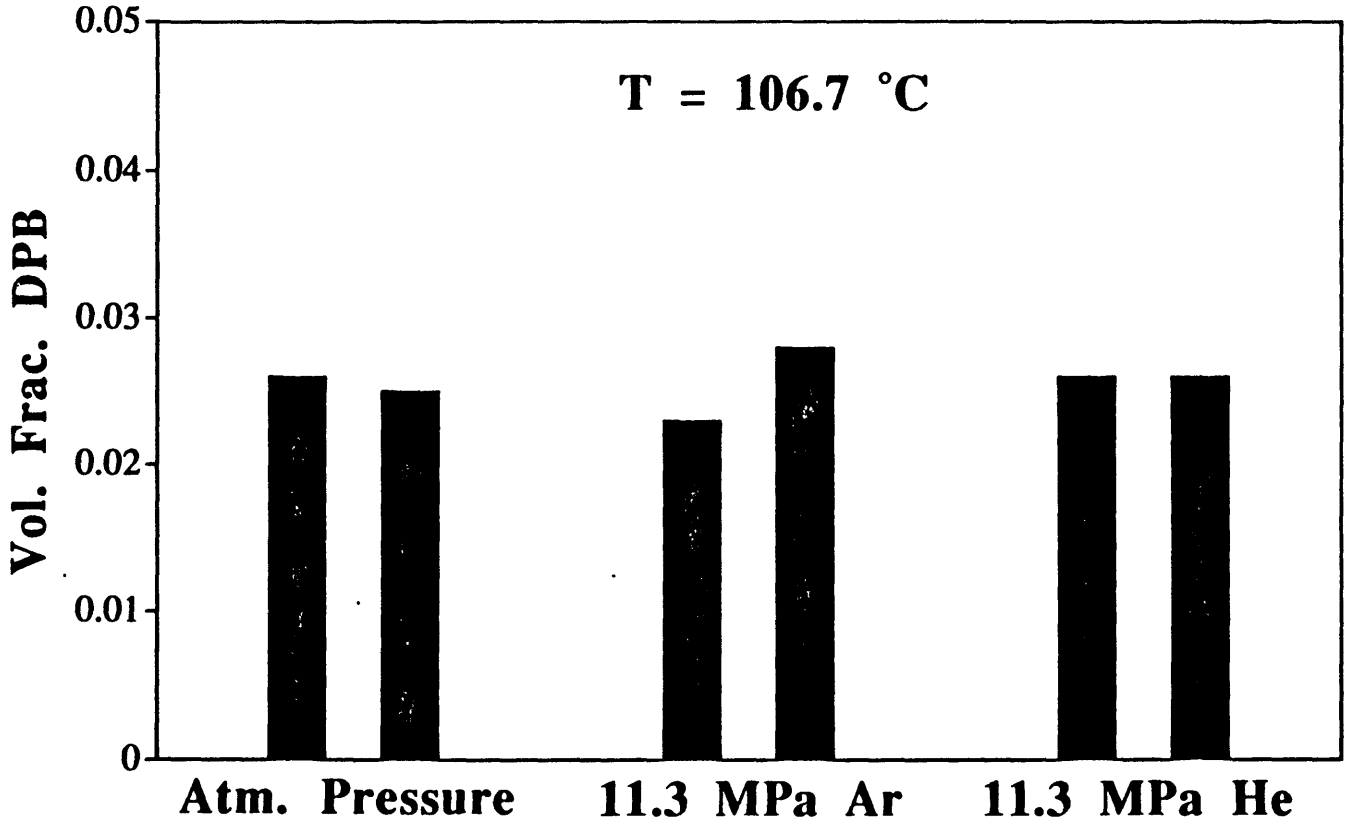

Figure 4.3 Solubility of dPB in PS determined from a number of different samples at 106.7 °C.

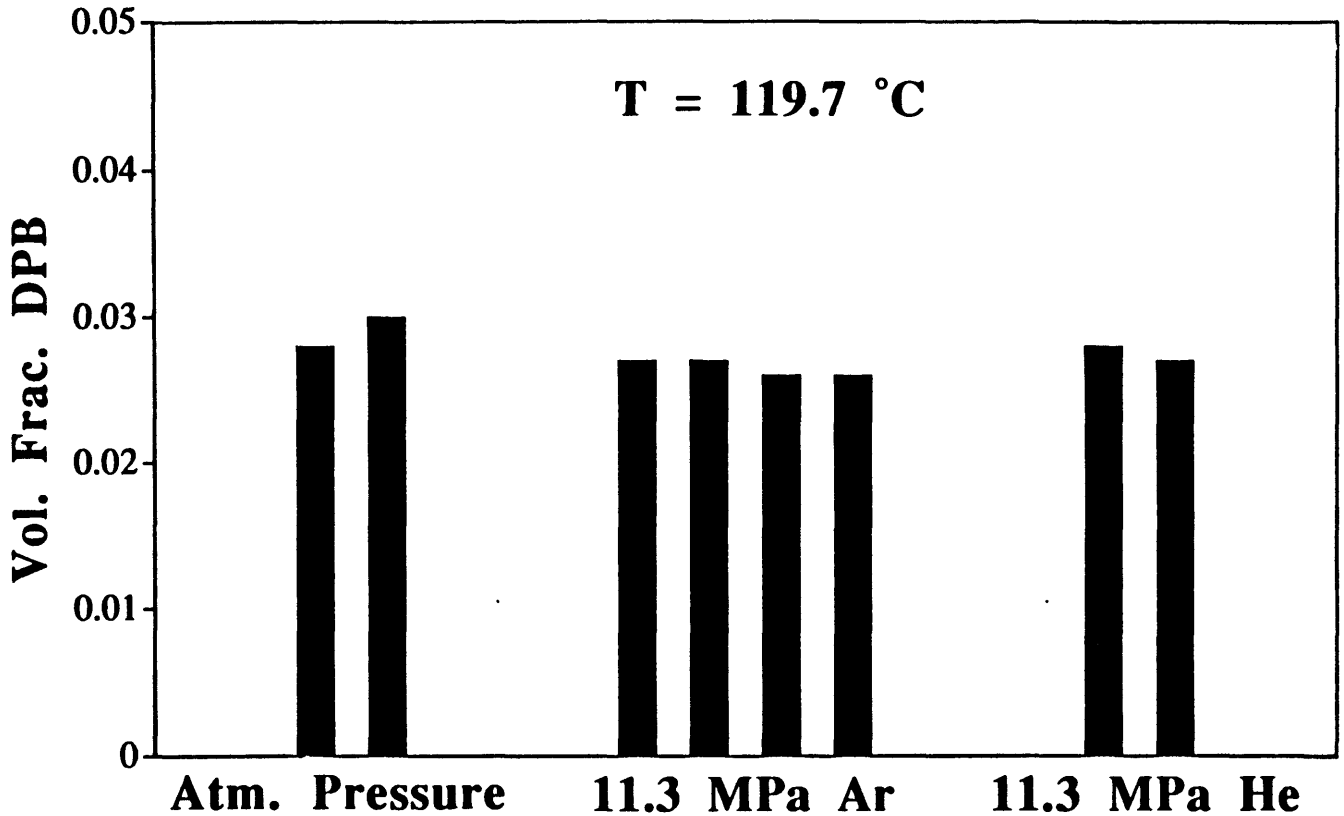

Figure 4.4 Solubility of dPB in PS determined from a number of different samples at 119.7 °C.

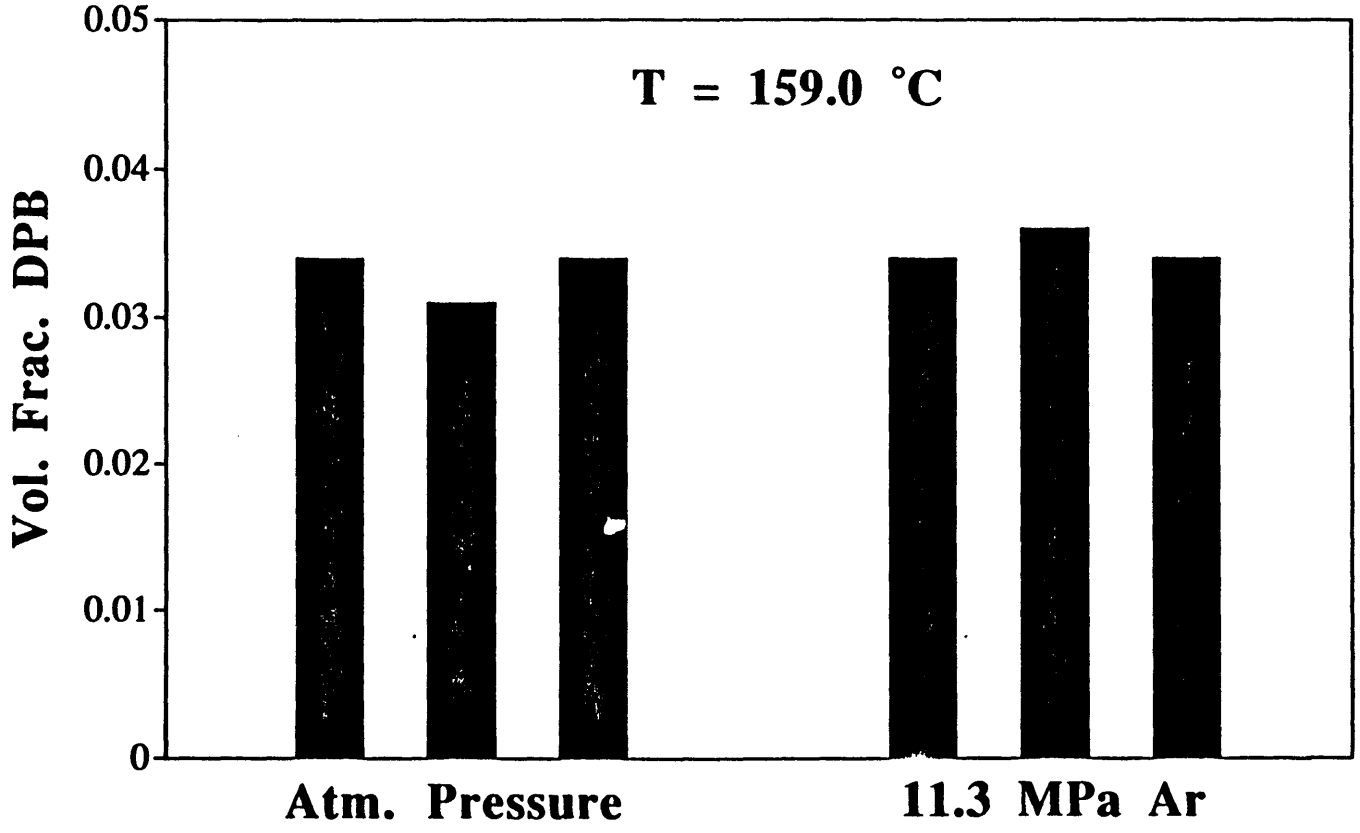

Figure 4.5 Solubility of dPB in PS determined from a number of different samples at 159.0 °C.

$$\Psi = \frac{C_\infty(P = P_2)}{C_\infty(P = P_1)} = \frac{\gamma_1}{\gamma_2}\exp\left[\frac{P_2^{res}V_{PB,2} - P_1^{res}V_{PB,1} - P_2^{blend}\bar{V}_{PB,2} + P_1^{blend}\bar{V}_{PB,1}}{RT}\right]. \quad (4.4)$$

Several interesting cases can be analyzed from Equation 4.4, but the most relevant here is $P_i^{res} = P_i^{blend}$ for i=1,2 which leads to the observation that the solubility ratio, Ψ, differs from unity only if the blend is non-ideal:

$$\Psi = \frac{\gamma_1}{\gamma_2}\exp\left[\frac{P_2(V_{PB,2} - \bar{V}_{PB,2}) - P_1(V_{PB,1} - \bar{V}_{PB,1})}{RT}\right]. \quad (4.5)$$

If, for example, $V_{PB,2}$ is larger than $\bar{V}_{PB,2}$ by 10 percent for 3000g/mol PB, P_2=11.3 MPa, P_1=0, T=100 °C, and the ratio of activity coefficients is unity, then Ψ=1.09. If the system is ideal, the molar volumes are identical to the partial molar volumes and the activity coefficients are unity so that $\Psi_{ideal} = 1$, and solubility is independent of pressure. To the extent that the non-idealities for our PB/PS system are expected to be rather small (C_∞ is on the order 0.04 volume fraction, compressibilities are low[13] and the maximum pressure achieved was on the order of 10 MPa (100 atm.), it is reasonable that we observed no measurable pressure dependence of C_∞ in this study.

Diffusion Experiments

Other samples were held at temperatures ranging from 115.2 °C to 89.0 °C for time periods of 15 to 1020 minutes with helium or argon gas pressure ranging from atmospheric pressure to 11.3 MPa. In these experiments the dPB/PS blend layer was approximately 35 nm thick and was 59 % dPB and 41 % PS by weight. The pure PS substrate layer was approximately 4 μm (4000 nm) thick. A schematic of a typical sample in the diffusion experiments is shown in figure 4.6. Diffusion times were chosen to obtain concentration profiles which would go to zero in penetration depths of order

200 nm. Figure 4.7 shows a representative sample which was held at 107.0 °C for 60 min at 5.7 MPa of helium pressure compared to an undiffused sample. The location of the interface between the thin blended reservoir layer of dPB on the surface and the initially homogeneous PS layer corresponds to a recoiled deuterium energy of approximately 1.46 MeV. Deuterium which recoils at energies below 1.46 MeV results from dPB which has diffused into the PS; the lower the energy, the deeper the dPB has diffused into the sample. Normalized yield is proportional to the concentration of dPB[1]. The dPB has clearly penetrated into the initially homogeneous PS layer. The solid lines through the data are best fits based on simulated samples for the two spectra. The undiffused sample is simulated as the bilayer structure depicted in figure 4.6. The consistent non-zero value for the counts of deuterium in the range of energy between the deuterium and hydrogen peaks, for example the data at energies below 1.43 MeV in undiffused sample in figure 4.7, is representative of all the samples and is accounted for as pile-up. These counts are attributed to events when two particles of lower energy reach the detector at the same time and are counted as one single higher energy particle. For the diffused sample, the simulation of the data assumes that the diffusion profile of dPB in the PS layer is consistent with Fickian diffusion of a species diffusing into a half space from a constant concentration at the interface. The constant concentration in this case is the equilibrium solubility limit, C_∞, of the dPB in PS at the temperature of the experiment. The concentration profile is given by[14]

$$C(x,t) = C_\infty \operatorname{erfc}\left[\frac{x}{\sqrt{4Dt}}\right] \tag{4.6}$$

where x is the depth of penetration, D is the diffusion coefficient, and t is time. The diffusion coefficients reported here are the values obtained from the best fits to the data using C_∞ and D as adjustable parameters. Another approach is to set C_∞ equal to the value determined in the solubility experiments at the temperature of interest and use only

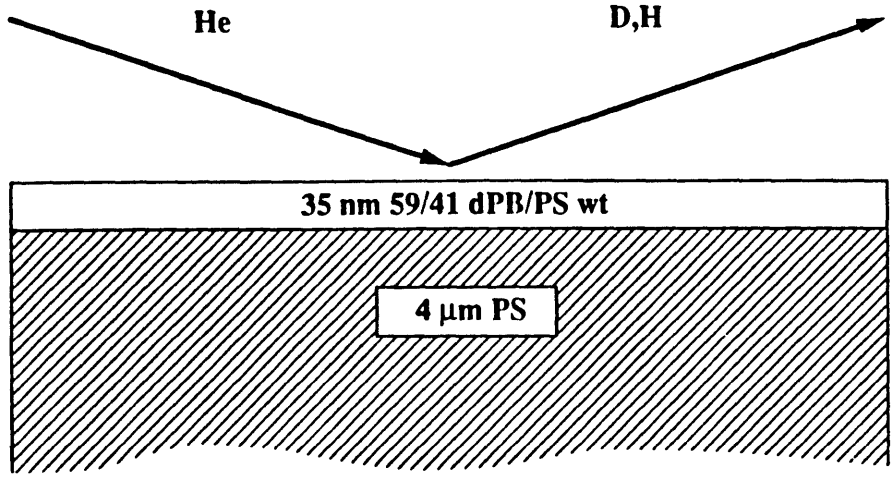

Figure 4.6 Schematic of a typical sample in the diffusion experiments.

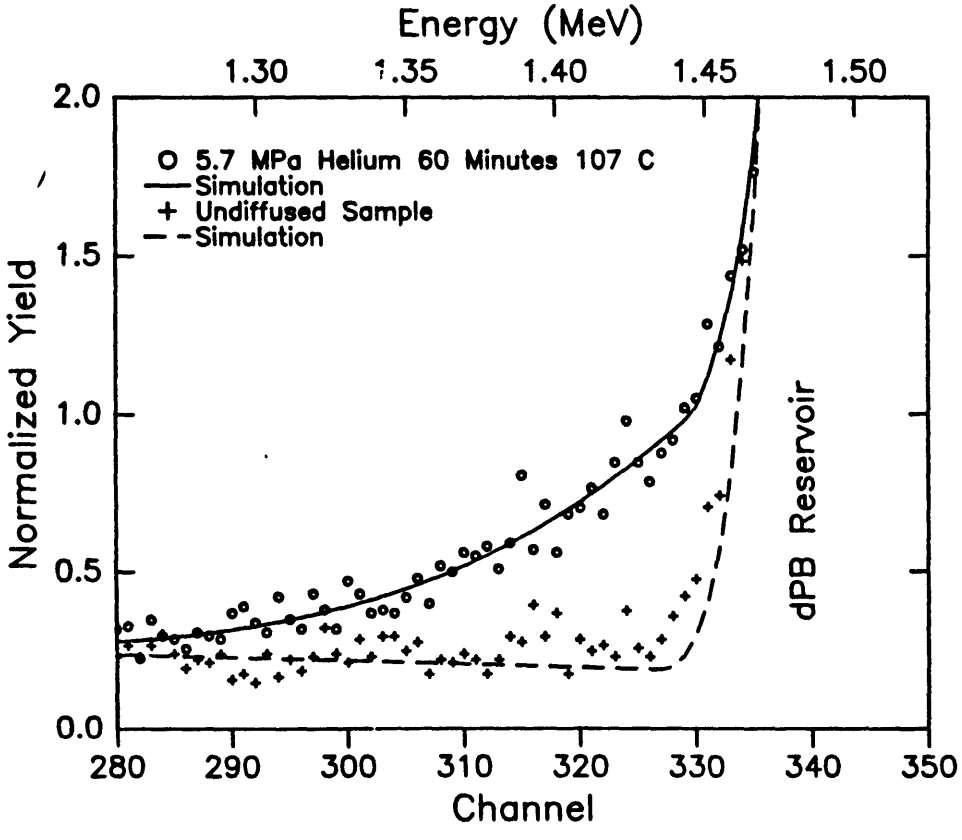

Figure 4.7 FRES data and simulations for an undiffused sample and for a sample held for 60 minutes at 107 °C with 5.7 MPa of helium pressure. The best fit to FRES data for the diffused sample is found with C_∞=0.035 and D=5.5 x 10^{-14} cm^2/s.

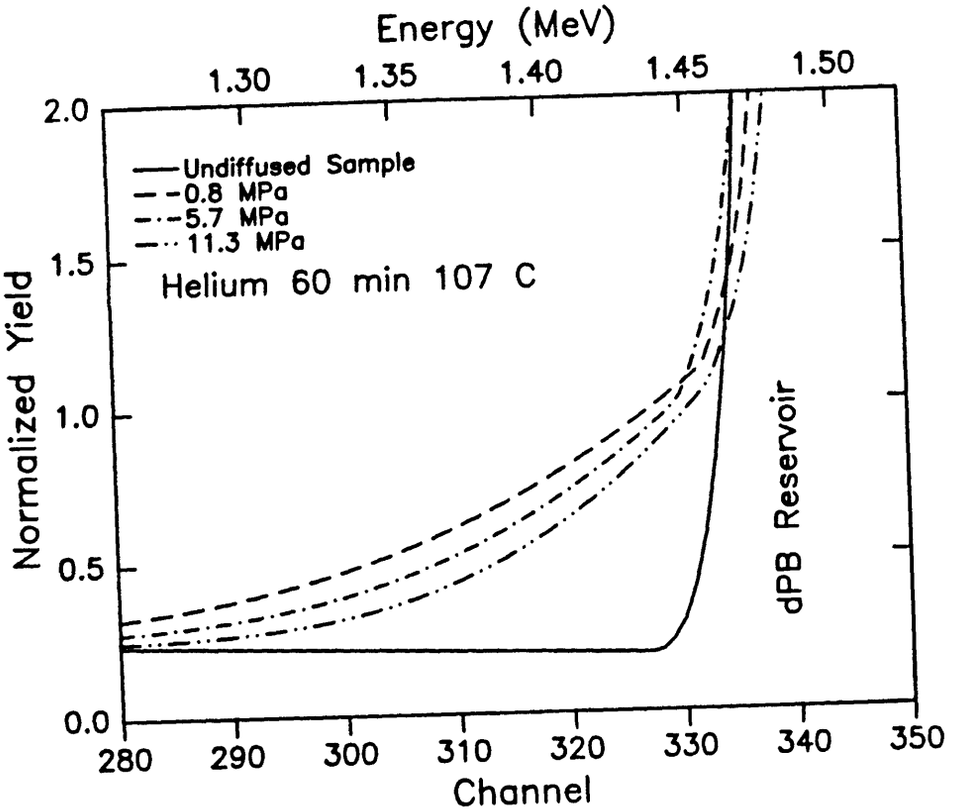

Figure 4.8 Best fits to FRES data for samples held at 107 °C with various helium pressures for 60 minutes.

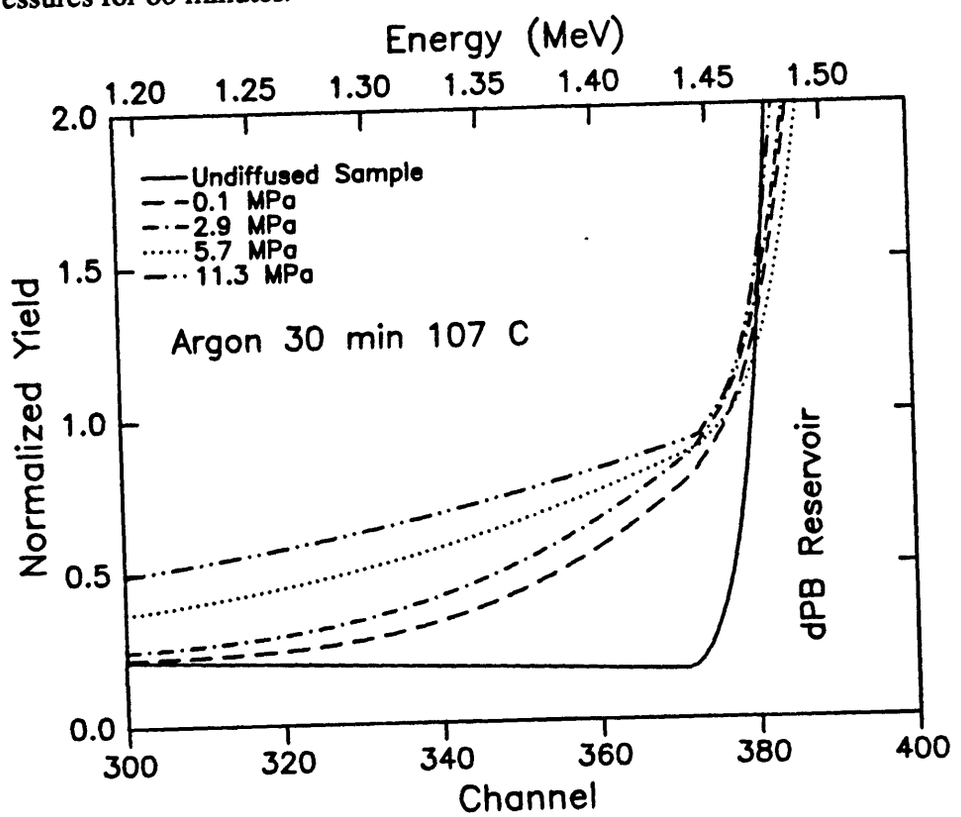

Figure 4.9 Best fits to FRES data for samples held at 107 °C with various argon pressures for 30 minutes.

D as an adjustable parameter. Both methods result in consistent and equivalent values of D within the error of the FRES experiment as discussed in detail in our previous work.[1]

Figure 4.8 shows fits to the FRES data from samples which were held at 107.0 °C for 60 min at 0.8, 5.7, and 11.3 MPa of helium pressure. The dPB has clearly penetrated further into the initially homogeneous PS layer at the lower pressure for the case of helium. Figure 4.9 shows fits to the FRES data for samples which were held at 107.0 °C for 30 minutes at atmospheric pressure, 2.9, 5.7, and 11.3 MPa of argon pressure. In these samples the penetration of the dPB in the PS layer increases with increased argon pressure, the opposite of the effect of the helium pressure.

Figure 4.10 shows the effect of both helium and argon gas pressure on the diffusion coefficient for dPB in PS at a constant temperature of 107 °C. As the argon pressure is increased from atmospheric pressure to 11.3 MPa, D increases from 1×10^{-13} to 1×10^{-12} cm^2/s. Conversely, as the helium pressure is increased from atmospheric pressure to 11.3 MPa, D decreases from 1×10^{-13} to 4×10^{-14} cm^2/s. The explanation for this behavior is the difference in solubility between argon and helium in PS. The diffusion coefficient for dPB in PS is dictated by the mobility of the PS matrix in these experiments. As mentioned in the Introduction, the mobility of PS is proportional to a temperature difference, $T_{experiment} - T_g$ (PS). The effect of hydrostatic pressure is to increase T_g and decrease D. Helium is effectively insoluble in PS, even at the higher pressures, and the decrease in D with increasing hydrostatic pressure is observed. Argon, however, is much more soluble in PS than helium. As the argon pressure is increased, the concentration of argon in PS increases and the PS becomes significantly plasticized. The plasticization decreases T_g, widens the gap between T_g and the temperature of the experiment, and increases D. When argon is the pressurizing medium, both the hydrostatic pressure effect to decrease D and the plasticization effect to increase D are present, and in the pressure range from atmospheric pressure to 11.3 MPa, the plasticization effect dominates. As described in the Introduction, Wang et al.[5] separated

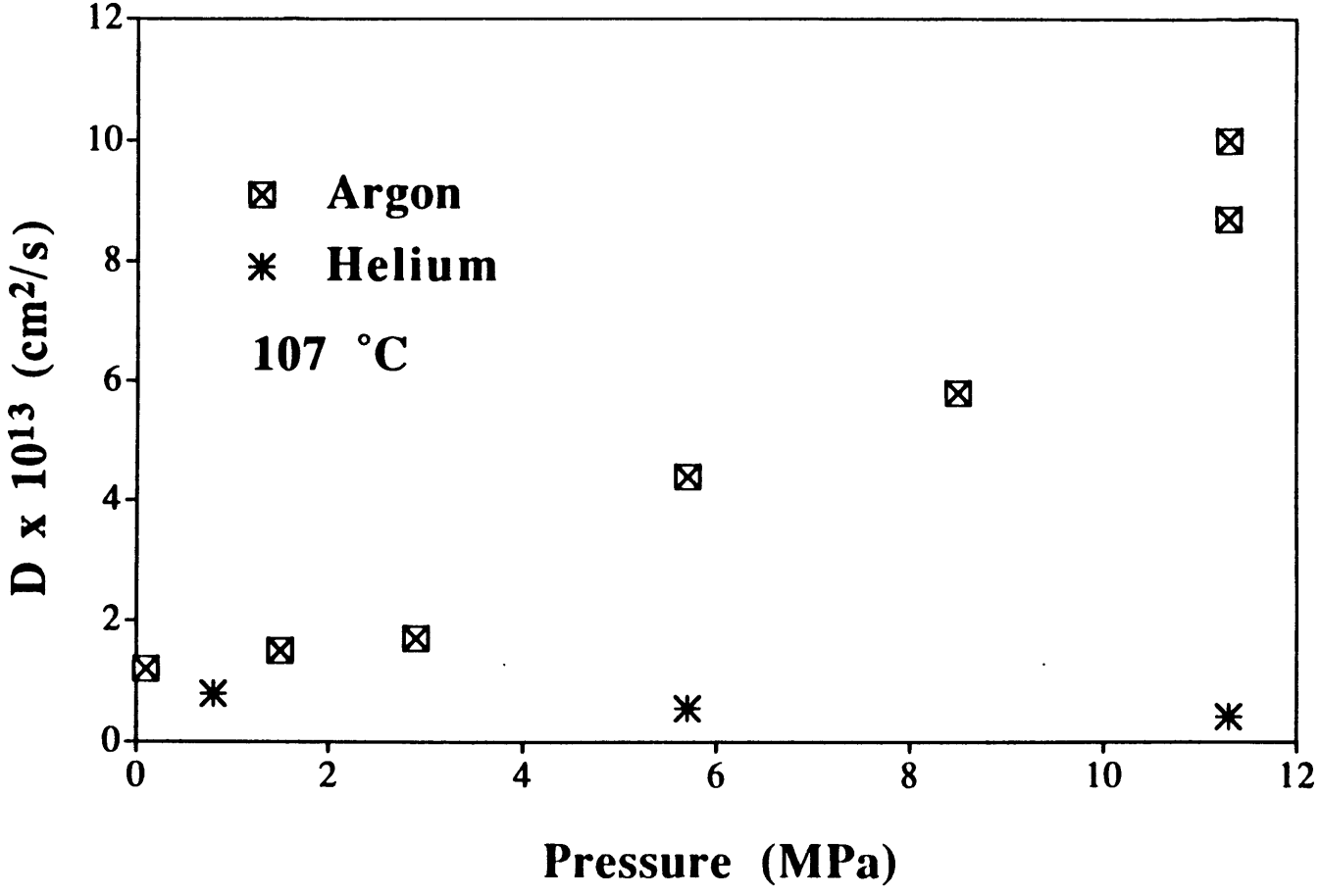

Figure 4.10 Plot of the diffusion coefficients determined from samples held at 107 °C with different argon and helium gas pressures vs. pressure.

these two effects in a framework to describe a minimum in T_g as a function of CO_2 pressure at approximately 20 MPa. Similarly, the diffusion coefficient for dPB in PS is expected to go through a maximum as T_g goes through a minimum at an argon pressure greater than the 11.3 MPa upper limit of our experimental setup.

Diffusion coefficients were also determined as a function of temperature at 11.3 MPa of helium pressure, atmospheric pressure,[1] and 11.3 MPa of argon pressure. These values are plotted in figure 4.11 versus 1000/T. As mentioned in the Introduction, the temperature dependence of D above the glass transition temperature is usually well described by a WLF equation which can account for curvature in the data. However, our data do not span a large enough range to merit a fit beyond an Arrhenius equation with a temperature-independent activation energy. The apparent activation energy, ΔE, is found for each data set from the best least squares fit of an Arrhenius equation to each set of data. The values of ΔE (figure 4.12) for the diffusion at 11.3 MPa of helium, atmospheric pressure, and 11.3 MPa of argon are 103, 99, and 96 kcal/mol respectively. If the lowest temperature point (89 °C) for the diffusion at 11.3 MPa of argon is omitted, ΔE is 81.3 kcal/mol and r^2 improves from 0.965 to 0.989 in the Arrhenius fit. The concentration of helium and argon in PS is a function of temperature as well as pressure. The fact that the ΔE values are the same for the case of helium at 11.3 MPa and the case of atmospheric pressure is expected because in these experiments the concentration of gas in the PS is negligible in the entire temperature and pressure range studied. At 11.3 MPa of argon pressure, however, the lower apparent activation energy is due to the increase in the concentration of argon in PS associated with the decrease in temperature. Thus the degree of plasticization increases with decreasing temperature. Similarly, Wang et al.[5] described enhanced plasticization of PS at lower temperatures with isobaric CO_2 pressure.

The diffusion coefficients found at 11.3 MPa of helium, atmospheric pressure, and 11.3 MPa argon can also be used to estimate the shift in T_g produced by hydrostatic

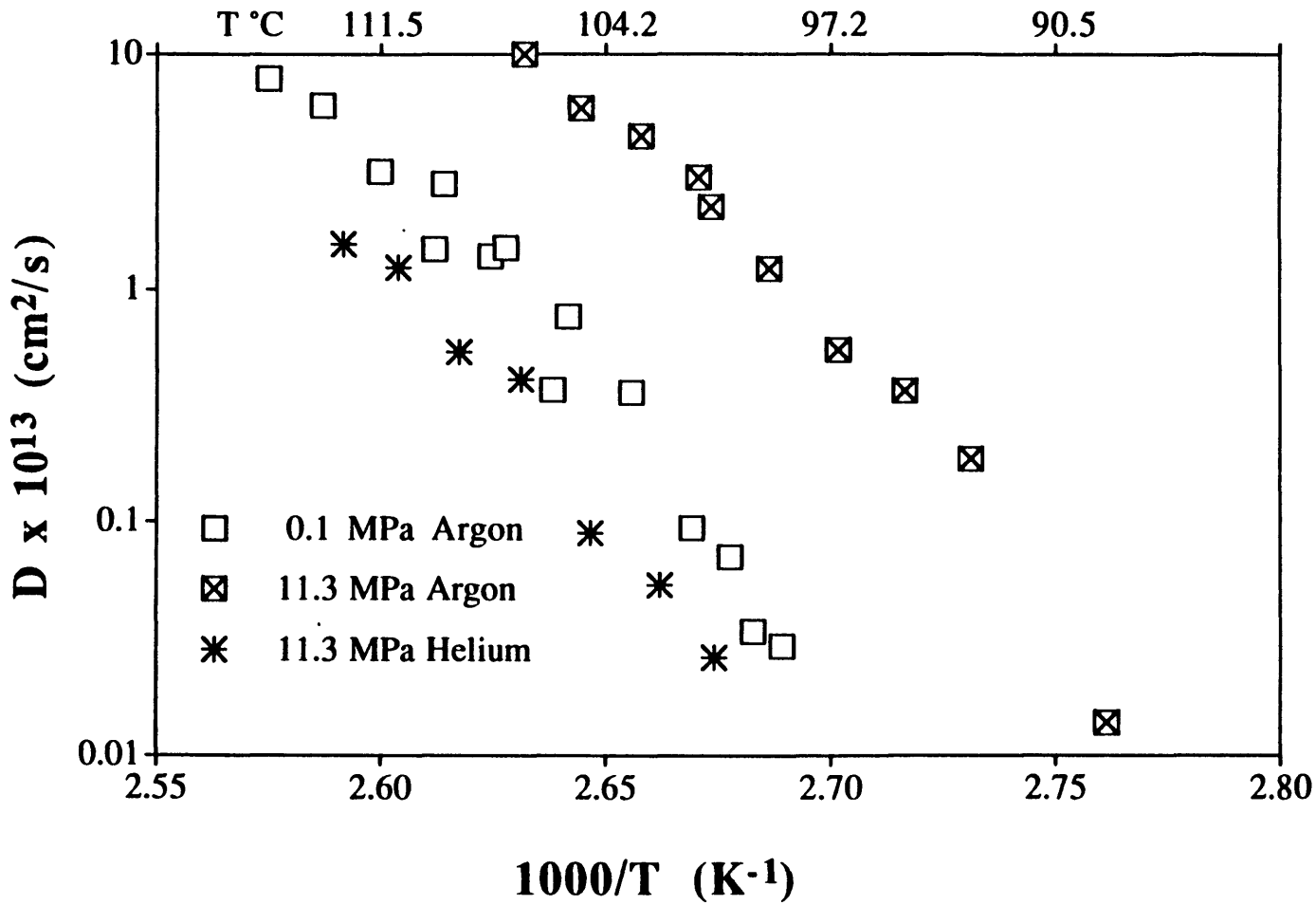

Figure 4.11 Semilog plot of D vs. 1000/T for samples with 11.3 MPa of helium pressure, atmospheric pressure, and 11.3 MPa of argon pressure.

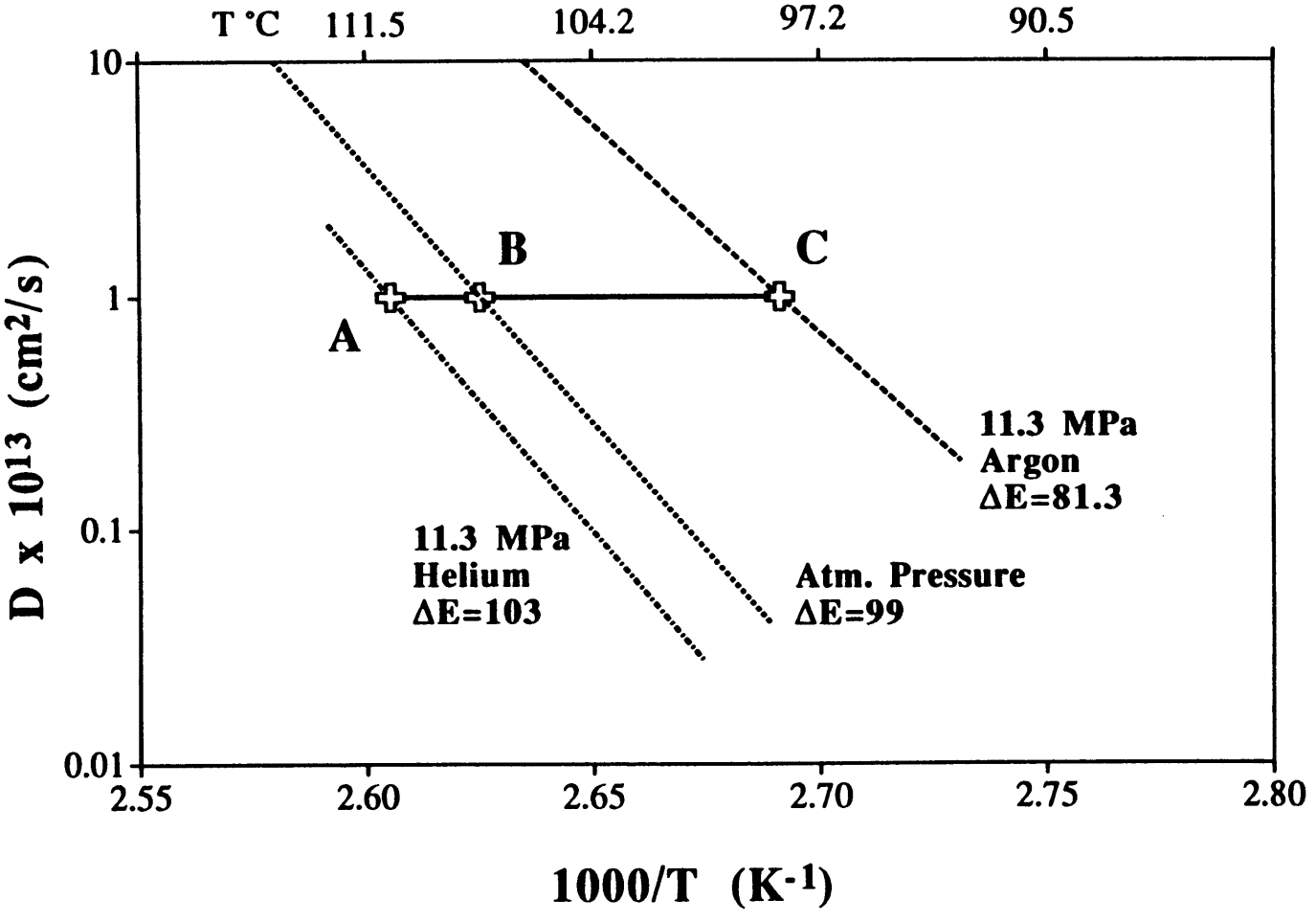

Figure 4.12 Best fits of Arrhenius equations to the data in figure 4.11. The solid line is drawn for D = 1 x 10^{-13} cm^2/s and the labeled crosses mark the intersection of this line with the Arrhenius fits.

pressure effect as well as by plasticization in the temperature range of the experiments. Either gas at atmospheric pressure, and helium at higher pressures, is considered effectively insoluble in PS. The upward shift in T_g produced by 11.3 MPa of hydrostatic pressure is determined from the increase in temperature required to obtain the same diffusion coefficient for a sample held at 11.3 MPa of helium compared to a sample held at atmospheric pressure. This temperature difference can be found from the points where the solid line drawn in figure 4.12 at a constant value of $D = 1 \times 10^{-13}$ cm^2/s intersects the Arrhenius fits to the diffusion coefficient data for the samples held at 11.3 MPa of helium and atmospheric pressure (segment $\overline{AB}$ in fig 4.12). The upward shift in T_g produced by 11.3 MPa of hydrostatic pressure is about 3 °C, which leads to a value of $\Delta T_g/\Delta P = 0.27$ degrees/MPa. This value agrees well with dTg/dP = 0.30 degrees/MPa reported by Gee.[4] The downward shift in T_g produced by dissolved argon acting as a plasticizer is determined from the temperature decrease required to obtain the same diffusion coefficient for a sample held at 11.3 MPa of argon compared to a sample held at 11.3 MPa of helium. This temperature difference is found from segment $\overline{AC}$ in figure 4.12. This downward shift in T_g produced by argon plasticization at this pressure and temperature is 12 °C.

The diffusion coefficient for dPB in PS is a sensitive probe of the mobility of the PS matrix into which it is penetrating. The experiments at 11.3 MPa of helium show that pressure or negative mean normal stress increases T_g and decreases D. It is probable that positive mean normal stress (triaxial tension) increases D and decreases T_g. During the tensile deformation of blends of a few volume percent low molecular weight polybutadiene (PB) and polystyrene at room temperature, the PB locally diffuses into PS in the neighborhood of crazes where the PS is under significant positive mean normal stress.[15, 16] An estimate for the diffusion coefficient for the PB in the PS craze material is 3×10^{-12} cm^2/s,[1] the same order of magnitude as the diffusion coefficients found near the glass transition temperature of PS in this study. If the PB molecule is acting as a probe of

PS matrix dynamics, then the deforming PS in the vicinity of a craze, at room temperature but under large positive mean normal stress, is as mobile as unstressed PS at much higher temperatures .

4.5 Summary

The solubility of 3000 g/mol perdeuterated polybutadiene in polystyrene is not a function of helium or argon gas pressure within the error of our experiments The diffusion coefficient for dPB in PS was found to be a sensitive probe of PS mobility. D decreased with increasing helium pressure because the effectively insoluble helium acts only to produce hydrostatic pressure which is known to increase T_g and decrease PS mobility. $\Delta T_g/\Delta P$ found from the diffusion coefficient data agreed well with the value of dT_g/dP reported by Gee[4] in this pressure range. D increased with increasing argon pressure because of plasticization effects. The concentration of dissolved argon in PS increases with pressure from atmospheric pressure to 11.3 MPa, and the resulting plasticization dominates the hydrostatic pressure effect to decrease T_g increase PS mobility and increase D.

4.6 References for Chapter 4

(1) Nealey, P. F.; Cohen, R. E.; Argon, A. S. *Macromolecules* **1993**, *26*, 1287-1292.

(2) Ehlich, D.; Sillescu, H. *Macromolecules* **1990**, *23*, 1600-1610.

(3) Kim , H.; Waldow, D. A.; Han, C. C.; Tran-Cong, Q.; Yamamoto, M. *Polymer Communications* **1991**, *32*, 108-114.

(4) Gee, G. *Polymer* **1966**, *7*, 177-191.

(5) Wang, W. V.; Kramer, E. J.; Sachse, W. H. *J. Polym. Sci. Polym. Phys. Ed.* **1982**, *20*, 1371-1384.

(6) Cheng, P. L. Ph D Thesis, Massachusetts Institute of Technology, 1986.

(7) Green, P. J.; Mills, P. J.; Kramer, E. J. *Polymer* **1986**, *27*, 1063-1066.

(8) Mills, P. J.; Green, P. F.; Palmstrøm, C. J.; Mayer, J. W.; Kramer, E. J. *Appl. Phys. Lett.* **1984**, *45*, 957-959.

(9) Feldman, L. C.; Mayer, J. W. ; ; Elsevier Science Publishing Co., Inc.: New York, New York, 1986.

(10) Doolittle, L. R. *Nucl. Inst. Meth.* **1985**, *B9*, 344.

(11) Doolittle, L. R. *Nucl. Inst. Meth.* **1986**, *B15*, 227.

(12) Guggenheim, E. A. ; Fifth ed.; North-Holland Publishing Company: Amsterdam, 1967.

(13) *Polymer Handbook*; Third ed.; Brandrup, J.; Immergut, E. H., Ed.; John Wiley &Sons: New York, 1989.

(14) Crank, J. ; 2nd ed.; Oxford University Press: Oxford, U.K., 1975.

(15) Argon, A. S.; Cohen, R. E.; Gebizlioglu, O. S.; Brown, H. R.; Kramer, E. J. *Macromolecules* **1990**, *1990*, 3975-3982.

(16) Gebizlioglu, O. S.; Beckam, H. W.; Argon, A. S.; Cohen, R. E.; Brown, H. R. *Macromolecules* **1990**, *23*, 3968-3974.

Chapter 5

Limited Supply Non-Fickian Diffusion in Glassy Polymers

5.1 Abstract

Non-Fickian diffusion of a flame retardant plasticizer, resorcinol bis(diphenyl phosphate) (RDP) in a glassy polyetherimide (Ultem™) was measured with Rutherford Backscattering Spectroscopy (RBS). Volume fraction versus depth profiles were obtained as a function of time, temperature, and externally applied stress in experiments where a limited supply of RDP was initially present on the surface of the Ultem™. The profiles of the plasticizer in the glassy polymer in all samples had sharp diffusion fronts with constant volume fraction behind the front. The limited supply boundary condition requires that the volume fraction, ø, of RDP in the plastized zone decrease as penetration depth increases. Isochronal values of ø decrease with increasing temperature. At long times, ø approaches a value such that the material in the plasticized zone has a glass transition temperature equal to the temperature of the experiment. At 140, 160, and 180 °C, ø decreased in direct proportion to the log of time. At 120 °C, two regimes of diffusion behavior were observed in a plot of ø versus the log of time. Short time, high ø behavior corresponds to case II diffusion, and long time, low ø behavior corresponds to anomalous diffusion. Only the anomalous regime was observed at the higher temperatures. Externally applied biaxial tensile or compressive stresses of order 10 to 40 MPa in the plane of the sample had no effect on the diffusion at 120 °C in experiments lasting 1 or 72 hours.

5.2 Introduction

A central process in a recently reported toughening mechanism observed in blends of a few volume percent low molecular weight polybutadiene rubber (PB) and high molecular weight glassy polystyrene (PS) is the diffusion of PB into PS in the immediate vicinity of crazes.[1,2] According to a previously proposed model, randomly dispersed pools of phase separated PB approximately 0.1 μm in diameter are tapped by crazes as they grow. A limited supply of PB wets the PS craze surfaces and diffusion is accelerated by positive mean normal stress which is present locally in these regions during the deformation process. The chemical potential of the PB dissolved in PS is altered by the presence of the stress field, and the solubility of PB in PS is increased.[3,4] Thus one effect of the stress field is to create a greater driving force for diffusion. The material that is drawn into crazes is plasticized and crazing occurs at a lower flow stress than in the homopolymer, ultimately resulting in larger strains to fracture and increased toughness. Diffusion is clearly the limiting process in this mechanism because the increased toughness of these blends disappears at high strain rates, low temperature, or when a higher molecular weight PB is used. Based on measured craze velocities at 25 °C[5] and a characteristic length in the system of 10 nm, the diameter of a craze fibril, the required diffusion coefficient for the PB in PS to account for the toughening mechanism must be of order 10^{-12} cm^2/s at room temperature. Tracer diffusion coefficients for 3000 g/mole PB in PS do not attain this magnitude until the temperature of the system is approximately 115 °C, well above the T_g of PS.[6] Perhaps a non-Fickian diffusion mechanism can account for the flux of PB into PS necessary to locally plasticize the material drawn into crazes. This scenario is closely related to Brown's model[4] for environmental craze growth in polymers.

Many plasticizer/glassy polymer systems have been studied which exhibit non-Fickian diffusion behavior. The history of experimental and theoretical developments in this field are documented quite well in a number of recent publications.[7-12] In all of these

studies, the polymer is in contact with an infinite reservoir of the plasticizer at constant activity. Under this boundary condition, the transport is characterized by an induction period followed by the formation of a diffusion front with a steep concentration gradient between swollen and unswollen material. The front propagates at a constant velocity and the mass uptake of penetrant is linear with time. Essentially the concentration behind the diffusion front is constant and equal to the equilibrium swelling ratio. The process zone in non-Fickian diffusion lies immediately ahead of the sharp interface. In this zone, entangled polymer chains are constrained in the unperturbed glassy polymer but are in close proximity to very mobile chains in the swollen plasticized material. Stresses on the order of the yield stress of the polymer can be generated in the glassy material just ahead of the diffusion front. The stress drives the diffusion and the time dependent mechanical response of the polymer is the rate controlling step.[13] The critical roles that stress and plasticization play in non-Fickian diffusion motivate us to explore the relevance of this mechanism to the diffusion process in the locally plasticized toughened PB/PS blends mentioned above.

Non-Fickian diffusion has been modeled by a number of groups for the boundary condition of an infinite supply of plasticizer in contact with the glassy polymer.[7-14] We will focus on models based on the work of Thomas and Windle[8,9,12,13] which appear to capture the fundamental aspects of non-Fickian transport. The Thomas and Windle model successfully incorporates the ideas that the diffusion is driven by the stress generated ahead of the diffusion front and is controlled by the creep deformation of the polymer. The stress is calculated with an osmotic pressure analogy and the creep deformation of the polymer is considered to be dependent on the elongational viscosity, η. Both the viscosity and the diffusion coefficient in the flux equation are strongly dependent on the local volume fraction of penetrant. Thus the diffusion coefficient and the physical properties of the polymer change dramatically across the narrow interface between the swollen, plasticized material and the unswollen glassy substrate.

Hui et al.[8,9] developed a model based on the work of Thomas and Windle[13] for the infinite supply reservoir boundary condition which is particularly useful for comparison to our limited supply non-Fickian diffusion problem. It is useful because many of the observable non-Fickian diffusion characteristics are described in terms of the volume fraction of the plasticizer, ø, in the plasticized zone, a parameter that we can measure in our experiments. In this study with a limited supply of plasticizer, ø is a function of penetration depth. Hui et al.[8,9] described in more detail the initial stages of non-Fickian diffusion, and defined a critical volume fraction, $ø_c$, below which the characteristic diffusion front will not form. As the ratio of $ø/ø_c$ (>1)increases, they calculate that the natural logarithm of the diffusion front velocity increases rapidly for ø slightly greater than $ø_c$, but that the rate of increase decreases for higher values of ø. The model of the Hui. et al. is compared quantitatively to diffusion profiles of iodohexane in polystyrene which were determined with Rutherford Backscattering Spectroscopy.

The integral sorption Deborah number, De, as defined by Wu and Peppas[12] provides an insightful means to understand transitions in diffusion behavior. Qualitatively, De is the ratio between the characteristic relaxation time of the glassy polymer and the characteristic time for diffusion in the plasticized zone. If De<< 1, then the diffusion mechanism will be Fickian. Non-Fickian diffusion behavior occurs when De is of order 1 and greater. De of order 1 is called anomalous diffusion, and De>>1 is called case II diffusion.

The goal of the present work is to observe non-Fickian diffusion of a model plasticizer in a glassy polymer when the plasticizer is present in limited supply in order to gain insight into the diffusion process of the toughening mechanism. The system we have chosen to investigate consists of a stable non-volatile plasticizer, resorcinol bis-(diphenyl phosphate)(RDP), and a glassy polyetherimide(Ultem™). Experiments were performed in the range of 120 to 160 °C, 95 to 55 °C below the T_g of Ultem™. At the end of each experiment the specimen was quenched to room temperature to 'freeze' the concentration

versus depth profiles. The profiles are determined via Rutherford Backscattering Spectroscopy in which the phosphorous atoms of the RDP provide an excellent tag to monitor the plasticizer volume fraction as a function of depth. The diffusion was measured as a function of time, temperature, matrix properties, and externally applied biaxial compressive and tensile stresses. The results for the limited supply boundary condition experiments are interpreted in terms of non-Fickian diffusion theory as developed for the infinite reservoir boundary condition.

5.3 Experimental

Materials

The glassy polymer employed in this study is a polyetherimide known as Ultem™ 1000 (Ultem™). The polymer was supplied by General Electric Company in pellet form. The chemical structure is shown in figure 5.1. Ultem™ was chosen because it has a high glass transition temperature (~215 °C) and is resistant to crazing[15]. The plasticizer chosen for this study is resorcinol bis-(diphenyl phosphate) (RDP). This flame retardant plasticizer, known as Fyrolflex RDP, was supplied by Akzo Chemicals Inc. in the form of a viscous liquid (~600 cp at 20 °C). The chemical structure of the compound is shown in figure 5.2. Approximately 70% of the material is the dimer where n=1, and the rest is higher order oligomers and a few percent triphenyl phosphate. This product is non-volatile (vapor pressure<1 mm Hg at 37.8 °C) and is stable to 370 °C.

Sample Preparation

Most of the samples were prepared in the following manner. A uniform film of Ultem™ greater than 2 μm in thickness was deposited on a piece of silicon wafer via spin coating at 1500 rpm from a 15 % by weight solution of Ultem™ in anisole. These films were dried in a vacuum oven for 8 hours at room temperature and then for 24 hours at approximately 220 °C, a temperature 5 °C above the T_g of Ultem™. The oven was then

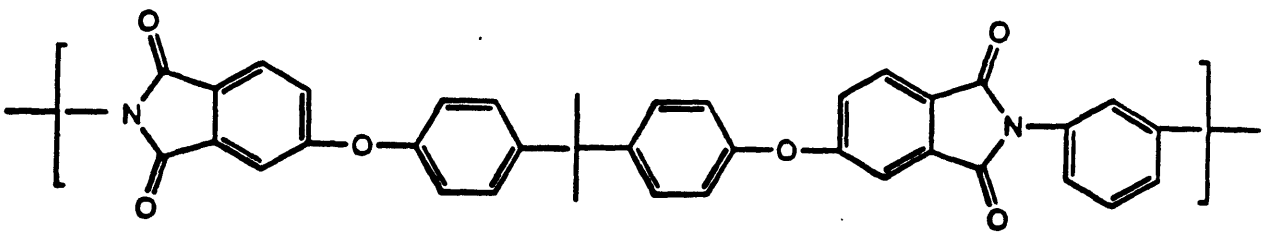

Figure 5.1 Chemical Structure of Ultem™.

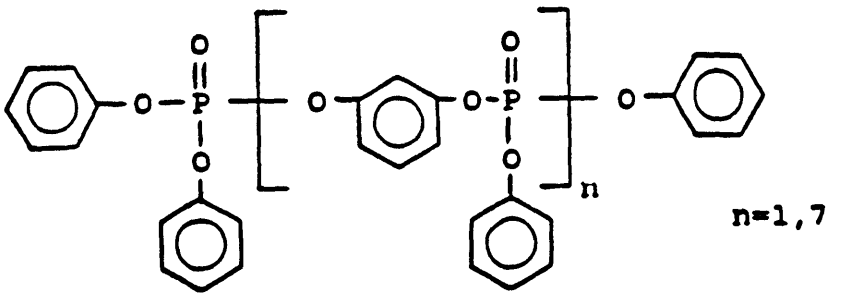

Figure 5.2 Chemical Structure of RDP.

allowed to slowly cool to room temperature over the course of about 4 hours. We tried to ensure that each sample would experience the same thermal history. Samples which were part of the same series of experiments were processed together in a single batch. Films approximately 70 nm thick which consisted of a 4:1 blend of RDP and Ultem™ were deposited on a clean glass slide via spin coating from a solution which was 4 % by volume RDP and 1 % by volume Ultem™ in anisole. Transmission electron microscopy performed on one of these films did not reveal phase separation and for the purposes of this study we consider the 4:1 blend to be homogeneous. The blended film was floated off the glass slide on to the surface of a water bath and picked up with the Ultem™ coated wafer. The bilayer samples were dried in a vacuum oven overnight at room temperature prior to placement in a thin-walled copper chamber which was subsequently immersed in an oil bath for a specific period of time. The minimum time period used in these experiments was 30 minutes to reduce the effects of temperature fluctuations which arise as the sample chamber initially heats up and the oil bath regains its steady state temperature.

Some samples were subjected to an externally applied stress in addition to being held for 1 hour or 72 hours at 120 °C. These samples were prepared from injection molded disks supplied by General Electric Company which were four inches in diameter and 1/8 inch thick. The polymer disks were sanded down to thicknesses of 0.5 to 1 mm and then polished with successively smaller diamond grit solutions starting with a 15 μm grit and ending with 1 μm. In this way bulk samples could be prepared with high quality surfaces suitable for ion beam analysis.[16] Stress was applied to the samples in a concentric ring arrangement depicted in figure 5.3. A load is applied to the smaller ring with radius R on one side of the disk and the other side of the sample is held by a larger ring with radius A. The biaxial stress, $\sigma_{biaxial}$, arises inside the smaller ring in the plane of the disk and is either compressive or tensile depending on which side of the sample is considered; $\sigma_{biaxial}$ is calculated as a function of the load, L, the reciprocal Poisson's ratio, n, the sample thickness, t, R, and A, with the following equation:[17]

$$\sigma_{rr} = \sigma_{\theta\theta} = \sigma_{biaxial} = -\frac{3L}{2\pi n t^2}\left[0.5(n-1)+(n+1)\log\left(\frac{A}{R}\right)-(n-1)\frac{R^2}{2A^2}\right] \qquad (5.1)$$

where $\sigma_{biaxial}$ is the surface stress in both the radial and tangential directions in the plane of the sample at distances less than R from the sample center. The applied stress normal to the plane of the sample, σ_{zz}, is zero. Two sample chambers with R and A equal to 11.1 and 23.8 mm, and 14.4 and 45.6 mm respectively were designed in which samples could be subjected to biaxial stresses and at the same time be immersed in an oil bath for temperature control. With these devices, loads of a few kilograms produce values of σ as high as 40 MPa. The large sample holder was used for samples in which the diffusion surface was held in tension, and the small sample holder for samples in which the diffusion surface was held in compression.

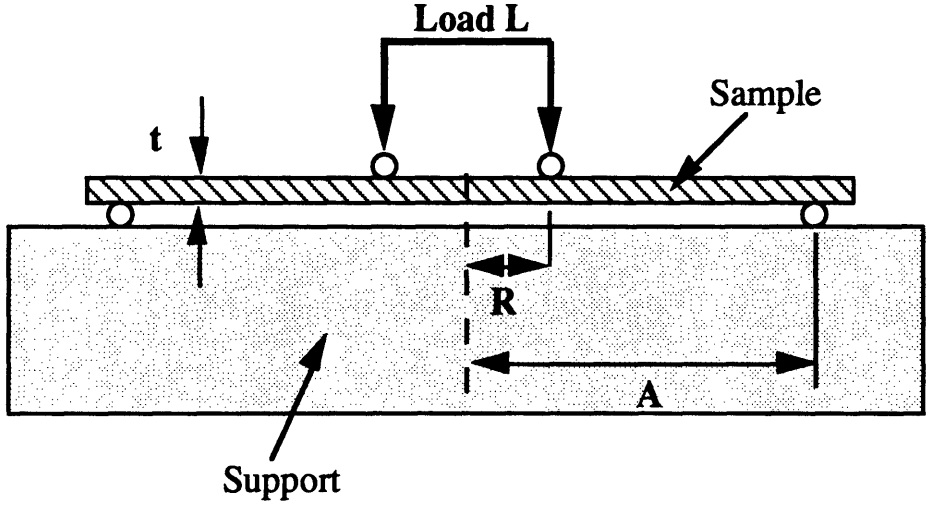

Figure 5.3 Configuration of concentric ring stress experiments.

Rutherford Backscattering Spectroscopy

All of the samples were analyzed with Rutherford Backscattering Spectroscopy(RBS) at the Cambridge Accelerator for Materials Science located at Harvard University. The model system of RDP and Ultem™ was chosen to allow the determination

of the phosphorous concentration as a function of depth which can be directly correlated to the volume fraction RDP in Ultem™ based on knowledge of the chemical formulae and densities of the species involved. We employed a 2 mm beam of 2 MeV alpha particles($4He^+$) which was directed normal to the sample surface. With an annular silicon surface barrier detector and a multichannel analyzer, the backscattered alpha particles in a subtended solid angle of 14.2×10^{-3} steridians centered at 176° from the incident beam were counted as a function of energy. The beam dose for all of the samples was 15 μC. The resolution in the experiments was 20 keV. Details of this experimental technique are described elsewhere.[18,19]

Differential Scanning Calorimetry

Bulk blended specimens which contained from 0 to 30 % by weight RDP in Ultem™ were prepared via evaporation of solvent from solutions of RDP and Ultem™ in methylene chloride. Solutions of approximately 10 % by weight polymer were poured into one inch diameter weighing pans and allowed to slowly evaporate over the course of a week in a partially sealed chamber. The samples were then dried in air for a few days, and finally in a vacuum oven at room temperature for more than one week. The specimens had thicknesses of approximately 0.5 mm. Glass transition temperatures for the blends were determined from Differential Scanning Calorimetry (DSC) experiments on a Perkin-Elmer model DSC7 operated at 20 °C/min in scans from 50 to 250 °C.

5.4 Results

Figure 5.4 shows the results from the DSC experiments on static cast homogeneous blends of RDP and Ultem™. As the volume fraction of RDP is increased from 0 to 0.3, the single glass transition temperature of the blended RDP/Ultem™ material decreases monotonically from 215 to 90 °C.

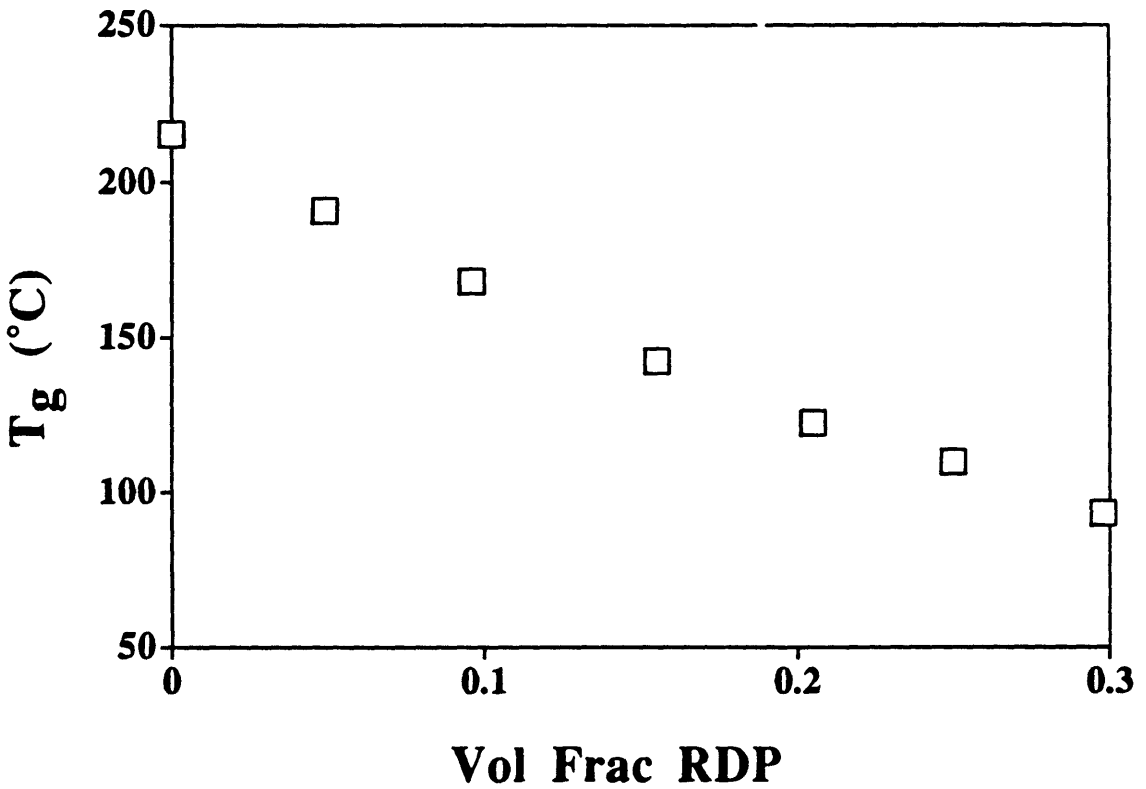

Figure 5.4 Glass transition temperature as a function of volume fraction RDP.

Typical RBS data from a sample held for 4.5 hours at 140 °C is shown in figure 5.5. Helium ions backscattered from elastic collisions with phosphorous atoms on the surface of the sample in the configuration of our experimental setup are detected at an energy of 1.19 MeV. The data at energies immediately lower than 1.19 MeV are from helium ions backscattered from phosphorous atoms below the surface of the sample; decreasing energy corresponds to increasing depth. Here an energy of 1.10 MeV in the phosphorous peak is equivalent to a depth of 275 nm. The data at energies below 0.75 MeV are a result of backscattered helium ions from oxygen, nitrogen, and carbon atoms in the sample. Since RDP is the only species in the sample which contains phosphorous, the yield of backscattered helium ions from collisions with phosphorous is directly proportional to the volume fraction of RDP in the sample. Thus a volume fraction versus depth profile of RDP in Ultem™ is obtained in the RBS experiments. The profile in figure 5.5 shows that the limited supply of RDP initially on the surface has penetrated into the initially homogeneous Ultem™ layer and a sharp diffusion front exists at a depth of 275 nm between swollen and unswollen material. The width of the interface is less than the 50 nm, the depth resolution of the technique. The concentration of RDP in the plasticized zone is constant within the experimental error. The normalized yield of backscattered helium from phosphorous atoms corresponds to a volume fraction of RDP in Ultem™ equal to 0.26 in the swollen layer. The existence of the sharp diffusion front with a constant concentration behind the front is indicative of non-Fickian diffusion.[8,13] If the diffusion were Fickian, the concentration versus depth profiles would resemble complementary error functions.[6,20] The shape of the profile shown in figure 5.5 is typical of all the samples analyzed in this study.

The solid line in figure 5.5 represents the best least squares fit of a simple model to the data. The model assumes that a step function in RDP volume fraction is formed via diffusion into the initially homogeneous Ultem™ substrate. The step function is convoluted with a gaussian function whose full width at half maximum is 20 keV, the

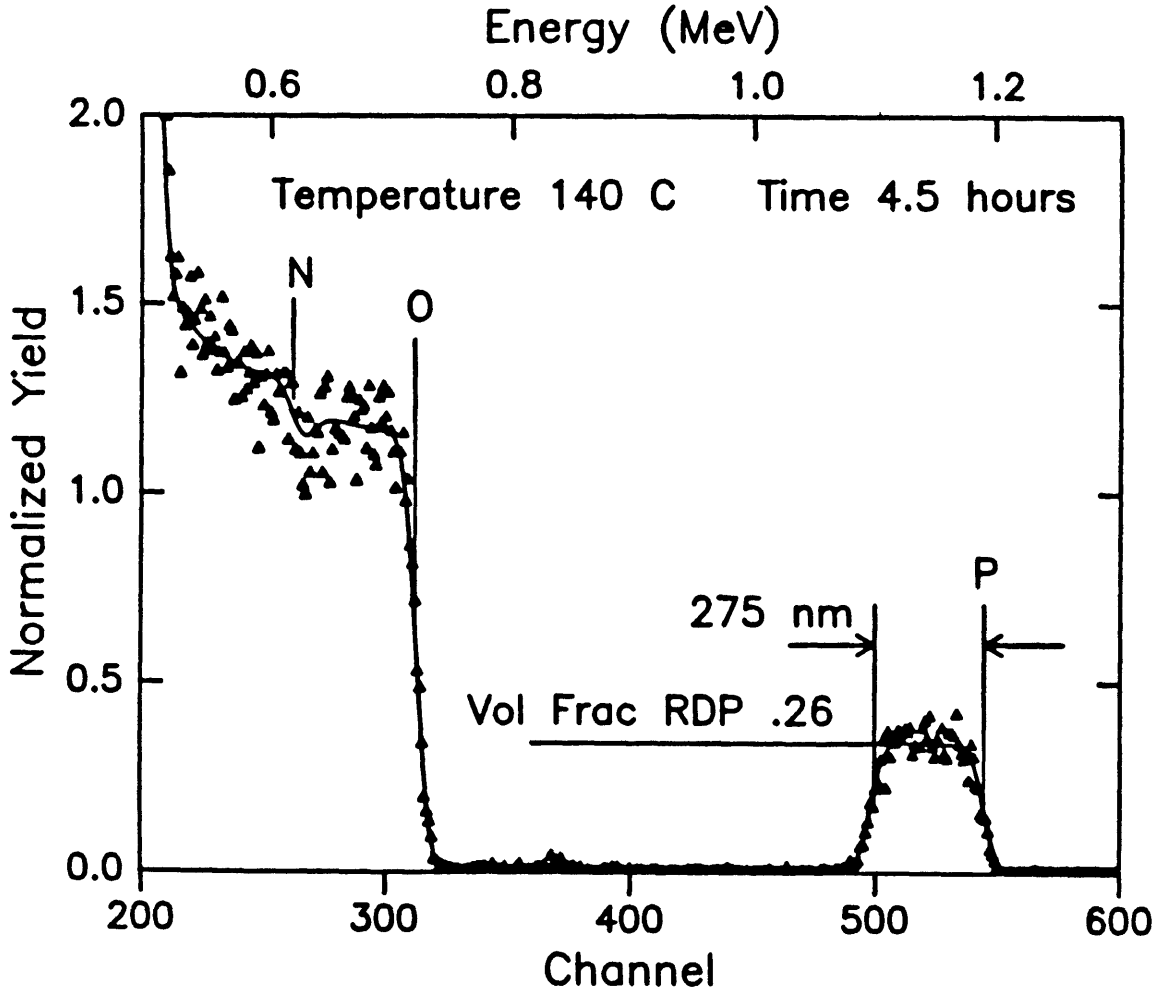

Figure 5.5 Typical RBS data for a sample held 4.5 hrs at 140 °C.

known resolution of the experiment, and the result is fit to the RBS data. The convolution with the gaussian function is responsible for the rounding of the step function edges. The gaussian function is determined independently and should not be considered a fitting parameter. Only the penetration depth and the volume fraction of RDP in that in the step function are varied to obtain the best two parameter fit. Data between about 0.5 and 0.7 MeV are used to normalize the yield or volume fraction axis for small errors in measured beam dose from sample to sample. These fits are performed with the aid of the RUMP software package developed at Cornell University.[21,22] The software was purchased from Computer Graphics Service in Lansing, NY. The program performs complex interactive fits to RBS data given the specific parameters of the experimental configuration and the physical and chemical properties of the species in the sample description.

Figure 5.6 shows the effect of changing the quantity of RDP in the limited supply boundary condition. Only the phosphorous peak is plotted with the axes labeled in terms of depth and volume fraction RDP. Each sample was held for 1 hour at 140 °C. One of the samples had twice as much RDP present initially on the sample surface. This was accomplished by simply picking up two RDP/Ultem™ supply films from a water bath as described above. The penetration depth of RDP in the sample with twice the supply of RDP present is almost but not quite twice that of the sample with the single supply layer. A higher volume fraction of RDP in the plasticized zone in the double supply layer sample is therefore also observed. This indicates that diffusional resistance in the swollen layer is an important component of diffusion front propagation at this time and temperature.

Figure 5.7 shows the RBS data for a series of samples which were held for 20 hours at temperatures which ranged from 120 to 180 °C. Only the phosphorous peak is plotted from the RBS data with the axes labeled in terms of depth and volume fraction RDP. In each sample, a sharp diffusion front exists between an unswollen homogeneous Ultem™ layer and a swollen layer with a constant concentration of RDP. The depth of penetration of the front into the initially pure Ultem™ layer increases as the temperature

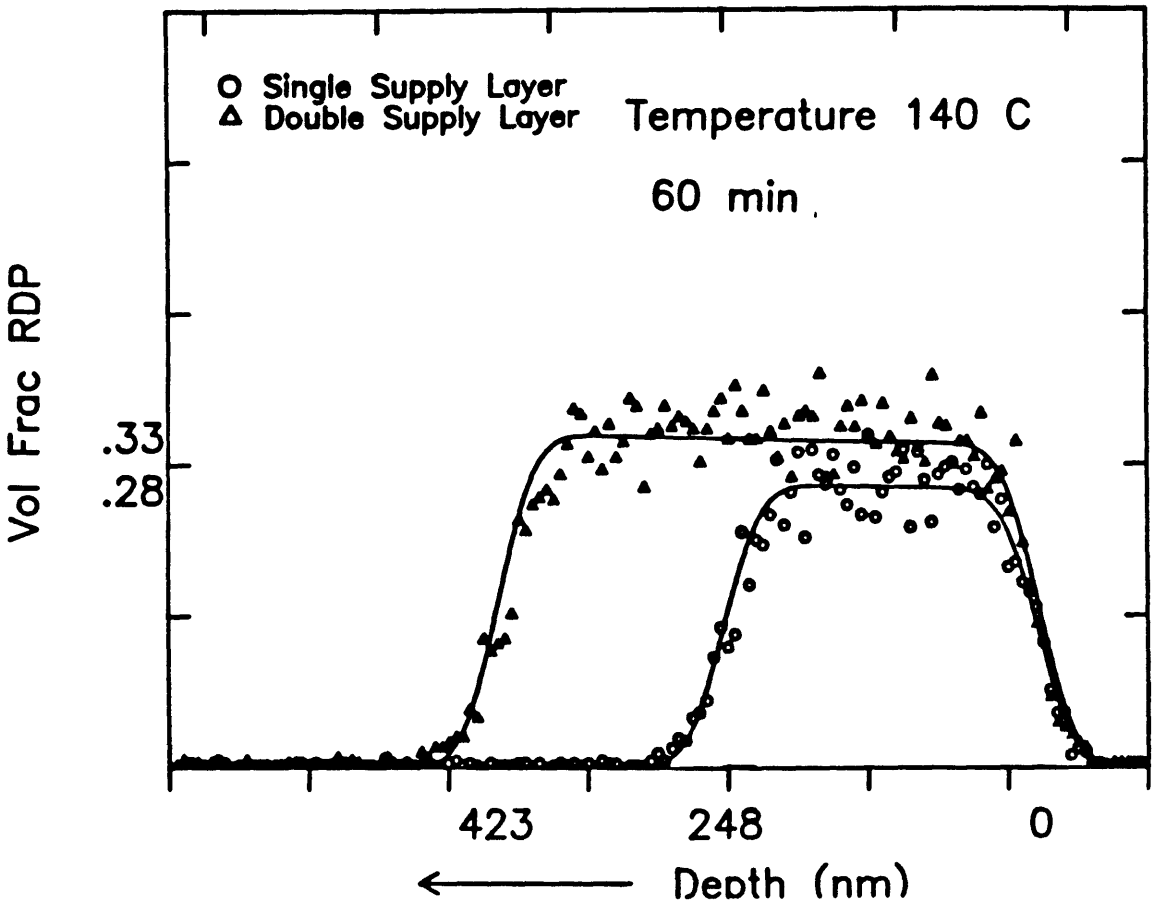

Figure 5.6 RBS data for single and double supply layer samples held fpr 60 minutes at 140 °C.

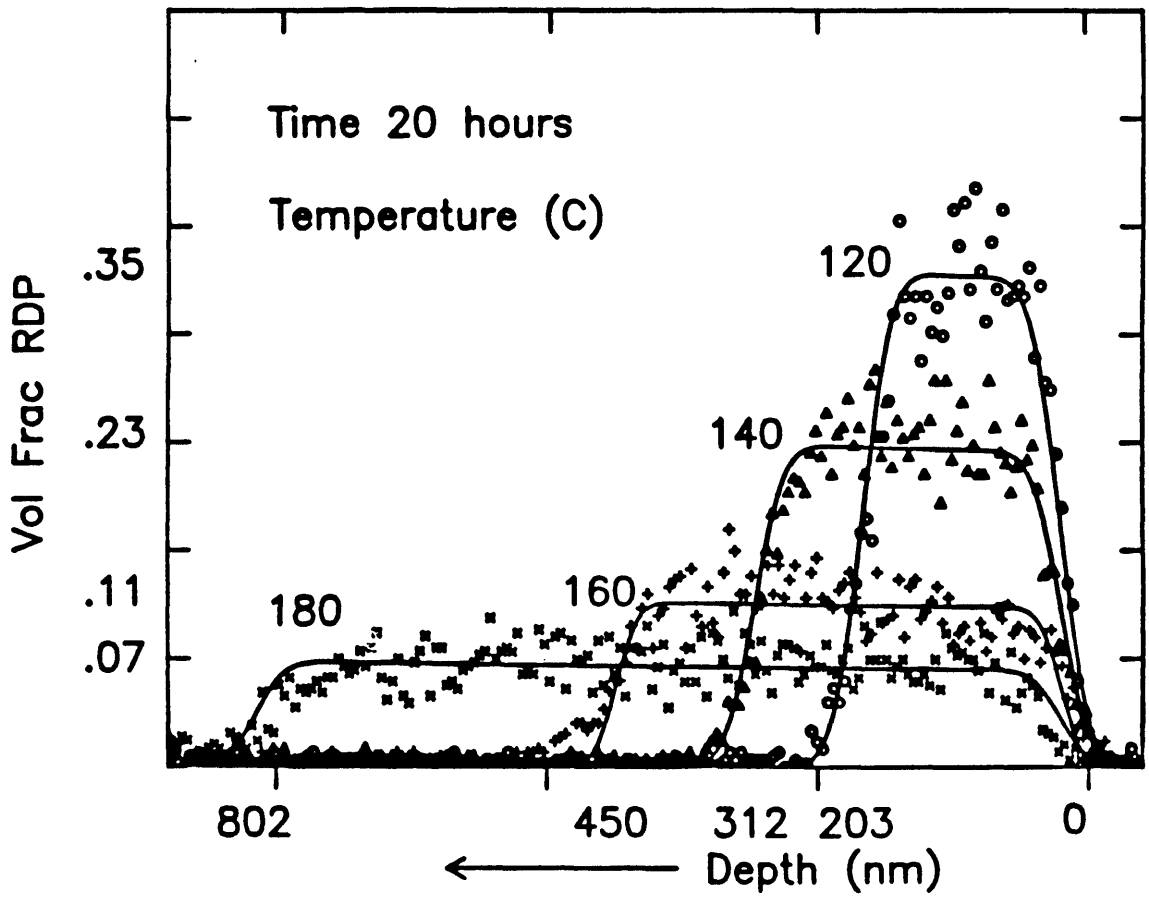

Figure 5.7 RBS data for samples held 20 hours at 120, 140,160, and 180 °C.

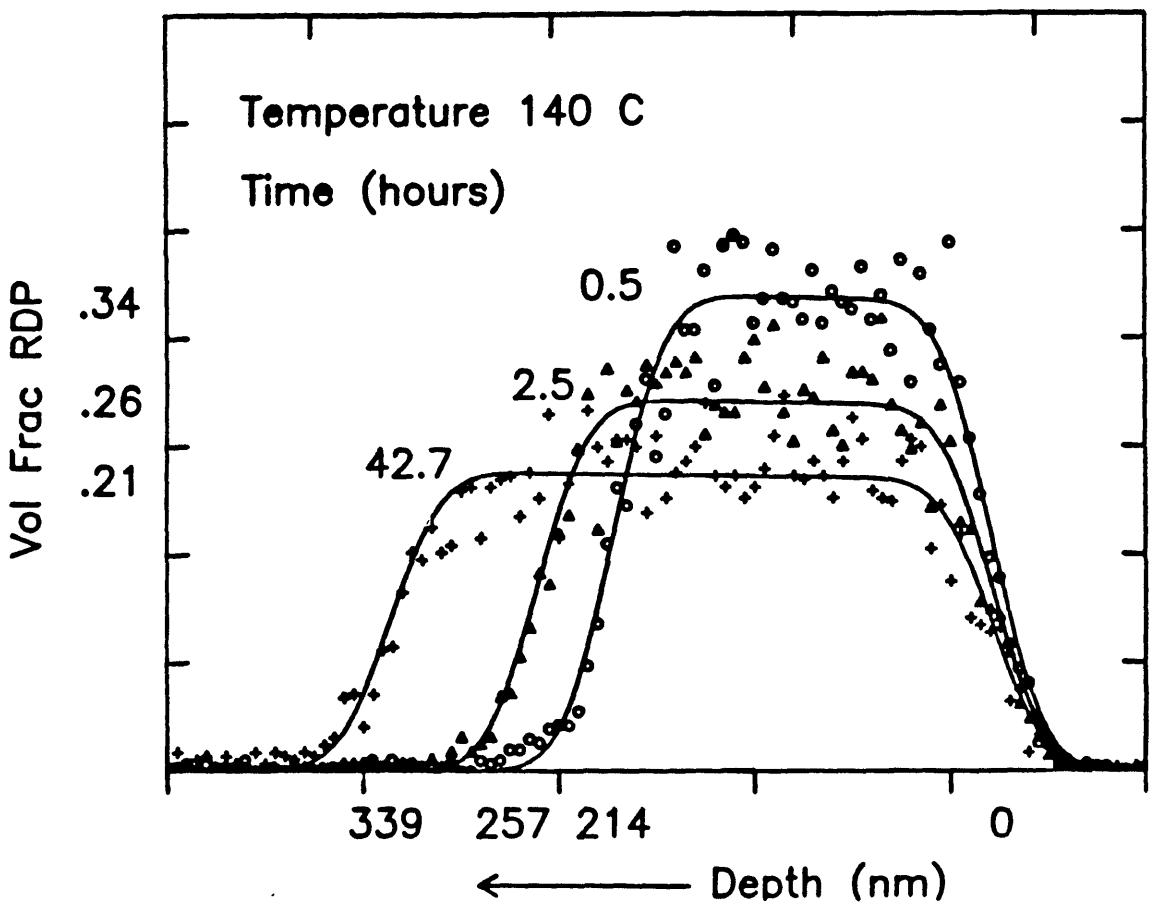

Figure 5.8 RBS data for samples held at 140 °C for 0.5, 2.5, and 42.7 hours.

increases. Each sample had approximately the same limited supply of RDP, and thus by the conservation of mass, the further the penetration the lower the volume fraction of RDP in the swollen layer.

In another series of samples, the temperature was held at 140 °C and the treatment time was varied from 0.5 to 42.7 hours. The phosphorous peaks of the RBS data from these samples are plotted in terms of volume fraction RDP versus depth in figure 5.8. The depth of penetration of the RDP diffusion front increases as the time of the experiment increases. However, the penetration depth clearly does not increase linearly with time. The front position changes from 214 nm to 257 nm for 0.5 to 2.5 hours, and then only reaches a value of 339 nm after 42.7 hours. A plot of the volume fraction RDP versus time for samples held from 0.5 hours to 72 hours at temperatures of 160 and 180 °C is shown in figure 5.9. For both temperatures, the volume fraction RDP, ø, in the plasticized zone decreases rapidly at short times and then decreases at a much slower rate at long times. The glass transition temperatures found in the DSC experiments are plotted as a function of blend composition on the right axis of figure 5.9. Notice that the slope of the volume fraction RDP data as a function of time goes to zero as ø approaches a value such that the material in the plasticized zone has a glass transition temperature equal to the temperature of the experiment. Plotted in figure 5.10 are the values of ø after 2 and 72 hours at 120, 140 , 160, and 180 °C. After 72 hours at 180 and 160 °C, the material in the plasticized zones have glass transition temperatures of approximately 180 and 160 °C respectively. The material in the plasticized zones after 72 hours at 140 and 120 °C have glass transition temperatures still well below 140 and 120 °C respectively. Significantly slower kinetics at the lower temperatures are responsible for the longer time required to reach a composition in the plasticized zone which has a glass transition temperature equal to the temperature of the experiment.

A series of experiments was performed to explore the effect of matrix properties on the propagation of the diffusion front. A two step process was used; one supply layer was

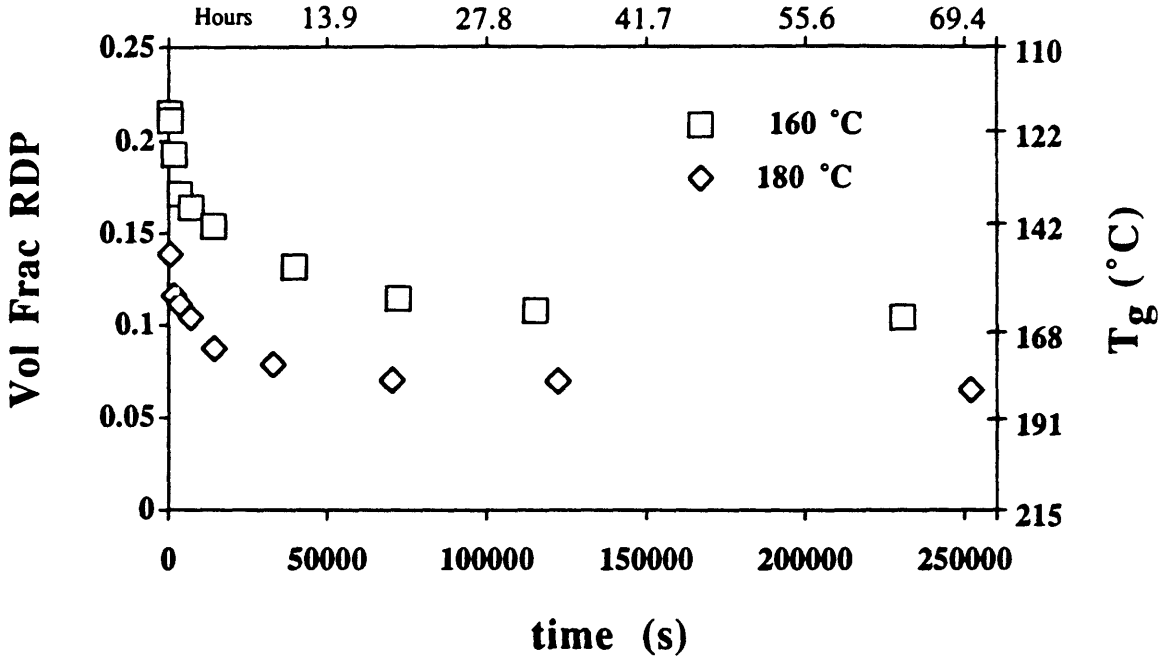

Figure 5.9 Plot of volume fraction versus time for samples held at 160 and 180 °C. T_g as a function of volume fractrion is shown on the right hand axis.

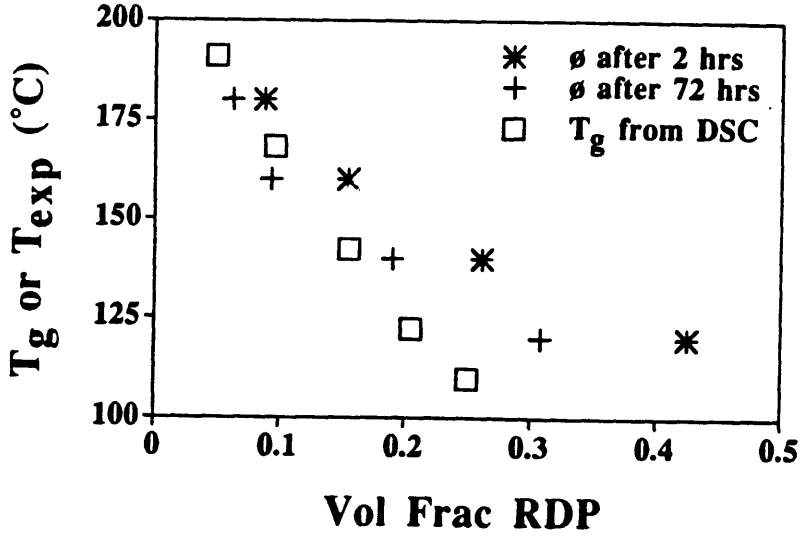

Figure 5.10 Plot of T_g, and ø after 2 and 72 hours as a function of volume fraction.

allowed to diffuse for 9 hours at 180 °C in all of the samples, and then a second supply layer was applied and allowed to diffuse for various time periods at 120 °C. RBS data and fits for two of these samples are shown in figure 5.11. A two step concentration profile is created in which the penetration to a depth of approximately 700 nm with a volume fraction RDP in the plasticized zone equal to 0.08 occurs at 180 °C, and the second front at higher volume fractions RDP is formed at 120 °C. In this process, the front which propagates at 120 °C does so in a material that is a 0.08 volume fraction blend of RDP in Ultem™. A plot of ø as a function of log time at 120 °C in pure Ultem™ is compared to ø(ln(t)) in the two step experiments in figure 5.12. Both sets of data exhibit two regimes of diffusion behavior where there is a clear change of slope in the semilog plot. At long times, the two sets of data eventually coincide and the effect of different matrix properties is minimal. At short times, however, the two sets of data diverge with an apparent shift in time and with different slopes in the data in the two regimes.

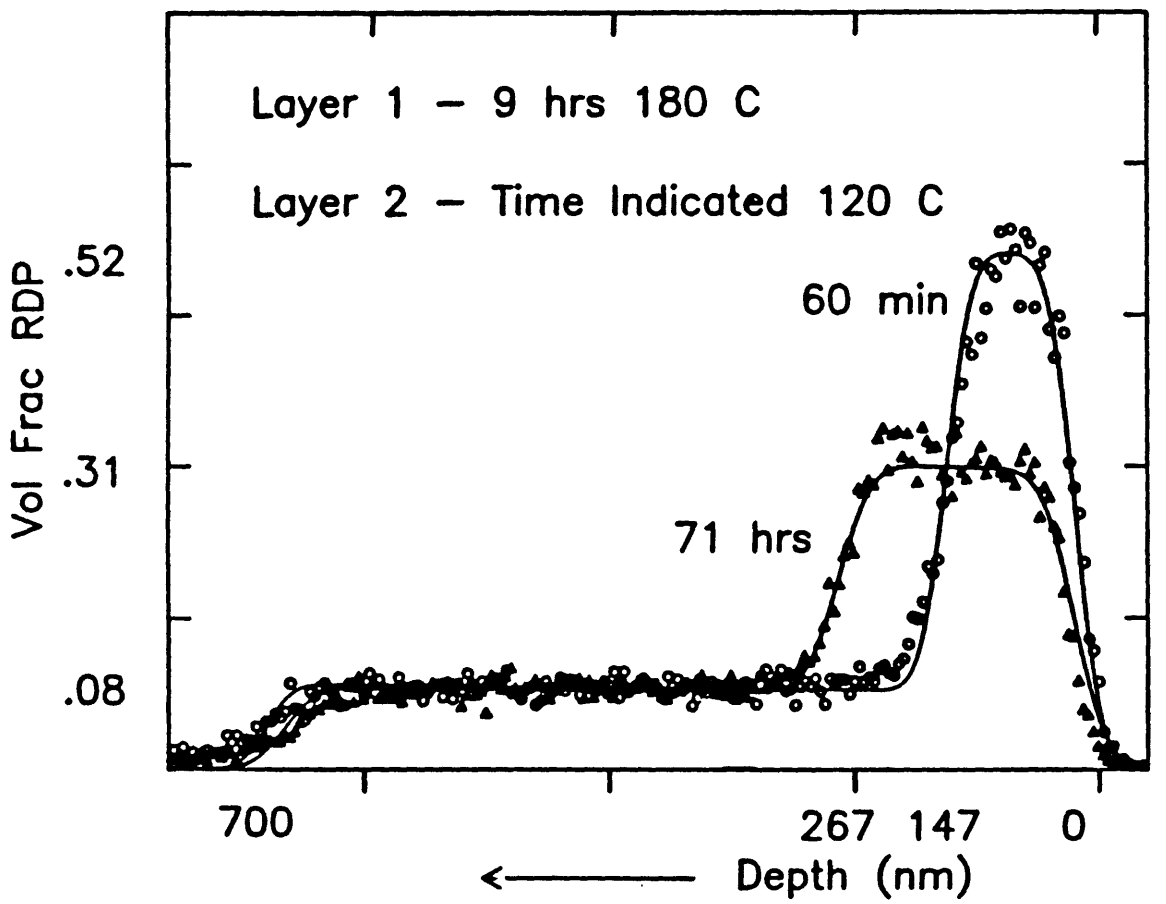

Figure 5.11 RBS data from two step diffusion experiments for samples held for 60 minutes and 71 hours at 120 °C during the second step.

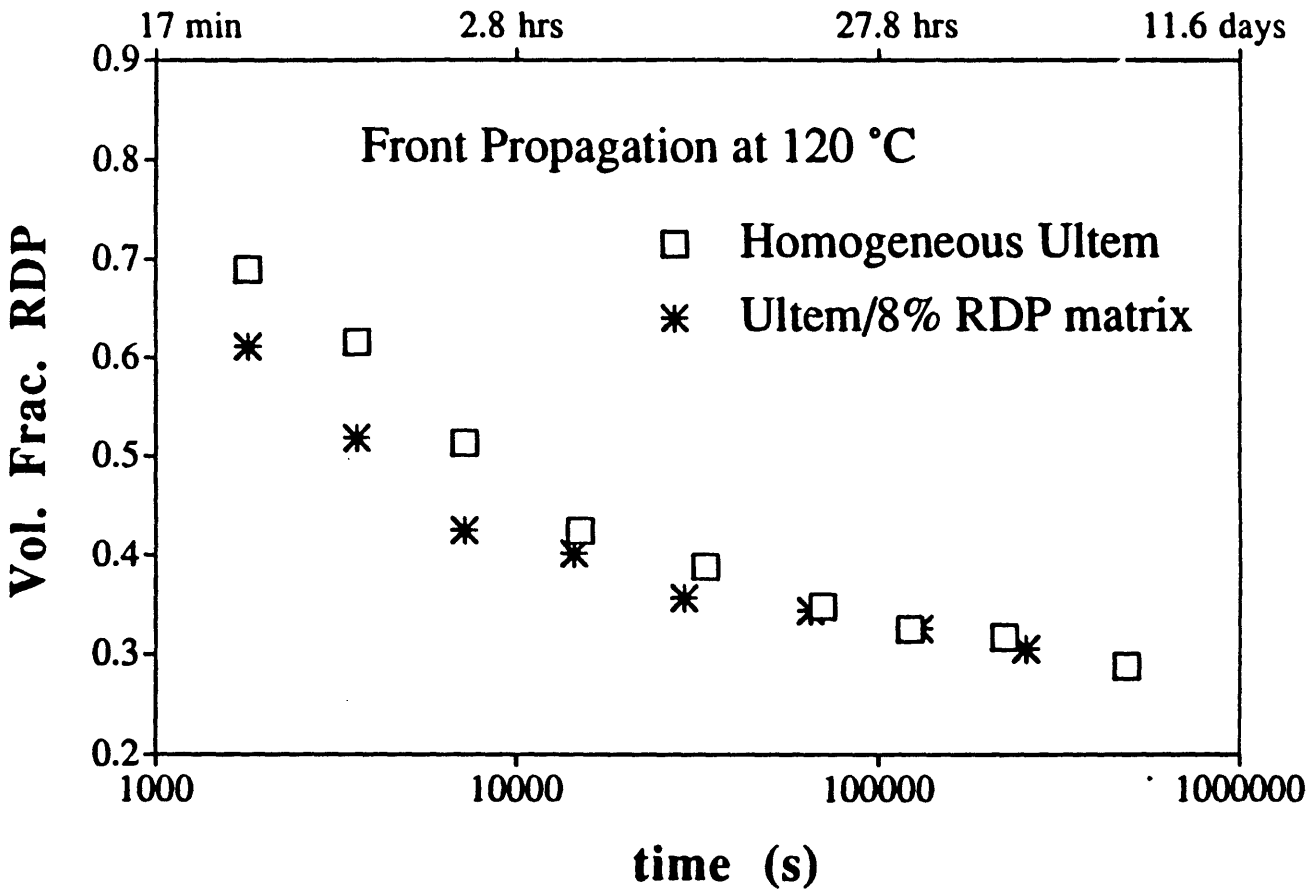

Figure 5.12 Plot of volume fraction versus log time for front propagation at 120 °C in pure Ultem™, and Ultem™ with 0.08 volume fraction RDP in the second step of the two step experiments

A summary of the results from samples which were subjected to externally applied stresses at 120 °C as described in the Experimental Section is given in Table 5.1.

Table 5.1 Results From Samples Subjected to an External Stress

Run Number	Time (hrs)	Stress (MPa) T=Tension C=Compression	Vol Frac RDP
1	72	0	0.33,0.34
		C 32.3	0.34
		T 19.8	0.28
2	72	0	0.27
		C 43.1	0.29
		T 26.7	0.27, 0.26
3	72	0	0.28
		C 12.7	0.27
		T 37.6	0.26
4	1	0	0.36, 0.35
		T 5.1	0.34
		T 9.9	0.38
		T 25.3	0.35

Despite the application of radial and tangential stresses in the plane of the sample as high as 40 MPa in tension or compression, there is no significant effect on the limited supply diffusion of RDP in Ultem™ after either 1 hour or after 72 hours.

5.5 Discussion

In order to compare the results of this investigation to previous work regarding non-Fickian diffusion in plasticizer/glassy polymer systems, we must find the means to compare diffusion with a limited supply boundary condition to diffusion with an infinite reservoir boundary condition. The differences which arise because of the boundary conditions are readily apparent. With the limited supply boundary condition, the propagation of the diffusion front is clearly not linear with time (figures 5.8 and 5.9), and the volume fraction RDP, ø, in the plasticized zone decreases with time and penetration depth. Therefore the properties of the material behind the front change with time and penetration depth. In contrast, in an infinite reservoir boundary condition, a fully developed diffusion front propagates with a constant velocity and ø does not vary with time and penetration depth. The properties of the material behind the front are constant. However, ø can be varied in the infinite reservoir experiments by changing the activity of the plasticizer in the reservoir. The front velocity, v, as a function of ø has been determined both experimentally and theoretically.[8] These results in the literature are compared to results in this study with the limited supply boundary condition by calculating an instantaneous front velocity as a function of ø in the RDP/Ultem™ system as described below.

Figure 5.13 is a plot of the volume fraction RDP in the plasticized zone at all the temperatures studied versus log time. The solid lines represent the best least squares fit of the equation,

$$\phi = -m \ln(t) + C \ , \qquad (5.2)$$

where t is the time in seconds, and m and C are constants. Equation (5.2) has been applied to the 120 °C data with different values of m and C in the two distinct regimes of behavior.

A discontinuity exists where the two solid lines meet at a volume fraction of approximately 0.43. The values of m and C for the different data sets are tabulated in Table 5.2.

Table 5.2 Values of m and C for the various data sets.

Temperature °C	m	C
120 (ø>0.43)	0.127	1.649
120 (ø<0.43)	0.039	0.794
140	0.025	0.502
160	0.019	0.33
180	0.012	0.212

Although equation (5.2) fits the experimental data quite well, it is not reported to have any physical significance.

Instantaneous front velocities are calculated as a function of ø in the following way. The conservation of mass requires that

$$\phi \bullet z = S, \tag{5.3}$$

where z is the penetration depth, and S is a constant. For the experimental data at 120 °C and 140 °C, S is equal to 72 nm ± 9 nm. The small discrepancies result from the reproducibility of sample preparation and experimental error. At 160 °C and 180 °C, the value of S systematically decreases at times greater than 4 hours from approximately 72 nm to approximately 50 nm. Perhaps there is a small evaporation rate at the higher

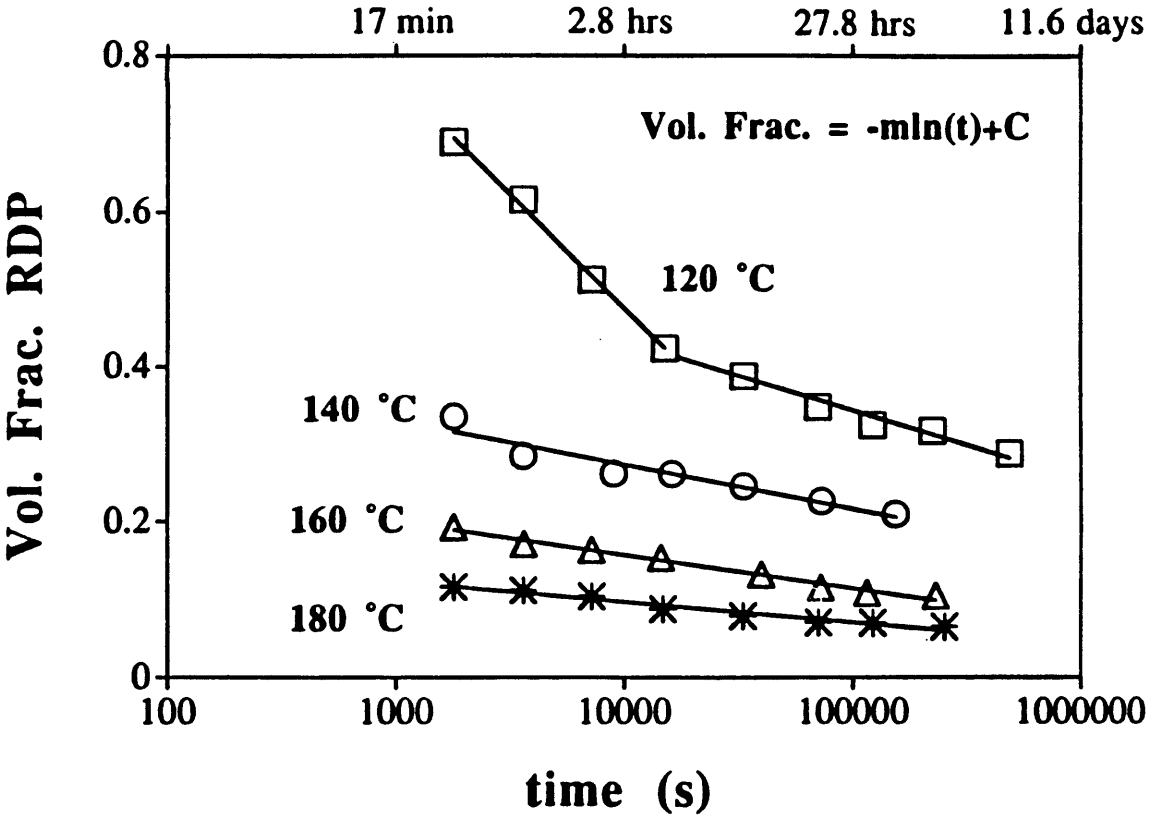

Figure 5.13 Plot of volume fraction versus log time for samples held at 120, 140, 160, and 180 °C with fits to the data of the equation ø=-mln(t)+C.

temperatures. For the purpose of the calculations, we use S=72 nm for all of the data. The instantaneous front velocity is given by

$$v = \frac{dz}{dt} = -\frac{z^2}{S}\frac{d\phi}{dt}. \tag{5.4}$$

Combining equations (5.3) and (5.4),

$$v(\phi) = \frac{S \bullet m}{\phi^2 \exp\left[\frac{C-\phi}{m}\right]}. \tag{5.5}$$

A semilog plot of the calculated instantaneous front velocities as a function the volume fraction of RDP in the plasticized layer is shown in figure 5.14. The most interesting data set is for the experiments conducted at 120 °C. At values of ø>0.43, v decreases slowly as ø decreases. Here the characteristic time for relaxation of the Ultem™ is very much longer than the characteristic time for diffusion in the plasticized zone, De>>1, and this regime is case II diffusion. The discontinuity in the calculated velocities at 120 °C is due to the simple discontinuous fit to the volume fraction versus time data (figure 5.11). At values of ø<0.43, v decreases more rapidly as ø decreases. These values of v and ø occur at the longer experimental times when the material in the plasticized zone is approaching its rubber to glass transition. In this regime, the characteristic time for diffusion in the plasticized zone is the same order of magnitude as the characteristic relaxation time of the Ultem™. De is of order 1 and the system shows anomalous diffusion behavior. At all temperatures above 120 °C, we only capture the anomalous diffusion behavior because experiments in the case II regime require time periods which are too short for accurate temperature control in our experimental setup. The instantaneous front velocities at temperatures above 120 °C are also expected to increase less rapidly at

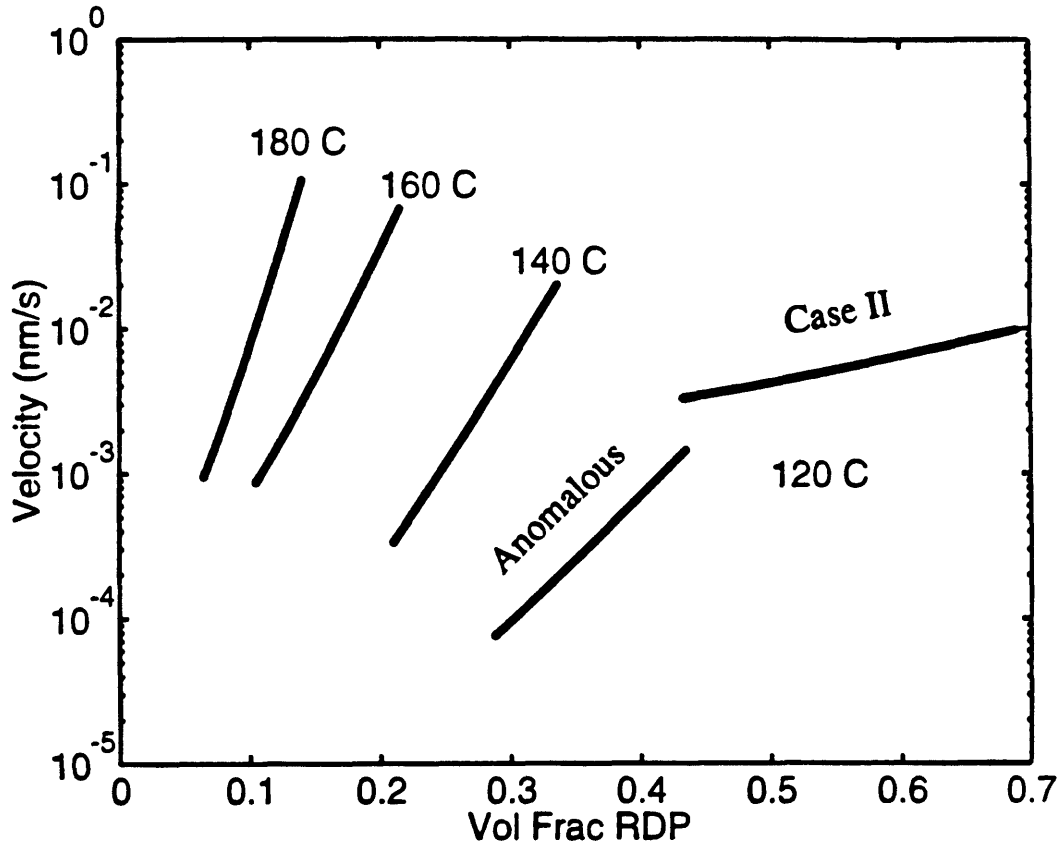

Figure 5.14 Semilog plot of instantaneous front velocity versus ø.

higher values of ø. The plots are expected to have the same form as the plot for the data at 120 °C. The shape of the semilog plot of v versus ø at 120 °C is qualitatively the same shape as the semilog plot of the normalized front velocity versus ø published by Hui et al.[8] in their theoretical treatment of non-Fickian diffusion. The results from the RDP/Ultem™ system with a limited supply boundary condition are therefore consistent with the existing theory of non-Fickian diffusion as it was developed for the infinite reservoir boundary condition.

Lasky et al.[23], and later Gall et al.[7] determined the diffusion profiles with RBS for iodohexane in PS, and 1-iodo-n-alkanes in PS, respectively, at low penetrant activities. From these experiments, the critical value of ø at the surface of the glassy polymer, $ø_c$, necessary for a sharp diffusion front to form and propagate is determined. After the front forms and starts to propagate into the glassy polymer, ø continues to increase slowly until a constant value is reached. The volume fraction in the plasticized zone is plotted as a function of time, and $ø_c$ is determined as the intercept of a fit to the data at a time equal to the induction time. The best fit of ø versus time is with ø in direct proportion to the log of time. In this study, a well established RDP front propagates into the Ultem™, but as it proceeds, the volume fraction of penetrant behind the front decreases due to the limited supply boundary condition. Here ø decreases in direct proportion to the log time (figure 5.13).

Hui et al. defined $ø_c$ as the composition where the diffusion coefficient, D(ø), undergoes a step change with $D(ø<ø_c)$ equal to the diffusion coefficient in the glassy polymer, D_g, and $D(ø>ø_c)$ equal to the diffusion coefficient in a rubbery polymer, D_r, with $D_r>>D_g$. They explicitly do not state that $ø_c$ corresponds to the material composition that has a glass transition temperature equal to the temperature of the experiment even though this seems to be implied in their definition of D(ø). Gall et al.[7] argue that the onset of case II diffusion occurs when the glassy polymer begins to yield, not when the T_g of the plasticized material drops below the ambient temperature. They cite evidence from

experiments with N-methyl pyrollidinone diffusing into an aromatic polyimide (not a glassy polymer) in which the swollen material is not above its T_g.[24] From the results discussed above (figures 5.9 and 5.10), ϕ_c in the RDP/Ultem™ system is identified as the composition at which a rubber to glass transition occurs at the temperature of the experiment. This supports the view that non-Fickian diffusion fronts form when the volume fraction of plasticizer attains a value such that plasticized zone is rubbery. The limited supply boundary condition is an innovative experiment to determine ϕ_c in that diffusion fronts are formed at values $\phi>\phi_c$ and then ϕ decreases with time and penetration depth towards ϕ_c. In other studies, ϕ is varied by changing the activity of the penetrant in the infinite reservoir throughout a series of experiments. A novel aspect of the model RDP/Ultem™ system is the non-volatile nature of the plasticizer and its compatibility with the glassy polymer. Comparisons were made between independent DSC measurements of T_g in static cast blends to compositions determined in the diffusion measurements to elucidate the significance of ϕ_c. Comparisons and experiments such as these were difficult or impossible to perform in previously studied systems where the penetrants in those studies were volatile.

The two step diffusion experiments provide a unique means to explore the effect of matrix properties on non-Fickian diffusion behavior and test some the principles of the Thomas and Windle theory. With this simple technique, ϕ is determined as a function of time for RDP penetrating into a modified Ultem™ matrix. The propagation of the diffusion front at 120 °C in the pure Ultem™ is compared to propagation of the front at the same temperature in a matrix which is a blend of 0.08 volume fraction RDP in Ultem™(figure 5.13). In the Thomas and Windle theory,[13] the mean normal stress ahead of the diffusion front is calculated with an osmotic pressure analogy. The osmotic pressure, P_{os}, is proportional to the difference in chemical potential between the actual penetrant concentration in any material element and the local equilibrium value in that element if the stress were relaxed to zero. The actual penetrant concentration profile exhibits a 'Fickian

tail' which extends into the glassy polymer ahead of the diffusion front, and the maximum in P_{os} occurs somewhere along the 'Fickian tail' where the actual concentration is small, the local equilibrium concentration is high, and the difference between the concentrations is the greatest. In the two step diffusion experiment, 0.08 volume fraction RDP is already in the matrix. Since the actual concentration of plasticizer can never attain values below 0.08 volume fraction, the calculated osmotic pressure as a function of depth must be significantly affected both in shape and magnitude. The velocity of the diffusion front in the two step experiments as compared to the experiments with pure Ultem™ (figure 5.15) is influenced by not only different matrix viscosity, in the Thomas and Windle framework, but by a different profile of the mean normal stress ahead of the front as well.

The effect of the altered matrix properties on front propagation at 120 °C in the case II regime(ϕ>0.43) is to essentially shift the ϕ versus time data to shorter time (figure 5.12). This implies that the induction time is shorter for propagation in the matrix with 0.08 volume fraction RDP. The material with 0.08 volume fraction RDP has a lower η_o than pure Ultem™. Thomas and Windle[13] predict that the induction time is a function of η_o only, and decreases with decreasing η_o. A promising avenue of future research is to take advantage of the compatibility and thermal stability of the RDP/Ultem™ system, to measure $\eta_o(\phi,T)$ and $D(\phi,T)$ independently, and use measured front velocities in various two step diffusion experiments to test the validity of non-Fickian diffusion models.

The results of the experiments where an external biaxial stress was applied in the plane of the sample and normal to the direction of the diffusion front velocity, z, are difficult to explain in the framework of the Thomas and Windle model. The mean normal tensile stress generated near the interface between the plasticized layer and the unswollen substrate is of order 50 to 100 MPa.[8,12,13] The largest externally applied biaxial stresses ($\sigma_{rr}=\sigma_{\theta\theta}=\sigma_{biaxial}$, $\sigma_{zz}=0$) correspond to mean normal stresses ($2\sigma_{biaxial}/3$) of order 20 MPa, a significant fraction of the stress generated near the diffusion front. The additional stress had no detectable effect on the diffusion behavior (see table 5.1). This is

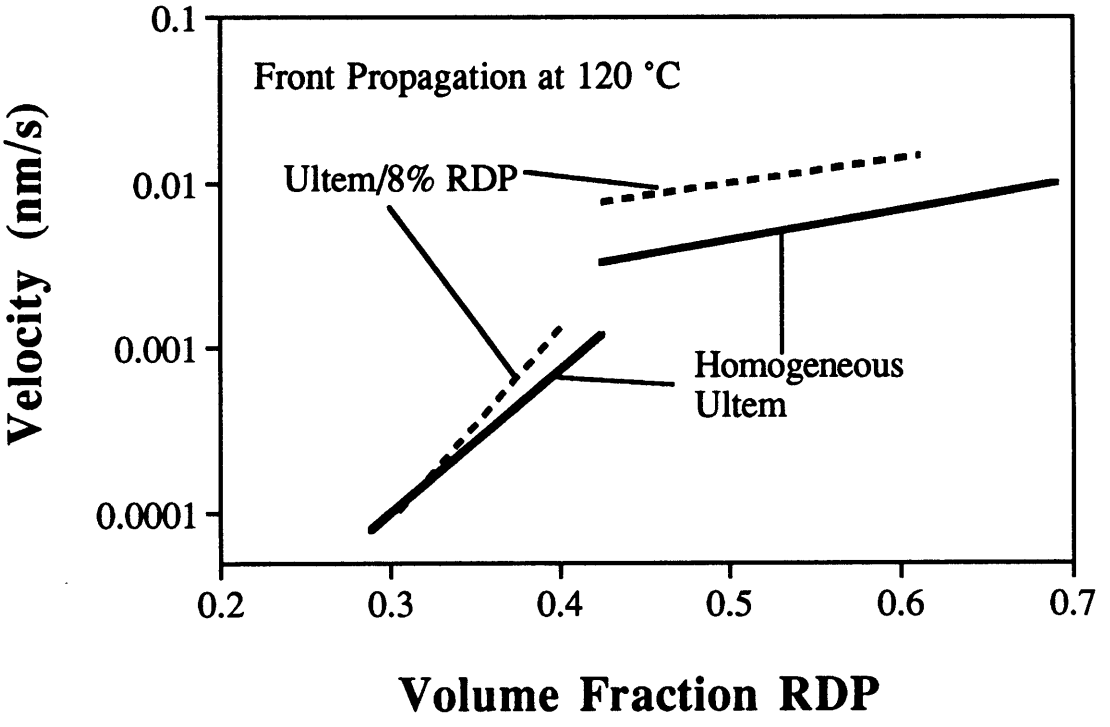

Figure 5.15 Semilog plot of instantaneous front velocities at 120 °C in pure Ultem™ and Ultem™ with 0.08 volume fraction RDP in the second step of the two step experiments.

surprising in that Thomas and Windle consider the swelling rate in the interfacial region to be linearly proportional to the mean normal tensile stress (or osmotic pressure in their terminology). Due to lateral constraints in the planar geometry of the experiment, the deformation or swelling of the polymer occurs only in the direction of penetration, z. Our results indicate that the swelling rate should perhaps be proportional to the component of stress in the penetration direction (σ_{zz}) rather than to the mean normal stress. The magnitude of σ_{zz} is unaffected by the externally applied stress and thus the diffusion behavior is unchanged. An experiment which would verify this hypothesis would be to apply an external stress in the penetration direction and monitor changes in the diffusion behavior.

Externally applied tensile and compressive biaxial stresses corresponding to mean normal stresses of order 20 MPa are expected to change the mechanical and diffusive properties of the glassy polymer matrix. Hydrostatic pressure, for example, is known to increase T_g by approximately 0.3 °C/MPa (Chapter 4). However, the two step diffusion experiments demonstrated that even the alteration of the matrix by the presence of 0.08 volume fraction RDP produced no change in the diffusion profile at 120 °C after 72 hours (figure 5.12), and so it is not surprising that externally applied stresses do not change the diffusion behavior at 120 °C after 72 hours. In order for the biaxial stress to affect the diffusion behavior after 1 hour at 120 °C, η_o and/or D_o of the matrix must be significantly changed. The externally applied stresses employed in this study apparently do not significantly alter either of these properties. This indicates that the diffusion behavior probably will not be affected until the external stresses are so large as to cause plastic deformation.

The primary objective of this research was to gain some insight into the diffusion process which occurs in the toughening mechanism mentioned in the Introduction. Fickian diffusion at room temperature can not account for the necessary flux of polybutadiene into polystyrene to locally plasticize the material drawn into crazes. The critical role that stress

and plasticization play in both the toughening mechanism and non-Fickian diffusion implies that perhaps diffusion via a non-Fickian mechanism can account for the required flux of polybutadiene plasticizer. This scenario would be similar to Brown's model[4] for environmental crazing in polymers. An estimate for the required velocity of a diffusion front is 10 nm/s based on a characteristic length in the system to be the diameter of a craze fibril(~10 nm), and a typical measured craze velocity of 10 nm/s at room temperature. These craze velocity measurements were made at room temperature, 70 °C below the T_g of PS. For comparison, we choose the RDP front velocities 70 °C below the T_g of Ultem™ at approximately 145 °C. Examination of figure 5.14 reveals that it is unlikely for the front velocity at 145 °C to ever reach a value as high as 10 nm/s, 1000 times the largest front velocity plotted for diffusion at 120 °C. In fact, even at 180 °C, the front velocity does not appear likely to attain a value of 10 nm/s. The physical properties of PS in the yielding state must be significantly different than the unperturbed polymer to account for the flux of PB in PS which occurs in the toughening mechanism. This observation is consistent with other examples of enhanced diffusion as a result of deformation are found in the literature. Miller and Kramer[25] describe an increase of orders of magnitude in the diffusion rate of Freon 113 in cross-linked PS and poly (para-methystyrene) in environmental deformation zone formation. Harmon et al.[26] have shown that deformed PMMA samples absorb methanol at much higher rates than undeformed samples.

5.6 Summary

Non-Fickian diffusion of RDP in Ultem™ was measured with RBS when the RDP was present in a limited supply initially on the surface of the Ultem™. The volume fraction versus depth profiles of the plasticizer in the glassy polymer were essentially step functions and had sharp diffusion fronts less than 30 nm in width. The limited supply boundary condition requires that as the plasticizer front penetrates deeper into the glassy substrate, the

volume fractions of RDP, ø, behind the front must decrease. At long time periods, ø approaches a value such that the material behind the front has a glass transition temperature equal to the temperature of the experiment. We identify this value of ø as the critical volume fraction of plasticizer, $ø_c$, as defined by Hui et al.[8,9], Lasky et al.[23], and Gall et al.[7] Data taken at 120 °C exhibits two regimes of non-Fickian diffusion behavior, anomalous and case II. Only the anomalous regime was observed at 140, 160, and 180 °C. The transition between regimes is interpreted in the framework of an integral sorption Deborah number introduced by Wu and Peppas.[12] Calculations of the instantaneous front velocities, especially for the 120 °C data, as a function of ø allow us to make a favorable comparison to the model of Hui et al.[8] Unique two step volume fraction profiles were produced by diffusion of a limited supply of RDP at 180 °C followed by diffusion of a second limited supply of RDP at 120 °C, and the effects of an altered matrix on front propagation at 120 °C were considered. Externally applied biaxial tensile and compressive stresses in the plane of the sample of order 10 to 30 MPa had no effect on diffusion at 120 °C in experiments in the case II or the anomalous regime.

5.7 References for Chapter 5

(1) Gebizlioglu, O. S.; Beckham, H. W.; Argon, A. S.; Cohen, R. E.; Brown, H. R. *Macromolecules* **1990**, *23*, 3968-3974.

(2) Argon, A. S.; Cohen, R. E.; Gebizlioglu, O. S.; Brown, H. R.; Kramer, E. J. *Macromolecules* **1990**, *1990*, 3975-3982.

(3) Nealey, P. F.; Cohen, R. E.; Argon, A. S. *Macromolecules* Submitted for publication.

(4) Brown, H. R. *J. Polym. Sci, Polym. Phys. Ed.* **1989**, *27*, 1273-1288.

(5) Spiegelberg, S. H. PhD Thesis, MIT, 1993.

(6) Nealey, P. F.; Cohen, R. E.; Argon, A. S. *Macromolecules* **1993**, *26*, 1287-1292.

(7) Gall, T. P.; Lasky, R. C.; Kramer, E. J. *Polymer* **1990**, *31*, 1491-1499.

(8) Hui, C.; Wu, K.; Lasky, R. C.; Kramer, E. J. *J. Appl. Phys.* **1987**, *61*, 5137-5149.

(9) Hui, C.; Wu, K.; Lasky, R. C.; Kramer, E. J. *J. Appl. Phys.* **1987**, *61*, 5129-5136.

(10) Lasky, R. C. Ph.D. Thesis, Cornell University, 1986.

(11) Lustig, S. R.; Caruthers, J. M.; Peppeas, N. A. *Chemical Engineering Science* **1992**, *47*, 3037-3057.

(12) Wu, J. C.; Peppas, N. A. *J. of Polym. Sci., Polym. Phys. Ed.* **1993**, *31*, 1503-1518.

(13) Thomas, N. L.; Windle, A. H. *Polymer* **1982**, *23*, 529-542.

(14) Durning, C. J. *J. of Polym. Sci., Polym. Phys. Ed.* **1985**, *23*, 1831-1855.

(15) Kambour, R. P. *Polymer Communications* **1983**, *24*, 292-296.

(16) Black, K. A., Ultrapolishing of polymers, personal communication.

(17) Roark, R. J. *Formulas for Stress and Strain;* Fourth ed.; McGraw-Hill: New York, NY, 1965.

(18) Chu, W. K.; Mayer, J. W.; Nicolet, M. A. *Backscattering Spectroscopy*; Academic Press: New York, NY, 1978.

(19) Feldman, L. C.; Mayer, J. W. *Fundamentals of Surface and Thin Film Analysis*; Elsevier Science Publishing Co., Inc.: New York, New York, 1986.

(20) Crank, J. *The Mathematics of Diffusion;* 2nd ed.; Oxford University Press: Oxford, U.K., 1975.

(21) Doolittle, L. R. *Nucl. Inst. Meth.* **1985**, *B9*, 344.

(22) Doolittle, L. R. *Nucl. Inst. Meth.* **1986**, *B15*, 227.

(23) Lasky, R. C.; Kramer, E. J.; Hui, C. *Polymer* **1988**, *29*, 673-679.

(24) Gattiglia, E.; Russel, T. P. *J. of Polym. Sci., Polym. Phys. Ed.* **1989**, *27*, 2131-2144.

(25) Miller, P.; Kramer, E. J. *J. of Mater. Sci.* **1990**, *25*, 1751-1761.

(26) Harmon, J. P.; Sanboh, L.; Li, J. C. M. *J. of Polym. Sci., Polym. Phys. Ed.* **1987**, *25*, 3215-3229.

Chapter 6

Summary

The motivation for this research was to gain insight into the complex diffusion process which occurs in a recently reported craze toughening mechanism for glassy polymers, an important class of thermoplastics. At room temperature and at strain rates below 10^{-3} s^{-1}, blends of a few volume percent of low molecular weight polybutadiene rubber (PB) in glassy polystyrene (PS) undergo significantly larger strains to fracture and craze at lower flow stresses than the homopolymer when the phase separated pools of PB in the PS matrix are less than approximately 0.2 μm in diameter. The central process of the toughening mechanism is the sorption of PB from submicron-sized phase separated pools into the fringe layers of crazes. This process locally plasticizes this material and facilitates craze growth. The solubility of PB in these regions is substantially increased by the positive mean normal stress which accompanies the plastic deformation in the region of a craze. In the model of Argon et al., the diffusion process is assumed to occur at a rate which is much faster than the rate of craze growth. Subsequent mechanical experiments at subambient temperatures or at strain rates higher than 10^{-2} s^{-1} show that the diffusion process is the limiting step. In order to probe and quantify the limitations of the toughening mechanism, and to develop a more complete model, information is required on the rate of diffusion of PB in PS in the fringe layers of crazes. The estimated minimum diffusion coefficient for low molecular weight PB in PS necessary for the diffusion process to occur within the same time frame as craze growth in the toughened blends is 10^{-12} cm^2/s.

To measure diffusion coefficients of this magnitude in experiments of reasonable time periods, concentration profiles must be determined over distances of order 0.1 to 1 μm. Forward Recoil Spectroscopy (FRES) and Rutherford Backscattering Spectroscopy (RBS) are ion beam analysis techniques which are suitable for this type of

measurement. In both experiments, a sample is irradiated with a high energy beam of alpha particles (2 to 3 MeV helium ions). A very small fraction of the incident ions have elastic collisions with nuclei in the sample. The energy of recoiled or backscattered particles is a function of the masses of the target nuclei thereby allowing relative concentrations of elements to be determined up to a depth of approximately 1 μm in the sample. In diffusion experiments, the diffusing species is labeled with deuterium for FRES, and any medium atomic weight element for RBS. These techniques have been used extensively for analysis of semiconductor materials, but have only recently been applied to polymers.

Tracer diffusion coefficients for 3000 g/mol perdeuterated PB in high molecular weight PS were measured with FRES. In the temperature range from 97 to 115 °C, the diffusion coefficients vary from 10^{-15} to 10^{-12} cm^2/s, and the apparent activation energy for the diffusion is 99 kcal/mol. The values of the diffusion coefficients and the activation energy are in good agreement with those found for the diffusion of smaller more rigid photoreactive dye molecules in PS in the same temperature range. This implies that the PB molecule acts as a probe of the PS matrix properties. The diffusion coefficient varies three orders of magnitude over 18 °C because this temperature range is near the glass transition temperature of PS. Small changes in temperature have a dramatic effect on matrix mobility. The thermally-induced tracer diffusion of PB in PS did not proceed at a rate equivalent to the estimated rate required by the toughening mechanism until the temperature reached 115 °C, a temperature well above the T_g of PS. Polystyrene in the vicinity of crazes at room temperature must behave as though it is at or above its T_g.

The effect of stress on diffusion in the PB/PS system described above was investigated by applying helium gas pressure. Hydrostatic pressure (negative mean normal stress) decreased the diffusion coefficient for 3000 g/mol perdeuterated PB in PS from 1.2×10^{-13} to 3.7×10^{-14} cm2/s as the helium pressure was increased from atmospheric pressure to 11.3 MPa. This result is explained in terms of the known effect of hydrostatic pressure to increase the glass transition temperature of PS by 0.3 °C/MPa. On the other

hand, positive mean normal stress (negative pressure) is expected to increase the diffusion coefficient and decrease T_g. Negative pressure in the fringe layers of crazes is at most 40 MPa. Therefore, unless the effect of positive mean normal stress is extremely asymmetric in comparison with the effect of negative mean normal stress with respect to diffusion at zero stress, negative pressure effects alone can not fully account for the rapid diffusion in the toughening mechanism at room temperature.

Tracer diffusion measurements of perdeuterated PB in PS exhibited volume fraction versus depth profiles which were Fickian in nature. The volume fraction of PB in PS never attained values large enough to significantly affect matrix properties. However, in the diffusion process in the toughening mechanism, the solubility of PB in PS is increased by the presence of negative pressure, and the PB is present in a more abundant supply than in the tracer diffusion experiments. In order to determine whether a non-Fickian diffusion mechanism could account for the flux of PB into the PS in the vicinity of crazes, a model plasticizer/glassy polymer system of resorcinol bis(diphenyl phosphate) (RDP) and a polyetherimide (Ultem™) was investigated. Volume fraction versus depth profiles of RDP in Ultem™ were determined as a function of time, temperature, and externally applied stress using RBS when RDP was initially present in a limited supply on the surface of the Ultem™. The profiles had sharp diffusion fronts with a constant volume fraction of RDP in the plasticized zone in all of the samples; the behavior was consistent with so-called anomalous and case II diffusion behavior. Instantaneous diffusion front velocities which ranged from 10^{-4} to 10^{-1} nm/s were determined for temperatures from 120 to 180 °C. Biaxial compressive or tensile stresses of order 30 MPa in the plane of the sample and normal to the penetration direction had no effect on the diffusion behavior. These experiments are comparable to the PB/PS system on the basis of the temperature difference, $T_g - T_{experiment}$. Under no experimental conditions did the front velocity attain a value of 10 nm/s, the minimum velocity required to account for the flux of PB in PS in the diffusion process of the toughening mechanism at room temperature.

Both the tracer diffusion measurements in the PB/PS system and the non-Fickian diffusion behavior observed in the RDP/Ultem™ system reveal that the physical properties of PS during the deformation process must be dramatically different from the unstressed polymer or the stressed polymer prior to plastic deformation. The diffusion process and the deformation process in the toughening mechanism are intimately linked.